POLITECNICO DI MILANO

Dept. Chimica, Materiali e Ingegneria Chimica “G. Natta”

Doctoral Program in Industrial Chemistry and Chemical Engineering

---

MODELING ACROSS DIFFERENT LENGTH SCALES: FROM KINETICS TO FLUID DYNAMICS

Doctoral Dissertation of:
STEFANO VALERIO RAVASIO
Matr. 768908

Supervisor:
Prof. Carlo Cavallotti

Tutor:
Prof. Maurizio Masi

The Chair of the Doctoral Program:
Prof. Tiziano Faravelli

Cycle XXVI
2011-2013

POLITECNICO DI MILANO

Dept. Chimica, Materiali e Ingegneria Chimica “G. Natta”

Doctoral Program in Industrial Chemistry and Chemical Engineering

---

MODELING ACROSS DIFFERENT LENGTH SCALES: FROM KINETICS TO FLUID DYNAMICS

Doctoral Dissertation of:
STEFANO VALERIO RAVASIO
Matr. 768908

Supervisor:
Prof. Carlo Cavallotti

Tutor:
Prof. Maurizio Masi

The Chair of the Doctoral Program:
Prof. Tiziano Faravelli

Cycle XXVI
2011-2013

Acknowledgments

I would like to thank people that have been with me in the last 3 years.

A special acknowledgement goes to my family for having kept to help me during this period.

Then I'd like to thank prof. Carlo Cavallotti for the possibility to do this interesting experience and for his availability to give me many useful advices to complete this path. Then I'm also grateful to all the members and friends of CFA lab, who spent much pleasant moments with me.

I'd also like to express my gratitude to prof. Sugiyama for the opportunity he gave me to stay 6 months in Tokyo. Another thank goes to prof. Momose and Yudai Suzuki who worked at strict contact with me and also to prof. Shimogaki and prof. Fuji who contribute to this research. Of course I'm obliged with all the members and friends of Sugiyama and Shimogaki groups who welcomed me in Tokyo and spent much pleasant moments with me, as well as with Yoshiko Sawayanagi who helped me to enter in Japan.

Finally I also thank all my friends in Italy and in Japan.

I'm extremely sorry that these acknowledgments are so plain and synthetic, but in this period I've really written too much, following the scientific formalism. So actually I'm not feeling creative enough. Probably I will rewrite them in a second moment in a more appropriate and poetic style.

Stefano

Publications and conferences

- Stefano Ravasio, Carlo Cavallotti, *'Analysis of the reactivity and energy efficiency of an atmospheric non thermal plasma used for the non oxidative conversion of methane' ,* Colloquium on chemical reaction engineering, 10-11-2011, Munich (GER) *'Chemical reaction engineering for methane valorization'*
- Stefano Ravasio, Carlo Ferrara, Carlo Cavallotti, '*Reactivity and energy efficiency of an atmospheric non thermal plasma used for the non oxidative conversion of methane' ,* AICHE annual meeting, 28-10-2012 / 02-11-2012, Pittsburgh (USA), 'Reaction engineering for combustion and pyrolysis II'
- Stefano Ravasio, Carlo Cavallotti, '*Analysis of reactivity and energy efficiency of methane conversion through non thermal plasmas'* Chemical Engineering Science 2012, Vol. 84, 580-590
- Stefano, Ravasio, Carlo Cavallotti, Maurizio Masi, *'Analysis of gas phase reactivity of chlorosilanes'*, the Journal of Physical Chemistry A 2013, Vol. 117, 5221-5231
- Stefano Ravasio, Takeshi Momose, Katsushi Fuji, Yukihiro Shimogaki, Carlo Cavallotti, Masakazu Sugiyama, '*Analysis and control of growth rate and composition in GaN MOVPE (2)',* SCEJ autumn meeting, 17-09-2013, Okayama (Japan), 'CVD & Dry Process - Reaction Engineering for the Structure/ Functions control', oral presentation
- Carlo Cavallotti, Filippo Rossi, Stefano Ravasio, Maurizio Masi, 'A kinetic analysis of the growth and doping kinetics of the SiC chemical vapor deposition process', Industrial & Engineering Chemistry Research 2014, in press
- '*Investigation of the mechanism active during GaN MOVPE by a combined modeling and experimental approach',* (provisory title), in preparation
- Carlo Cavallotti, Stefano Ravasio, '*A new approach to determine transitional partition functions for loose transition states',* in preparation, to be submitted to Physical Chemistry Chemical Physics

Summary

This work is focused on the study of advanced kinetic mechanisms in several systems where there is an interaction between some components in a gas phase and an activated surface. Basically the gaseous reagents enter in a reactor where they undergo various chemical reactions. The energy necessary to promote such reactivity is supplied through a solid surface, located inside the area where the conversion takes place. Also material exchanges occur at the interface and a considerable part of the gaseous precursors might be deposited on the active surface. The control of the growth of such solid is a key aspect both in case that product is the target of the process, and when it is the result of an undesired side conversion. Hence the transport phenomena between the two phases act an important role in determining the performances of these systems, as well as the reaction kinetics.

The industrial applications of this type are actually countless, including the huge branch of chemical vapor deposition and a consistent part of catalysis. The reactors are designed on the basis of classical chemical engineering and the operative parameters should be selected in the best way to optimize the global performances. In particular, in this study there were analyzed four different processes where it is valid what stated

above. The first one is a technology still in phase of investigation for the future use in the industrial scale that is the non oxidative conversion of natural gas in atmospheric non thermal plasmas. The others instead have been applied for decades to produce semiconductor materials, which are the chemical vapor deposition (CVD) of polycrystalline silicon, the chemical vapor deposition (CVD) of SiC and the metal organic vapor phase epitaxy (MOVPE) of gallium nitride.

In all of the processes mentioned above, despite the wide interest for the large scale production, the kinetic mechanism has not yet been clarified and the reactors are actually managed following the results of a trial and error approach. Thus a better understanding of the fundamental chemistry and of how the kinetics is influenced by the heat and material exchanges can potentially lead to significant advantages. Indeed it should be a very useful tool for the optimization of the operative conditions and the reactor design with the final purpose to enhance the productivity of those systems, but also to limit the energetic costs, or to improve the quality of the products.

The aim of this phd thesis is to investigate the most critical aspects in the systems cited above, focusing in particular on their kinetics an fluid dynamics. The main issue was to develop a general methodology, which can be extended to other cases. As final result the method should provide useful guidelines to improve the global performances. The approach adopted was thus conceptually the same. The initial part consists in assembling the kinetic scheme. A preliminary set of reactions is determined including what already proposed in the literature. Moreover a thermodynamic analysis helps to identify the most stable intermediates, which may have a significant role in the mechanism. After that, additional new classes of conversion routes are hypothesized for the first time. Accurate *ab initio* calculations are performed to evaluate the kinetic parameters of such new reactions, based on transition state theory. The precision of the computational techniques herein used is generally higher

with respect to those previously utilized in other studies about the processes investigated. The approach followed in this work combines the advantages of fast DFT with those of more rigorous techniques. When relevant the low vibrational frequency associated to torsional motions is replaced by a 1D hindered rotor model. This improves the prediction of the pre exponential factors. Therefore also the constants taken from the literature are re evaluated in order to avoid comparing reaction pathways using kinetic constants calculated at different levels of theory. Then the whole kinetic scheme is combined with a literature surface mechanism and tested with a program simulating a simple bi phase PSR reactor model. With that micro kinetic analysis is possible to find the most sensitive reaction pathways and to discard from the mechanism those without any noticeable effect on the global conversion rates. However the transport phenomena in fact heavily influence the performances of real reactors. Thus fluid dynamics models are developed and finally solved including the new proposed mechanism. The methodology described was applied to all the four processes, but paying more attention at different aspects in each of them, depending on the respective focuses and background of knowledge.

The first part of the work was dedicated to the non oxidative valorization of natural gas through non thermal plasmas. The simulations are consistent with the results reported in the literature, that have demonstrated the possibility to achieve elevated acetylene yields with energy efficiencies comparable with those of thermal processes. Moreover one of the main findings of this study is that the temperature evolution in the plasma volume plays a key role in determining the system reactivity and its energy consumption. Among the conclusions of this study are included a set of guidelines that may be useful to improve the energy efficiency of plasma methane conversion.

Then it was studied the silicon CVD from trichlorosilane. A micro kinetic analysis revealed that a radical chain mechanism, never proposed before

in the literature, should be predominant in the gas phase of industrial Siemens reactors. Furthermore it was pointed out a strong inter relation between the reactivity in the two phases because of the consumption of the corrosive HCl in the gas, produced during the deposition. Thus operating Si CVD in conditions in which the gas phase reactivity is favored (i.e. at high gas phase temperatures) should enhance the precursor conversion and the film growth rate, though at the expense of an increased production of tetrachlorosilane. These conversion pathways have lately been proved to be effective also during SiC growth, even if the products distribution changes considerably because the operative conditions are completely different. Those simulations predict that the surface kinetics of atomic Si can influence the SiC deposition profile.

Finally this research was also focused on GaN MOVPE. Such project was in cooperation with two groups in the University of Tokyo and part of the phd thesis was spent in there. An important aspect of this work was the description of particles formation. Therefore the model was improved by including a set of equations based on the second order method of moment, in order to represent the particles dynamics. In particular a new correlation was here proposed to describe the scavenging of active precursors on the droplets surface. A reasonable agreement between simulations and experiments was achieved. With the hypothesis proposed it has been possible to clarify the various phenomena that take place in the reactor during the film growth and to explain the effect of several operative parameters. Thus the model can be used as a means to achieve higher growth rates, as well as to reduce the powders drop on the substrate.

In conclusion the methodology here proposed was successfully proved to be a useful tool to optimize the operative conditions for different type of processes with a subsequent improvement of their global performances.

Index

List of figures

Chapter 1. Introduction

Chapter 2. Theoretical background and methods

Chapter 3. Non oxidative conversion of CH_4 in plasmas

Chapter 4. Chemical vapor deposition of Si and SiC

Chapter 5. Metal organic vapor phase epitaxy of GaN

List of tables

CHAPTER 1

Introduction

The aim of this phd thesis is to investigate the most critical aspects in systems where there is an interaction between some components in a gas phase and an activated surface, focusing in particular on their kinetics an fluid dynamics. The main issue is to develop a general methodology, which can be extended also to other cases. In particular there were analyzed four different processes. The first one is a technology still in phase of investigation for the future use in the industrial scale that is the non oxidative conversion of natural gas in atmospheric non thermal plasmas. The others instead have been applied for decades to produce semiconductor materials, which are the chemical vapor deposition (CVD) of polycrystalline silicon, the silicon carbide CVD and the metal organic vapor phase epitaxy (MOVPE) of gallium nitride. As final result the method should provide useful guidelines to improve the global performances of the systems studied. In the present chapter it is provided a general description of those processes, underlying their related most critical aspects.

1.1 Conversion of activated gases to higher value products

Nowadays a huge number of applications in the chemical industrial field still rely on systems where there is an interaction between some components in a gas phase and an activated surface. Basically the gaseous

reagents enter in a reactor where they undergo various chemical reactions. The final products are higher value chemicals or materials, which can be in the gaseous or in the solid state, depending on the type of process. The energy necessary to promote such reactivity is supplied through a solid surface, located inside the area where the conversion takes place. Also material exchanges occur at the interface and a considerable part of the gaseous precursors might be deposited on the active surface. The control of the growth of such solid is a key aspect both in case that product is the target of the process, and when it is the result of an undesired side conversion. Hence the transport phenomena between the two phases act an important role in determining the performances of these systems, as well as the reaction kinetics.

The applications of this type are countless, including the huge branch of chemical vapor deposition and a consistent part of catalysis. The reactors are designed on the basis of classical chemical engineering and the operative parameters should be selected in the best way to optimize the global performances. However despite the wide interest for the large scale production, in many cases the kinetic mechanism has not yet been clarified and the reactors are actually managed following the results of a trial and error approach. Thus a better understanding of the fundamental chemistry and of how the kinetics is influenced by the heat and material exchanges can potentially lead to significant advantages. Indeed it should be a very useful tool for the optimization of the operative conditions and the reactor design, with the final purpose to enhance the productivity of those systems, but also eventually to limit the energetic costs, or to improve the quality of the products.

1.2 Plasma processes

The initial part of this study was dedicated to the non oxidative valorization of natural gas with non thermal plasmas. Before describing that process, a general overview of plasma applications is given.

1.2.1 General aspects about plasmas

It is normally defined as plasma an ionized gas, which is thus characterized by the presence of electrons not bounded to atoms or molecules. The latter are consequently converted to ions positively charged, bringing to the maintenance of the macroscopic electrical neutrality of the volume. The non negligible concentration of charge carriers confers to a plasma enhanced electrical conductivities so that it responds strongly to electromagnetic fields. As its properties are very different with respect to those of gas, liquids or solids, plasma is considerate as a further distinct state of the matter. Contrary to how it can be believed, such kind of state is quite frequent in nature, for instance lightings and aurora borealis are common examples. Anyway plasma is the main constituent of the universe as ordinary matter, most of which is in the rarefied intergalactic plasma and in stars.

Plasma can also be generated artificially by inducing ionization with a strong electromagnetic field formed with a laser or a microwave generator, or by applying an electric field on a gas between two electrodes. One widespread actual technology based on this principle is neon lighting, but also the more recent plasma displays. Indeed they both contain rarefied ionized gases electrically charged. Besides plasmas have also several other industrial applications. In material processing for electronic industry, weakly ionized plasma assisted treatments are commonly applied for the etching procedures. It is generally utilized to remove from the surface a desired amount of thin solid film in an anisotropic way. Furthermore plasma enhanced chemical vapor deposition can be used to grow particular materials as grapheme, diamond films or amorphous silicon for solar cells. Finally plasma processes are also important for other types of industries, like biomedical, automotive, toxic waste management, aerospace and steel.

The features of those industrial systems are not only affected by the classical physical parameters, but they also depend on electronic

properties, as ions and electron concentrations and electronic temperature. The latter is the mean temperature of the electrons accelerated by the electric field. Indeed, as such kind of systems are multi component, they may have different temperatures. Consistently with the kinetic gas theory, the temperature in plasma is determined, like in common gases, by the mean energy of its constituents and by how that energy is distributed in its degrees of freedom (transactional, rotational, vibrational and electronic). The electrons receive energy from the electric field during their free path, losing only a portion of that energy trough the collisions with heavier particles. For that reason the electron temperature in plasma is initially higher with respect to that of the rest of the gas. In the subsequent moments the electrons and the heavier molecules may compensate their energy difference through collisions, except if the energy or the time are not sufficient to allow it, or in case of intense cooling. If the thermal equilibrium between all its constituents is achieved, the plasma is called thermal, otherwise it is called non thermal. The elevated temperatures, above 3000 K, in thermal plasmas make them not so attractive for industrial applications. In fact in such conditions the materials undergo a considerable stress and conspicuous electric powers are needed, most of those wasted into the gas heating.

The most common way to prevent the stabilization of a thermal regime is to operate in vacuum. Indeed on that condition the mean free path of the accelerated electrons is increased and the energy equilibration through collisions can be prevented. Thus at low pressures it is possible to generate macroscopic stationary plasmas, or macro discharges. A typical configuration of a macro discharge reactor is reported in Figure 1a. At this category belong several types of apparatus, where the formation of the plasma is implemented with different techniques. For instance in microwave plasmas, the discharges are generated by electromagnetic waves, whose wavelengths are of few centimeters and interact with the plasma in a quasi optic way. Radio frequency capacitive coupled plasmas

(RF-CCP) instead are sustained by the application of a voltage pulsated in the regime of radio frequencies. Finally in inductively coupled plasmas (RF-ICP) the energy is supplied by electric currents produced by electromagnetic induction, due to the time variation of a magnetic field.

The transition to the thermal regime can be prevented also if it is not given enough time to reach the thermal equilibrium between free electrons and the heavier molecules in the gas. Thus the discharge breakdowns should be rapidly stopped in limited times (10-100 ns), then the electric voltage is reversed and new discharges are formed. On this way plasmas are not developed uniformly in the inter electrodes gap, but in the form of small filaments, with diameters between 0.1 and 1 mm. One important related property is the memory effect, which is the repetition of the breakdowns exactly at the same points. That phenomenon occurs because, though after electron current termination there are no longer electrons or ions in the main part of the channel volume, in that area it remains a high level of vibrational and electronic excitation. Such type of microscopic periodically repeated plasmas are called micro discharges and with respect to macro discharges, it is easier to operate at atmospheric pressure. In Figure 1b is represented a schematization of a micro discharge reactor. The simplest technique to obtain the pulsation of the electron avalanches is the dielectric barrier discharge (DBD), that consists to include a dielectric material between the electrodes. The generation of weakly ionized plasmas takes place until the local electric field collapses for the charges accumulated on the dielectric surface. A common alternative reactor is the pulsed corona. For that it is required a more complex power generator, able to apply the electric voltage only during an imposed periodic time interval. The electrodes configuration consists of a coaxial coupling between a cylinder and a pointed extremity, in order to better localize and intensify the electric field. Therefore the charge density is considerably higher than in DBD.

Other examples of micro discharges are gliding arcs, pulsed spark and pulsed streamers.

Non thermal plasmas generated in the reactors described above have been object of recent wide researches [1], aimed to develop new technologies suitable for the large scale application. The explanation is that though the considerable amount of electric powers consumed, they have some interesting features, which are intriguing from the industrial point of view. One appealing peculiarity is the considerable concentration of active species like electrons, ions, excited molecules, photons and radicals. Therefore the reactivity of those systems is very enhanced and radical mechanisms take place at high velocity even at room temperature. Furthermore such systems can easily operate far from the thermodynamic equilibrium and provide high concentrations of species chemically active.

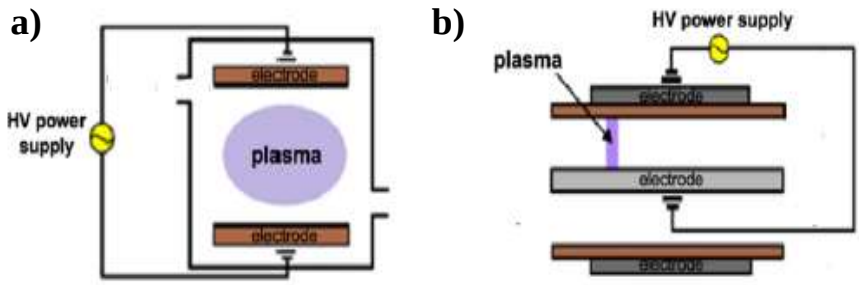

Figure 1: Schematizations of typical a) macro discharges; b) micro discharges.

1.2.2 Non oxidative conversion of natural gas with plasmas

One of the most investigated new processes based on non thermal plasmas is the conversion of methane into higher value products. Indeed, though the actual huge availability of natural gas, it is yet a greatly underutilized resource for the production of chemicals and liquid fuels. The traditional industrial way for the reactive activation of this raw material is its partial oxidation to syngas, that is subsequently converted to heavy hydrocarbons through Fisher Tropsch synthesis or to chemical commodities. However partial oxidation is very energetically expansive,

thus for decades considerable resources have been invested with the purpose to develop alternative technologies. Unfortunately this task is complicated, due to the high chemical stability of methane that made difficult its exploitation in processes different to the combustion. Plasmas overcome this problem because the electrons generated during the discharge are able to promote the homolytic dissociation of methane into radicals. After that a kinetic mechanism can easily take place. In particular the non oxidative conversion of natural gas promoted by electric discharges leads to the formation of hydrogen and higher hydrocarbons, as ethane, ethylene and acetylene, consistently with the following global reactions:

T1) $2CH_4 \rightarrow C_2H_6 + H_2$

T2) $2CH_4 \rightarrow C_2H_4 + 2H_2$

T3) $2CH_4 \rightarrow C_2H_2 + 3H_2$

Up to now, the only plasma technology for converting methane to acetylene demonstrated on an industrial scale and used in Germany for more than 50 years is the thermal arc plasma (Huels process), schematized in Figure 2. The electrical energy is transferred by direct contact of the high temperature arc and the natural gas feedstock. The products are quenched with water and heavier liquid hydrocarbons to prevent back reactions. In the Huels process a conspicuous amount of carbon is deposited on the electrodes, thus a periodic shut down of the reactor is required to allow their cleaning. Moreover single pass acetylene yield is quite limited (around 40%) and a huge electric power is consumed, mostly wasted into the gas heating. Therefore such process is not so attractive for the economical point of view, but subsides by the German government have helped to keep it in production.

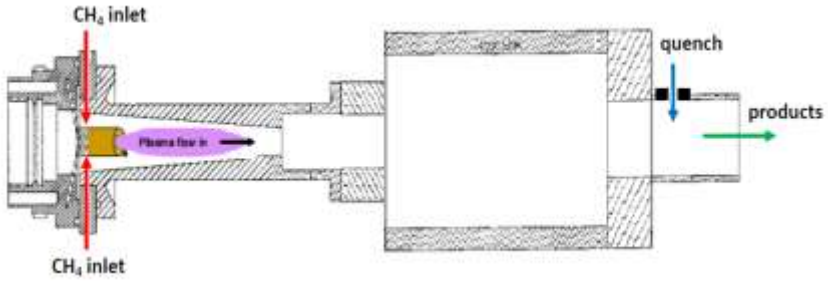

Figure 2: Reactor used in the Huels process for methane non oxidative conversion.

Most of the disadvantages related to the Huels process can be avoided using non thermal plasmas because a greater part of the electrical energy goes into the production of energetic electrons rather than into the gas heating. Hence with the improvement of the techniques described in Section 1.2.1, their possible industrial application for the non oxidative conversion of natural gas has recently attracted much attention. Other authors [2-7] have been able to obtain experimental high acetylene yields, with energetic expenses comparable with the thermal methane dissociation. However, this process could be competitive on the industrial scale only by reducing the specific power consumption. On this way it would be possible to conspicuously reduce both the operative and investment costs related to the electricity utilization and to the electric power generator.

1.3 Chemical vapor deposition

The other types of system of interest in this phd thesis are both based on chemical vapor deposition. In this section is first provided a basic definition of chemical vapor deposition and then a general description of the specific processes in exam.

1.3.1 General aspects about chemical vapor deposition

Chemical vapor deposition (CVD) is a generic name for a group of chemical processes that involve the deposition on a substrate of thin films

of solid materials from a gas phase. Nowadays this technique is mature and widely diffused in the electronic industry. The gas supplier is usually a bubbler because precursors are often liquid in normal conditions. A reaction chamber is used, into which the volatile reagents are introduced to decompose and interact with the heated substrate and then to form the desired product layer. The gaseous by products of the reactions are then desorbed and evacuated from the reaction chamber. In Figure 3 are represented the main phenomena that occur during CVD.

Depending on the process conditions amorphous, poly crystalline or epitaxial layer can be obtained. From the operative point of view the substrate temperature has a key role in determining both the homogeneous and heterogeneous reactivity. It should be noted indeed that chemical reactions don't take place only on the solid substrate, but also in the rest of the reactor volume. Another fundamental requisite is to reach conditions as much uniform as possible inside the reaction chamber. Only on this way the growth can be achieved with good thickness and resistivity uniformities and with satisfactory crystal quality. Besides the inter phase diffusion should be favored to enhance the deposition rate.

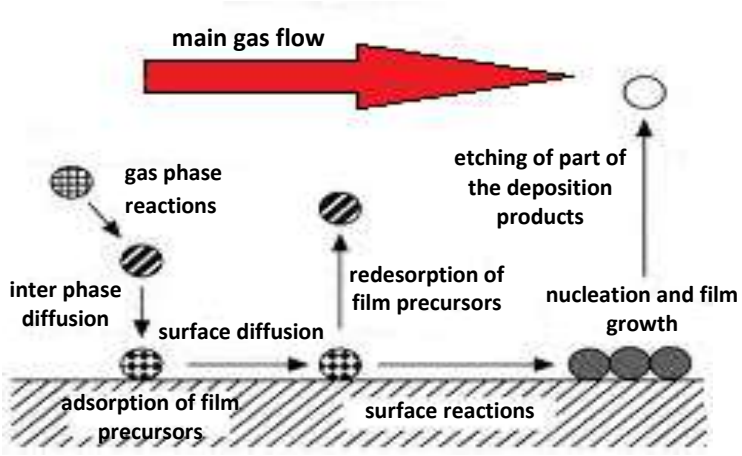

Figure 3: Representation of the main phenomena active during chemical vapor deposition.

There are several criterions to classify the various CVD processes. For instance one of these is based on the operating pressure. Atmospheric

pressure CVD systems (APCVD) work around the atmospheric pressure, low pressure CVD (LPCVD) instead operates in vacuum, whereas ultra high vacuum CVD (UHVCVD) is run below 10^{-6} Pa. When precursors are not volatile, they can be vaporized ultrasonically in aerosol assisted CVD (AACVD), or they can be supplied through injectors in a vaporization chamber in case of direct liquid injection CVD (DLICVD). Another criterion is based on the heating method. A reactor is said to be hot wall if it uses a heating system that heats up not only the wafer, but the walls of the reactor itself, whereas cold wall reactors use heating systems that minimize the heating up of the reactor walls, while the wafer is being heated up. Hot wire CVD (HWCVD) uses a hot filament to chemically decompose the source gases, while atomic layer CVD (ALCVD) deposits successive layers of different substances to produce layered, crystalline films. Then, in metalorganic CVD (MOCVD) the precursors supplied are metalorganics compounds. Plasma enhanced CVD (PECVD) exploits plasma to enhance the chemical reaction rates of the precursors. PECVD processing allows deposition at lower temperatures, which is often critical in the manufacture of semiconductors. The lower temperatures are also required for the deposition of organic coatings. In addition to the techniques cited above there are also many others, because the number of industrial processes based on chemical vapor deposition is very elevated. For that reason CVD actually constitutes a vast branch of the chemical engineering.

1.3.2 Poly crystalline silicon

Chemical vapor deposition is the main method adopted for the large scale production of poly crystalline silicon. That material is so extensively present in our lives that it is hard to recognize its importance. Since more than 50 years, both the integrated circuit and the photovoltaic technologies still rely on its massive production at a very high quality and low price. All these applications have as central product the hyper-pure

polycrystalline silicon to be used in the casting processes for the photovoltaic industry or in the Czochralski pulling for microelectronics. Because of the dramatic rise of its demand in the photovoltaic field, the today production capacity of poly-silicon reached the 350 kton/year from the 26 kton/year of the beginning years of this century. In this actual commercial scenario the paramount parameters are the product purity and cost. Definitively, one of the most consistent part of the overall process costs is inherent in the gaseous reagents reduction to solid silicon. This process relies on the use of silane or trichlorosilane as precursor gases to deposit Si from the gas phase and it is performed either in the traditional Siemens reactors or in the emerging fluidized bed reactors [8-11], represented respectively in Figures 4a and 4b.

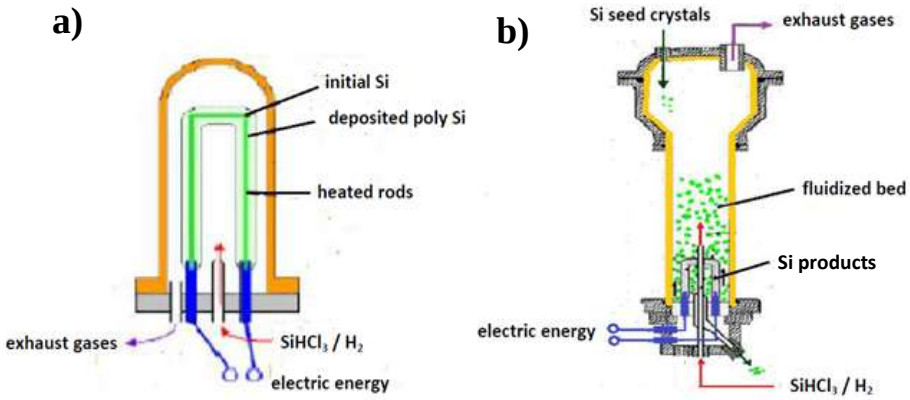

Figure 4: Reactor layouts for Si CVD a) Siemens; b) fluidized bed.

These two equipments present management issues of different nature, being the former a batch reactor and the latter continuous. Moreover, these reactors operate in conditions significantly different from those usually addressed in silicon chemical vapor deposition microelectronic processes, being the latter run either at reduced pressure or in diluted conditions, as summarized by the data reported in Table 1. In fact, these very large scale reactors work at high pressures (approaching 10 atm) and with a feed constituted of almost pure precursors.

In particular purified trichlorosilane is the most used reactant to growth silicon for photovoltaic applications, because of the low price related to such raw material. The conversion takes place following the heterogeneous reaction T4. However the process face limited single pass silicon yield and huge energy dissipation, very critical when the heating is performed by electricity. Moreover the HCl released during the deposition consume the main part of the precursor in the gas through T5, and $SiCl_4$ is abundantly formed as side product. Such component doesn't contribute to the film production because of its low tendency to react on the solid surface. Summing up, the global reaction active during the substrate growing is T6. Therefore it is necessary to reconvert $SiCl_4$ to $SiHCl_3$ in a side reactor at high temperature and H_2 partial pressure.

T4) $$SiHCl_3 + H_2 \rightarrow Si\downarrow + 3HCl$$

T5) $$3SiHCl_3 + 3HCl \rightarrow 3SiCl_4 + 3H_2$$

T6) $$4SiHCl_3 \rightarrow Si\downarrow + 3SiCl_4 + 2H_2$$

Table 1: Summary of the process conditions adopted to deposit poly silicon.

	film epiSi	**film polySi**	**mass polySi**
Precursor	$SiHCl_3$	SiH_4	$SiHCl_3$
Inlet mole fraction	0.05	1.00	0.5 <
Pressure	1 atm	1 torr	10 atm
Temperature	1200°C	800°C	1000°C
Growth Rate (micron/min)	1.0-5.0	0.4-0.5	3.0-20.0

Despite the great industrial relevance of this process, the kinetic mechanism active during the deposition has not yet been clarified. Thus a better understanding of reactivity of those systems can potentially lead to the improvement of the global performances. The subsequent reduction of

the operative costs would have a conspicuous impact from the economic point of view.

1.3.3 Silicon carbide

Besides polycrystalline silicon, in the last decades the semiconductor industry has been searching continuously for novel materials to be used for high-tech innovative devices. Among them silicon carbide (SiC) presents unique characteristics such as large band gap, high thermal conductivity, high breakdown field, and good corrosion resistance. These properties allow the realization of more reliable and smaller devices, able to work at higher voltages and current densities than possible with other semiconductors that make it an extremely suitable material for high power and high temperature applications [12, 13].

The large scale production of silicon carbide powder begins in 1893 for use as an abrasive. The grains of silicon carbide can be coagulated together to form very hard ceramic materials that are widely used in applications requiring high endurance, like for example car clutches, car brakes, and ceramic plates in bulletproof vests. Electronic applications of silicon carbide as light-emitting diodes (LED) and detectors were first demonstrated in 1907, and actually SiC is widely utilized in high temperature, high voltage semiconductor electronics.

Though the growth of SiC has been the object of active research for many years, its use on the industrial scale is still limited by various difficulties, some of them related to the production of high quality single crystalline ingots from which the substrates are then cut by. Although the possibility of producing large diameter wafers has been proved, there are still problems in producing ingots diameters larger than 3 inches, while the current standard for massive technological development is considered the 6 inches diameter substrate. Moreover the quality of the substrate today available on the market does not meet the high standard of thickness

uniformity and the absence of defects (mainly represented by micropipes) requested by the microelectronics and semiconductor industry [13, 14].

Chemical vapor deposition is almost the only one route to industrially perform epitaxial SiC growth, because of the very high temperature involved in the process and the level of control and purity that is required. The traditional recipe is based on the use of silane and light hydrocarbons, as Si and C precursor. The typical operating temperature is around 1500-1600°C with precursors highly diluted in H_2. Normal growth rate is around 5 μm/h, which render long deposition times to produce the structures of interest. The explanation is that this process evidences many practical problems related to the generation of Si particulate. Their formation results in saturation of the deposition rate, because if the gas flow is not able to flush them out of the growth zone, they drops on the substrate, affecting the film quality. In the attempt to overcome this inconvenient, high temperature and low pressure processes have been developed, keeping elevated feed rates to favor their outflow from the deposition area. Another high throughput production processes imply the use of chlorinated precursors and it is recently emerged as the most promising route in SiC technology [15, 16]. That process occurs through the reactions T7 and T8, which result to the global T9, using for instance $SiHCl_3$ and C_2H_4 as growth precursors. They are in fact quite similar to those for poly Si deposition from $SiHCl_3$.

T7) $$2SiHCl_3 + C_2H_4 \rightarrow 2SiC\downarrow + 6HCl$$

T8) $$6SiHCl_3 + 6HCl \rightarrow 6SiCl_4 + 6H_2$$

T9) $$8SiHCl_3 + C_2H_4 \rightarrow 2SiC\downarrow + 6SiCl_4 + 6H_2$$

High quality models of the deposition process can be extremely useful in order to optimize the SiC deposition process. From this point of view, there are valid similar considerations with respect to those valid for poly Si CVD.

1.3.4 Gallium nitride

Also in the last part of this phd thesis the issue was an industrial process based on chemical vapor deposition, specifically the gallium nitride MOVPE. Nowadays GaN is probably the most important semiconductor material since silicon. Its related large band gap (3.4 eV), that makes it particularly suitable for high power and high frequencies optic devices in the visible short wavelength and UV region. Indeed it has been widely used in bright light emitting diodes (LEDs) and laser diodes since the 1990s. Moreover GaN is also employed in the electronic and photovoltaic fields. Then the mixture of GaN with other elements as In (InGaN) or Al (AlGaN) allows the manufacture of devices emitting in a wider wavelength spectrum, with a band gap dependent on the composition of the material. Anyway the multibillion dollars market of GaN is in continuous expansion, as the number of its applications is increasing more and more with the recent improvements in the research [17-20]. For example GaN high electron mobility transistors have been offered commercially since 2006, and have found immediate utilization. In particular what is mainly pushing to the creation of this new sector of GaN based devices is the success in achieving reliable p-type doping [20].

However achievement of its full potential has been still refrained by a dramatic lack of GaN bulk single crystals. GaN has high melting temperature and very high decomposition pressure, hence it is not possible to use conventional techniques utilized for Si, Ge, or GaAs growth as Czochralski or Brindgman growth. Consequently the production of GaN based tools still relies on heteroepitaxy, as HVPE or MOVPE. The most common substrates are the cheap sapphire and SiC, though their thermal expansion coefficients and lattice parameters are not well matched to GaN. Therefore the growth of GaN on any substrate first requires the deposition of a buffer layer, with the purpose to partially compensate the mismatch. Anyway the epitaxial growth generates huge densities of defects, which limit the performances and operating lifetimes

of the devices based on this material. The research of efficient methods to reduce those defects is still an open field and currently great efforts are dedicated to that technological task.

The preferred industrial process to deposit GaN is the metal organic vapor phase epitaxy (MOVPE). Currently all optoelectronic commercial device structures are fabricated using MOVPE. The actual industrial systems operate at substrate temperatures between 900 and 1100 °C and pressures up to 1 atm. The growth rates are adjusted in base of the required film quality. For instance it is necessary to limit the deposition rate to 1-2 μm/h for the production of thin epi-layers, whereas it can be optimized to higher values in case of bulk growth, up to about 50 μm/h. The gallium precursor can be either trimethyl or triethylgalium, while the most appropriate nitrogen source is ammonia, supplied in large excess with respect to the gallium alkyl. Hence GaN is deposited following the global reaction T10 if $Ga(CH_3)_3$ is utilized. The precursors are diluted in H_2, and sometimes also N_2 is co fed as inert gas.

T10) $$Ga(CH_3)_3 + NH_3 \rightarrow GaN\downarrow + 3CH_4$$

A schematization of the reactor chamber is reported in Figure 5. Aiming to obtain a GaN layer as much homogeneous as possible, the substrate is located atop a rotating disc. One of the most problematic aspects of GaN MOVPE is the parasite formation of solid particles in the gas phase. Such powders contribute to the scavenging of part of the reagents, affecting the deposition yield [19, 21-28]. Furthermore if they drop on the substrate, the quality of the GaN film may be compromised for the generation of local defects and areas of preferential growth. Thus in order to limit this highly undesired phenomenon, the reaction chamber is specially designed to avoid the premature mixing between NH_3 (group V) and the gallium alkyl (group III).

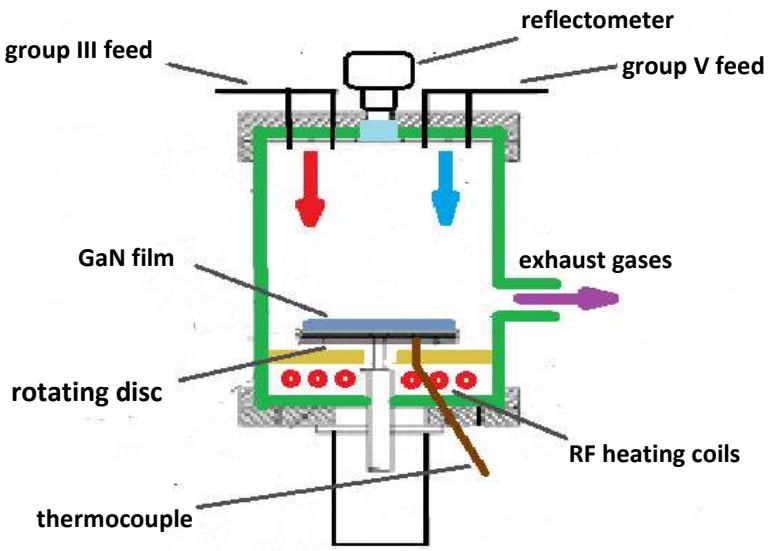

Figure 5: Schematization of a reaction chamber for GaN MOVPE.

Like in the case of silicon and SiC CVD, the deposition mechanism of GaN has not yet been clarified. Besides also the reactivity that leads to particle formation is still unknown. Consequently the selection of the operative conditions of the process, as well as the reactor design, is actually based on the trial-and-error approach. Studies focused on the reaction kinetics are thus an essential requisite to formulate models that can potentially be used as a helpful tool to achieve better performances.

CHAPTER 2

Theoretical background and methods

In modeling chemical processes, engineers very often have to face the critical task to determine key parameters not available in the literature or not easily estimable using correlations of the classical chemical engineering. Those parameters can be of different types and can affect for example chemical reactivity, thermodynamics, or transport phenomena.

A typical approach is to choose such constants in the most suitable way to fit the experimental data. However a pure fitting is usually unreliable to make predictions in operative conditions far from the experimental range explored, especially if the number of constants determined on this way is elevated. Thus, though fittings are still wide used to describe industrial reactors and sometimes they are even necessary, the modern research and development is oriented to reduce the number of unknown parameters through the improvements of appropriate theoretical methods. In spite of the reduction of the number of the fitting constants may make more difficult to achieve calculated profiles close to the experimental data, the potential advantages may be extremely satisfactory. Especially with a model obtained with a limited contribution of fitting, it is more probable that the hypothesis stated is correct, hence such model can be successfully applied for the scale up from laboratory to industrial apparatuses. Moreover also variables which are not possible to measure experimentally can be predicted, providing a more complete picture of the phenomena

occurring during the process at different scales. The immediate consequence of a better understanding should be to exploit it to project new operative reactors able to achieve better global performances.

In this section are summarized the main theoretical methods used in modeling the processes described in Chapter 1 and it is described the main approach followed in this thesis. Such techniques are actually becoming more and more critical in the modern studies of the reaction kinetics. It is also provided a brief explanation of the theoretical fundamentals, which constitute the basis of those methods.

2.1 Fundamentals of quantum chemistry

When dealing with systems whose reaction kinetics is unknown, the first step in order to create models able to describe their behavior, is to provide reliable estimations of the kinetic parameters of the chemical reactions involved in the process. Therefore the ability to determine accurately the rate coefficients of elementary key reactions has a drastic importance. A very powerful tool that has assisted researchers for decades in such critical task is transition state theory. That theoretical method is based on quantum mechanics and it can be applied following several approaches, with different related levels of precision and computational efforts. The improvements in such *ab initio* techniques both in the methodology and in computer technology, has been dramatic over the last years. Consequently their contribution is becoming more and more effective in the assembling of complex kinetic schemes.

2.1.1 The Shrödinger equation

Quantum mechanical methods give a mathematical representation of the physical properties of particles, through the direct solution of the Shrödinger equation, reported as Equation 1 in its time independent form.

It was proposed for the first time in 1925 by the Austrian physicist Erwin Shrödinger. The results of this equation are the energy of a particle or molecule (*E*) and its related wavefunction (Ψ), which characterizes its quantum state and behavior. The Hamiltonian operator (*H*) can be written as a function of kinetic energy (*T*) and potential energy (*U*), due to electrostatic interactions, as shown in Equation 2. For a multi atom system those terms account the contributions of every nucleus (*n*) and electron (*e*) present in the molecule. Besides the solution of the Shrödinger equation in general depends on all their related spins (*s*) and position coordinates (*Y*).

$$H\,\Psi(\bar{s},\bar{Y}) = E\,\Psi(\bar{s},\bar{Y}) \qquad (1)$$

$$H = [(T_n + V_{n-n}) + (T_e + U_{e-e} + U_{n-e})] \qquad (2)$$

However the two effects of nuclei and electrons can be separated by the introduction of the Born-Oppeneimer approximation. That assumption relies on the fact that electrons velocities are very much higher with respect to those of nuclei, hence the first ones are [29] able to reach an equilibrium position faster than the latter. As the coupling between the velocities of nuclei and electrons is neglected, the Shrödinger equation can be solved as the product of two wavefunction contributions. They refer respectively to the nuclei (Ψ_n) and to the electrons (Ψ_e), with the former depending only on the nuclear positions, as reported in the Equation 3.

$$\Psi(\bar{s},\,\bar{Y}) = \Psi_n(\bar{Y}_n)\,\Psi_e(\,\bar{s},\,\bar{Y}) \qquad (3)$$

Introducing that functional form in Equation 1, the Shrödinger equation can be written for the electrons only, whereas the nuclei are treated apart as classical particles that affect the electrostatic field where the electrons move. The total energy can thus be calculated as the sum of the electronic energy (E_e) and that related to the nuclei, according to Equation 4.

$$E = \frac{(T_n + U_{n-n})\Psi_n(\bar{Y}_n)}{\Psi_n(\bar{Y}_n)} + E_e \qquad (4)$$

The result of the Shrödinger equation is related to a particular configuration of the atoms coordinates (single point energy). Anyway it is not guaranteed that such configuration correspond to the real one, which is most stable as possible. The electronic energy can be mapped out as a function of the nuclear positions for a number of different nuclear configurations. From the mathematic point of view such function is a multi dimensional surface, called 'potential energy surface' (PES). Therefore it is necessary to find the molecular geometry that minimizes the total energy, which correspond to the absolute minimum of the PES. Coherently with the basic mathematical properties valid for any kind of function, if the optimized configuration corresponds to a local minimum the energy gradient should be null and all the eigenvalues (λ_i) of the Hessian matrix should be positive. Then once achieved the most stable configuration of the atoms in a molecule, from the features of the PES in the proximity that minimum and from the structural geometry there can be calculated the physical properties related to such particle.

Summing up, it is possible to evaluate the electronic energy of a specific molecule and its most stable geometrical configuration by solving the Shrödinger equation for different nuclear coordinates. The optimal geometry is found with the minimization of the PES. Finally the properties of interests can be estimated using the information obtained. Nowadays these and other features are commonly implemented in several commercial software packages as Gaussian [29], Molpro [30] and Gamess [31]. However the analytical solution of the Shrödinger equation is available only for the very simple case of the hydrogen atom. Hence it is necessary to numerically approximate the wavefunction (Ψ), with the selection of an appropriate *ab initio* computational model with respect to the corresponding level of approximation. Those models can also make indirect reference to experimental data.

2.1.2 Quantum mechanical approaches

The first essential expedient adopted in all the computational techniques to obtain a numerical solution of the Shrödinger equation is the introduction of a basis set [32]. A basis set consists in the expansion of the molecular orbital wavefunctions (ϕ_k) in a finite number (N_b) of known basis functions (χ_i), as reported in Equation 5.

$$\Phi_k(\bar{s}, \bar{Y}) = \sum_{i=1}^{N_b} c_{ik}\ \chi_i(\bar{s}, \bar{Y}) \qquad (5)$$

However not all the orbitals are occupied by electrons, but only those at lower energies. In principle the highest is the number the basis functions (χ_i), the most the approximated wavefunction (ϕ_k) could approach the real one (Ψ_k). Anyway a greater computational effort should be paid because it is necessary to solve an increased number of degrees of freedom (c_{ik}). Another important issue is the appropriate selection of the shape of the basis functions to be included in the Equation 5, that is the functional dependence upon the radial coordinate. In particular two kinds of basis functions exist: the Slater type orbitals (STO) and the Gaussian type orbitals (GTO). The smallest number of functions possible is referred to as the minimum basis set. The most common minimal basis set is STO-nG [ref], where n is an integer. This n value represents the number of Gaussian primitive functions comprising a single basis function. In these basis sets, the same number of Gaussian primitives comprises core and valence orbitals. Minimal basis sets typically give rough results that are insufficient for research quality publications. Then improved double-zeta (DZ) and triple zeta (TZ) basis functions have been proposed, which contain respectively twice and three times as many functions as in the minimum basis set, and so on. A further category relies on contracted basis functions, which are linear combinations of full sets of primitive basis functions into smaller ones. The aim is to describe also the less energetic, but relevant from the chemical point of view, electrons far from the nuclei. One very popular example is the Pople basis sets. Besides, also non localized basis sets can be used. This is the case of plane-waves, very

diffused in calculations involving periodic boundary conditions, like in solid crystals.

The Shrödinger equation can be solved with different modeling approaches by the introduction of functional forms of the wavefunctions and adopting one the basis sets described above. Electronic structure methods consider the dynamics of multi electrons systems by treating the electrons as independent particles. This implies that the electron-electron interaction is approximated as an average effect. The first technique developed is the Hartree Fock (HF) [32]. The Hamiltonian operator is separated in N_e terms called Fock operators, with N_e is the number of the electrons. It is adopted a simple functional, which satisfy the anti symmetric condition. The global wavefunction (ϕ) is simply assumed as a product of orbitals, that are rearranged in the Slater determinant, shown in Equation 6.

$$\Phi(\bar{s},\bar{Y}) = \frac{1}{\sqrt{N_e!}}\begin{vmatrix} \Phi_1(s_1\bar{Y}_1) & \Phi_2(s_1\bar{Y}_1) & \dots & \Phi_{N_e}(s_1\bar{Y}_1) \\ \Phi_1(s_2\bar{Y}_2) & \Phi_2(s_2\bar{Y}_2) & \dots & \Phi_{N_e}(s_2\bar{Y}_2) \\ \vdots & \vdots & \ddots & \vdots \\ \Phi_1(s_{N_e}\bar{Y}_{N_e}) & \Phi_2(s_{N_e}\bar{Y}_{N_e}) & \dots & \Phi_{N_e}(s_{N_e}\bar{Y}_{N_e}) \end{vmatrix} \quad (6)$$

As just pointed out, in the HF method the problem to take into account the electron-electron repulsion is solved by using a self consisted field, hence one electron feel the influence to the other ones in an averaged way. Such approximation doesn't take into account the instantaneous electrostatic interactions, as well as the quantum mechanical effects on electron distributions and the correlate feature of relative motions between the electrons. Adopting a large basis set it is possible to achieve 99% of the solution. However the remaining 1% is still very significant to the description of chemical bonds.

The difference between the HF energy and the lowest possible one in an assigned basis set is the electron correlation energy. Several methods try to evaluate the correlation energy in different ways, starting from the solution of the HF and then improving it to the approximation to the exact

solution. Therfore those techniques are generally called as post Hartree Fock. There are three main post Hartree Fock methods: configuration interaction (CI) [33], many-body perturbation theory (MBPT) [34] and coupled cluster (CC) [35]. In the HF computations, only the lowest energy molecular Slater orbital is occupied. In post HF methods instead is accounted the possibility of the electrons to partially occupy also the higher energetic orbitals. The precision of these approaches in the estimation of the molecular energies is very elevated, with accuracies around 1-2 kcal/mol, thus comparable with the experimental uncertainties. On the other hand unfortunately, they are extremely demanding from the computational point of view. Therefore their application to large systems with many atoms can be not affordable at the actual state of computer technology.

An alternative very popular quantum chemistry approach relies in the density functional theory (DFT), developed by Hohenberg and Kohn [36]. This type of methods has the remarkable advantage to be quite computationally cheap. DFT is based on the assumption that the ground state electronic energy and all the other ground state properties are uniquely determined by the electron probability density (ρ). The total energy (E) is calculated trough Equation 7, with the electron density (ρ) depending on the wavefunctions (ϕ_i) by the Equation 8. The electron density (ρ) is thus approximated as a set of one electron molecular orbitals, each for one of the N_e electrons considered. The kinetic (T), potential (U) and exchange correlation (E_{xc}) energies are functionals of ρ and their related wavefunctions are called Kohn-Sham orbitals [37].

$$E[\rho] = T[\rho] + U_{n-e}[\rho] + U_{e-e}[\rho] + E_{XC}[\rho] \qquad (7)$$

$$\rho = \sum_{i=1}^{N_e} |\Phi_i|^2 \qquad (8)$$

The various DFT methods differ in the way the exchange correlation energy (E_{xc}) is calculated, or in the choice of the functional form related to this term. Indeed, though exact functionals for the E_{xc} are unknown, the

use of some approximations allows a relatively accurate evaluation of several physical properties. For instance, in case of hybrid functionals a portion of the exact solution from HF theory is incorporated. One of the hybrid functionals most utilized in the literature consists in the Becke-Lee-Yang-Parr (B3LYP) [38, 39]. B3LYP is based on the generalized gradient-corrected approximation (GGA), in which E_{xc} depends not only by the local value of the electron density (ρ), but also by its gradient. However though the structures optimization and the evaluation of vibrational frequencies are generally quite reliable, the electronic energies are affected by conspicuous uncertainties. For instance in some cases, the error of the ΔE associated to a given chemical reaction can be even of 10-15 kcal/mol. To partially overcome this critical inconvenient, new generation functionals have been developed ad hoc to better describe some particular classes of chemical interactions, keeping into account corrections inferred from some experimental databases. One example consists on the Minnesota hybrid functionals [40], like the M06-2X. Hence the selection of an appropriate DFT functional is a crucial step to determine the properties of a given chemical component, with results that can be more or less satisfactory.

Finally it is also possible to extrapolate the calculations to systematically larger basis sets. This is the case of quantum chemistry composite methods [41], which aim to reach high precisions by taking into account the results of several calculations. Their basic principle is to combine methods with a high level of theory but small basis sets with methods that employ lower levels of theory but larger basis sets. Two examples are the semi empirical complete basis set approaches (CBS) [42] and the restricted open shell complete basis set (ROCBS) [43]. The difference between then is that the latter use spin restricted wavefunctions, more suitable to describe also particles affected by spin contamination. Such approaches are able to provide energy estimations with accuracies comparable with those calculated with post Hartree Fock techniques, but

the computational time can be considerably lower, though still quite onerous.

2.1.3 Estimation of thermodynamic parameters

As mentioned in Section 2.1.1, the aim of ab initio calculations is to provide a theoretical estimation of some physical properties in a given system. Once achieved the most stable configuration of the atoms of a molecule, consistently with the statistical thermodynamics, all its properties can be obtained knowing its molecular partition function (Q). Its estimation requires determining all the possible energetic levels of the molecule, or in other words how that molecule is able to store the energy. The energy is distributes in four different forms. The first three depends on the movements of the atoms and they are respectively the kinetic energy due to the rigid translation of the molecule, the inertial rotational energy due to the rotation of the structure and the internal elastic energy related to the vibrations of the nuclei. The characteristic vibrational frequencies (ν_i) of a given molecular structure can be calculated from the eigenvalues (λ_i) of the Hessian matrix of the PES, following the simple relation reported in the Equation 9.

$$\nu_i = \sqrt{\frac{\lambda_i}{4\pi^2}} \qquad (9)$$

The last contribution is then due to the electronic energy, related to the interactions between electrons and nuclei and that is responsible of the chemical bonds. The global partition function can be thus written as the product of the single partition functions associated to the four types of contributions, according to the Equation 10.

$$Q = Q_{tran} Q_{rot} Q_{vib} Q_{el} \qquad (10)$$

As already mentioned the state of that system is characterized by the partition functions (Q) of the particles present in the volume (V) of

interest, which depends on the energetic levels accessible for all the molecules. Consistently with the Equation 10, the molecular partition function can be split in four terms, due to the various ways in which the energy can be stored. The solution of the time independent Shrödinger equation makes possible the quantification of those contributions. The first one is related to the translational kinetic energy and in case of a particle with mass *m* at a certain temperature *T*, can be calculated with the Equation 11. Where k_b and *h* that are respectively the Boltzman and the Planck constants. The rotational partition function is instead expressed for a poly atomic molecule with N_a atoms by the Equation 12. It depends on the moments of inertia *I* of that molecule around its principal axes *x, y, z* and by its rotational symmetry number σ_R. To obtain the information necessary to estimate these first two contributions it is thus required the optimization of the atomic structure at the energetic minimum. Then as explained above, the vibrational partition function, reported in Equation 13, is accessible if is known the Hessian of the PES around that minimum. Indeed as evidenced in Equation 4, the $3N_a$*-6* normal vibrational frequencies ν_i are related to its eigenvalues. Finally the electronic partition function is directly related to the electronic energy E_{el} of the molecule at its fundamental state. It is reported in the Equation 14, and it is also function of the degeneracy number g_{el}, that is the number of unpaired electrons plus 1.

$$Q_{tran} = \frac{(2\pi\, m\, k_b T)^{3/2}}{h^3} V \qquad (11)$$

$$Q_{rot} = \frac{8\pi^2 (2\pi k_b T)^{3/2} \sqrt{I_x I_y I_z}}{\sigma_R h^3} \qquad (12)$$

$$Q_{vib} = \prod_{i=1}^{3N_a-6} \frac{exp\left(-\frac{h\nu_i}{2k_b T}\right)}{1 - exp\left(-\frac{h\nu_i}{k_b T}\right)} \qquad (13)$$

$$Q_{el} = g_{el} exp\left(-\frac{E_{el}}{k_b T}\right) \qquad (14)$$

Once obtained the total partition (Q) is then possible to calculate the main molecular thermodynamic properties as entropy (S_0), enthalpy (H_0) (considering a referring enthalpy H_{ref}) and heat capacity at constant pressure (C_p), as shown in the following expressions.

$$S_0 = k_B ln(Q) + k_B T \frac{\partial ln(Q)}{\partial T} \qquad (15)$$

$$H_0 = E_{el} + k_B T^2 \frac{\partial ln(Q)}{\partial T} + k_B T - H_{ref} \qquad (16)$$

$$C_P = 2k_B T \frac{\partial ln(Q)}{\partial T} + k_B T^2 \frac{\partial ln(Q)}{\partial T^2} + k_B \qquad (17)$$

Also in case of chemical reactivity the relations above can be applied to evaluate the thermodynamic parameters associated to a given reaction involving a certain number of species N_{sp}, with stoichiometric coefficients θ_i. In particular the equilibrium constant k_{eq} can be re elaborated in the form of the Equation 18, with N_{Av} is the Avogadro number. Thus every thermodynamic parameter can be in principle evaluated once knowing the partition functions of all the species involved. Such information can be provided from *ab initio* calculations.

$$k_{eq} = \prod_{i=1}^{N_{sp}} \left(\frac{Q_i}{N_{Av} V}\right)^{\theta_i} \qquad (18)$$

2.1.4 The 1D hindered rotor model

As it can be inferred from the previous section, having an accurate value of the partition function (Q) of a given particle is a critical requisite for the theoretical calculation of its physical properties. For that reason wide studies have been dedicated to the development of methodology aimed to provide more reliable evaluation of the terms which constitutes the partition function (Q). Besides the wide branch of approaches dedicated to the electronic energy (E_{el}), briefly summarized in Section 2.1.2, also

the vibrational partition function (Q_{vib}) requires particular attention. Indeed Equation 13 relies on the approximation that all the vibrational motions can be treated as harmonic oscillators. Generally that assumption is reasonable, especially when dealing with internal motions having high associated frequencies. However at lower frequencies atoms are less strongly linked to their equilibrium positions. Therefore the oscillations are wider and the hypothesis of harmonic vibrations becomes less adequate. This happens especially in large molecules for bendings or torsions around the axis of some bonds. In particular the latter is quite frequent. In Figure 6 is shown an example found in the present work, which is the torsion with related low vibrational frequency around the Si-Si bond in Si_2HCl_5.

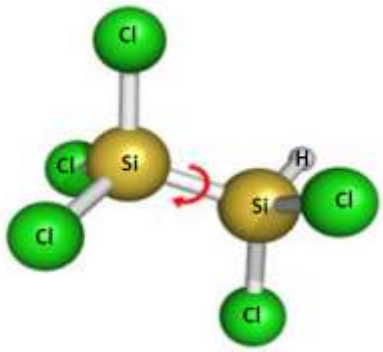

Figure 6: Low frequency torsional vibration around Si-Si bond in Si_2HCl_5.

Those motions should be treated as internal rotations rather than harmonic rotors. Thus the 1D hindered rotor (HR) approximation [44] provides a more reliable description of poly atomic systems by replacing the partition functions associated to the lowest torsional vibrational frequencies with specific contributions calculated using this theory (Q_{IR}). Such rotations are subject to hindrance due to a torsion energy barrier. In Figure 7 is plotted the rotational PES in the case of Si-Si torsion in Si_2HCl_5.

The hindrance potential shown in Figure 7 is necessary for the estimation of the Q_{IR}. Furthermore the other parameters required are the internal symmetry number (σ_R) and the reduced internal momentum of inertia (I_r)

that can be approximated as in the Equation 19. It is hence a function of the two inertia moments (I_{top} and I_{bottom}) computed about the axis containing the twisting bond and with respect to the moieties at both the extremities of such bond [45].

$$I_r = \frac{I_{top} I_{bottom}}{I_{top} + I_{bottom}} \qquad (19)$$

A common method adopted for the treatment of 1D hindered rotors is based on the assumption that it is possible to account separately the contribution of each degree of freedom. Consequently each rotor is treated with one effective 1D Hamiltonian. The energy levels are computed solving the 1D rotational Shrödinger equation, whose only spatial coordinate explicit dependence is that by the rotational dihedral angle. From this information is finally possible to calculate the partition function of the rotor (Q_{IR}). The 1D HR assumption can be also applied in the estimation of reaction kinetic constants, in order to improve the accuracy of the pre exponential factors.

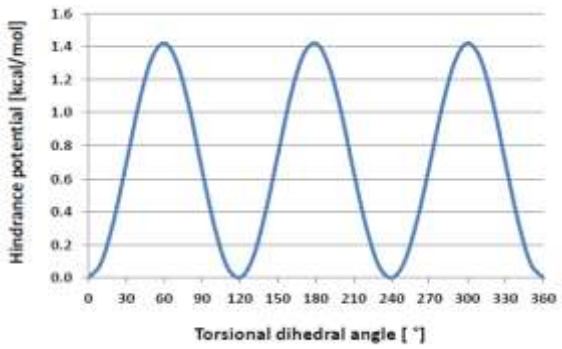

Figure 7: Torsional PES around Si-Si bond for Si_2HCl_5.

2.1.5 Transition state theory

Computational quantum mechanics can be used as a very useful tool for the *ab initio* calculation of kinetic constants of elementary chemical reactions. A common methodology relies on the transition state theory (TST) [46] first proposed in 1935 by Eyring and Evans and Polanyi. The

main assumption is that there exists a transition state or "activated complex" that separates the reactants from the products. In other words the reactants need to rearrange their structures to be converted into products and the transition state constitutes the rate determining step of that phenomenon. The molecular configuration change following the minimum energy path of the PES that links the reactants region to the products region. The position along that path can be mapped by defining a reaction coordinate (λ) which follows that most favored conversion way. The potential energy of the system varies along the reaction coordinate, for example as reported in Figure 8a. If it is present an evident maximum in that energy curve, the *tight* transition state [47] correspond to that maximum. The positions of the N_a atoms in the transition state are optimized by minimizing all the other $3N_a$-7 spatial degree of freedoms, orthogonal to the reaction coordinate. Hence that structure is a saddle point in the PES and one eigenvalue of the Hessian matrix is negative, with a related imaginary vibrational frequency along λ.

After making several assumptions, including the postulation of a quasi-equilibrium between the transition state and the reagents, from the TST it is possible to calculate the reactive flux that passes through a dividing surface in the configuration multi space. As direct consequence, the kinetic rate constant (k) of a given reaction can be expressed by the Equation 20, depending by the partition functions of the reactants (Q^R) and that of the transition state ($Q^{\neq}$). The activation energy E_{act} is equal to the energy barrier between the reactants and the transition state, including also the zero point correction.

$$k(T) = \frac{k_B T}{h} \frac{Q^{\neq}}{Q^R} exp\left(-\frac{E_{act}}{k_B T}\right) \qquad (20)$$

The canonical TST can be applied also to reactions without an evident energetic maximum along the reaction coordinate [47], as shown in Figure 8b. A typical example is given by the homolytic dissociations to

radicals. Anyway, on this case is not possible to univocally define the molecular structure of such *loose* transition state and it is necessary to apply the variational principle to calculate the related kinetic constant. Basically the transition state corresponds to the atomic configuration along the reaction coordinate which minimize the flux of reactive molecules that are converted from reactants to products. Therefore the *ab initio* procedure for the estimation of the kinetic parameters for *loose* transition states is more elaborated respect to that for the *tight* ones. Indeed it consists in evaluating several structures along the reaction coordinate and to select that with the lowest related kinetic constant. Typically the position of the *loose* transition states change with the temperature because structures more close to the products (referring to Figure 8b) are not favored from the energetic point of view, but more stable from the entropic ones. Hence at higher temperatures the atomic configuration with the related minimum kinetic constant shifts slightly towards the reagents.

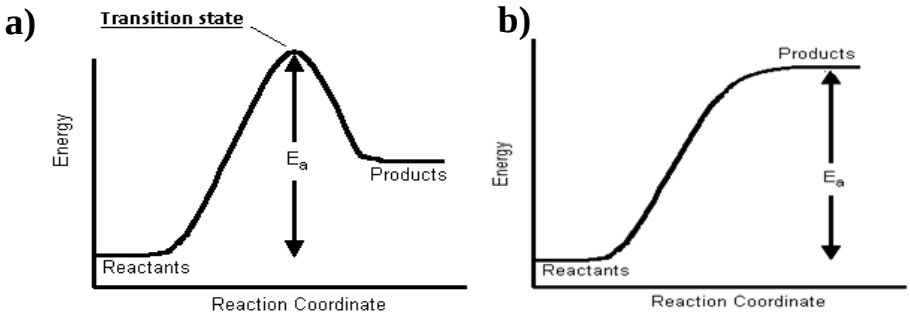

Figure 8: Potential energy along the reaction coordinate for a reaction with a) tight transition state; b) loose transition state.

2.2 Kinetic gas theory

The procedure to calculate kinetic constants by applying the transition state theory can be quite time consuming, especially for large molecules. In alternative as a first very rough approximation, some types of reactions can be determined with the more simple kinetic gas theory [48]. It was developed around 1860 by Clausius and Maxwell and is based on

classical physics. The theory is able to describe the particle motions for an ideal gas. The molecules are in a constant random movement in the gas volume with a velocity distribution function that depends by their kinetic energy. These rapidly moving particles constantly collide with each other and with the walls of the container. Kinetic theory explains macroscopic properties of gases, such as pressure, temperature, viscosity and thermal conductivity, by considering their molecular composition and motion.

Anyway focusing on reaction kinetics, from such theory it can be obtained the average number (*Z*) of intermolecular collisions occurring per unit volume and unit time. Indeed the bimolecular reactive processes are determined by effective inelastic collisions between particles in the gas. If the consequence of every collision is a chemical reaction, the bimolecular reaction rate will be equal to *Z*. Thus the reaction constants estimated on this way constitutes the superior limit of the real ones. Considering for instance a reaction between two molecules A and B, which can be approximated as spheres with respective diameters d_A and d_B and mass m_A and m_B, the related collisional kinetic constant k_{coll} can be expressed by the Equation 21, with μ_{AB} is the reduced mass reported in Equation 22.

$$k_{coll} = \pi \left(\frac{d_A + d_B}{2}\right)^2 \left(\frac{8\, k_B T}{\pi \mu}\right)^{0.5} \qquad (21)$$

$$\mu_{AB} = \frac{m_A m_B}{m_A + m_B} \qquad (22)$$

Such approximation can be quite reasonable only for a few classes of reactions, like radical combinations. However most of chemical transformations need to overcome an energy barrier, hence this idealization is completely inadequate. Furthermore the kinetic gas theory finds also application to evaluate kinetic constants k_{coll} of collisional processes between gasses and surfaces, as in the Equation 23, for a chemical specie A. This is the case for example of not activated adsorptions.

$$k_{coll} = \left(\frac{k_B T}{2\pi\, m_A}\right)^{0.5} \qquad (23)$$

2.3 Approach used for the estimation of kinetic constants

In order to study systems with complex reaction kinetics, having an accurate estimation of the kinetic constants is a key requisite. In Section 2.1 and Section 2.2 it is given a brief description of the methods available to accomplish that task. Here instead it is explained how those theoretical tools were applied during this thesis for the estimation of the reaction parameters. The approach described has been followed for the *ab initio* calculations of the kinetic constants in all the processes object of this work, except in the non oxidative plasmas for natural gas conversion. Indeed wide reliable data are present in the literature for systems similar to the latter.

In fact there are several papers about the theoretical estimation of kinetic constants of gaseous elementary reactions for the chemical vapor depositions of interests [16, 26, 49-69]. These works mostly relies on DFT methods which, as explained in Section 2.1.2, though they imply a limited computational effort, on the other hand, the related uncertainties could be conspicuous, especially in the estimation of the activation energies (even 10-15 kcal/mol). The precision of the computational techniques herein used instead is higher [47]. The *ab initio* calculations were implemented using Gaussian 09 computational suite [29]. With such method there were also determined the thermodynamic parameters of the chemical species involved in the mechanism.

The approach followed in this work is based on the transition state theory for the evaluation of the kinetic parameters of the elementary reactions involved in the kinetic schemes. It combines the advantages of fast DFT with those of more rigorous techniques. Indeed it has been demonstrated [70-72] that DFT allows predicting kinetic constants at a good level of

approximation if combined with a high level estimation of the energy. Thus the structures and the vibrational frequencies of all the stationary points were first determined at B3LYP/6-31+G(d,p) level [38, 39] in the case of silicon and SiC CVD, and at M062X/6-311+G(d,p) [40] for GaN MOVPE. Then the energies of all the optimized stationary points were re determined with more precise CCSD(T) calculations [73] extrapolated to the infinite basis set using the augmented cc-pVDZ and cc-pVTZ [74] basis sets, as proposed by Martin [75] for silicon and SiC CVD, whereas the ROCBS-qb3 [43] was utilized for GaN MOVPE. The uncertainties in the activation energies are around 2 kcal/mol. The kinetic constants so determined were then fitted to the modified Arrhenius form over a temperature range comprised between 300 and 2500 K for Si and SiC CVD and between 500 and 1500 K for GaN MOVPE. The maximum error in the regression was less than 10%.

When relevant the low vibrational frequencies associated to torsional motions were replaced by 1D hindered rotors. The corresponding partition functions were in such cases determined using the quantum eigenvalues, calculated as described in previous works [76, 77]. On this way it was improved the prediction of the pre exponential factors. Besides, if two reaction channels with comparable rates were possible, global reaction rates were computed as the sum of the rates of the two channels. In case of elementary reactions that do not present an evident saddle point, their transition state was determined using canonical variational transitional state theory. The reaction path was scanned through constrained energy minimizations along the length of the breaking bond with the unrestricted DFT functional and, thus allowing the partial occupation of the LUMO orbital. The PES was then re-scaled over reaction energies evaluated at higher level of accuracy.

The drastically more simplified kinetic gas theory was instead applied to estimate reactions like not activated adsorptions of chemical species on a solid substrate with a unitary sticking coefficient. In addition also for

preliminary analysis aimed to select the reactions to be included in the kinetic scheme, some radical combinations were treated using such principle. Anyway if important, they were lately re evaluated with more accurate techniques, with the only exceptions of particles nucleation (see Section 5.3).

The selection of an appropriate theoretical method and basis set is a very important point to determine the success of the approach followed. Therefore a preliminary analysis was performed with some sample reactions and reactants in the kinetic scheme before to calculate all the other. The selection of the DFT approach used for the structure optimizations was made by testing several different functionals. The results were compared with those of the more accurate coupled cluster calculations. Then it was chosen the functional which gives estimations closer with those of the coupled cluster ones. In parallel progressively larger basis sets were used. The estimated parameters changed till reaching asymptotic values when the basis set was large enough. Hence it was selected a basis set that gave previsions close enough to the most accurate one, in order to limit the computational effort without a significant loss of accuracy.

Finally, it can be interesting to provide information also concerning the criterion for the selection of the method used for the re estimation of the energies. For Si CVD it was chosen CCSD(T) with a very large basis set simply because the intent was to achieve results as much accurate as possible. Then, the related computational time was not extremely long because it was not performed a geometry optimization. However since in the GaN MOVPE kinetic model are present heavier and more complex molecular structures with respect to those involved in the other mechanism, it was necessary to reduce the computational effort, especially for the energy re estimation. For that reason in substitution of the CCSD(T), it was utilized the faster ROCBS-qb3, which should guarantee a similar accuracy. Indeed making a comparison of the

activation energies of some samples reactions in both cases (aug-cc-PVTZ basis set for CCSD(T) one) the maximum difference was around 1 kcal/mol.

2.4 Method of moments developed

Another important aspect of this work was the description of particle formation in GaN MOVPE, whose global effect is explained in Section 1.3.4. For this purpose a FORTRAN program used to solve the material balances in 2D cartesian systems was substantially modified with the addition of equations based on the second order method of moments and their corresponding analytic Jacobian. Further details about the chemical and kinetics aspects related to this phenomenon are provided Chapter 5.

2.4.1 Approach used to solve the population balance

The particle formation is described by using the population balance approach [78], otherwise known as general dynamic equation. This type of method is common for example to predict the particles growth dynamics in aerosol, but also for polymer kinetics. The terms accounted in the population balance for the specific problem under examination are shematized in Figure 9. Particles could be approximated as spherical aggregates composed by n monomeric units with volume Δv each. Therefore in principle it should be necessary to solve infinite material balances for aggregates of every possible dimensions, or n ranging from the minumum number of units to infinite. Obviously this is not feasible, but it is necessary to express the population balance with a finite number of equations.

One approach to solve the population balance uses the discrete sectional model [78], has been lately applyed to this kind of problem. The discrete part solves the detailed interaction of the monomers and small droplets

size, up to a pre determined dimentios. The sectional part intead handles the upper size distribution by approximating it as a finite number of sections. However for discrete sectional model there are required high computational powers.

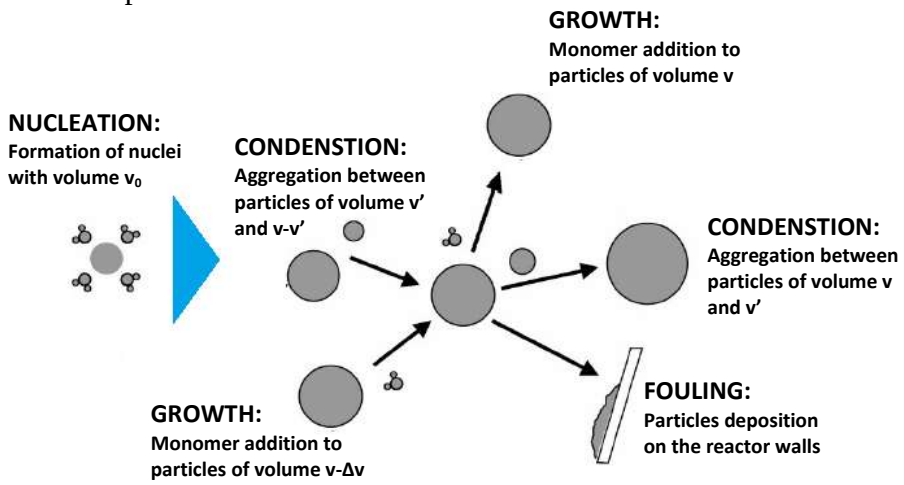

Figure 9: Representation of the terms included in the particles population balance.

Another very common approach is instead based on the method of moments [78]. As anticipated it was indeed this principle that it has been chosen to describe particles dynamics because it is able to provide a reasonable description of the phenomenon with a limited computational effort. Most of the correlations here assumed were taken for the work of Kim and Pratsinis [79] because their model is quite suitable to be implemented in the starting 2D program, providing estimations with an acceptable precision. Moreover this research group has already used it previously for aerosol dynamics [80]. Method of moments has been also applied for the specific case of GaN MOVPE in the commercial software developed by the STR group [81, 82], which relies on a conspicuous fitting on wide experimental data. As underlined in one of their articles [83], the clusters can be considered as a pseudo gas of heavy particles because above the substrate their average free path is several orders of magnitude greater than their average diameter. A consequence is that they can be assumed in free molecular regime. Such hypothesis has been

verified a posteriori and definitely confirmed for the operative condition explored.

The method of moments implemented treats the particles population balance by assuming a size distribution function *F(v)* of the particles volumes (*v*). Such distribution function is described through its moments of *kth* order (μ_k), defined as in the Equation 24. In theory it is required an infinite number of moments to fully reconstruct the shape of the distribution function. Anyway it is generally plausibly approximated with a unimodal log-normal function, reported in Equation 25 [79]. Thus the particles distribution size is expressed knowing 3 parameters that are respectively: their total concentration in the gas (μ_0), their geometric mean volume (v_G) and the standard deviation (σ_{log}).

$$\mu_k = \int_0^\infty v^k F(v) dv \tag{24}$$

$$F(v) = \frac{\mu_0}{3\sqrt{2\pi}\ ln\ \sigma_{log}} \frac{1}{v}\ exp\left[-\frac{ln^2(v/v_G)}{18\ ln^2\ \sigma_{log}}\right] \tag{25}$$

Consequently, the mathematical operator μ_k applied to the Equation 2 generates three different balance equations for the moments μ_o, μ_1 and μ_2. The first two have a specific physical meaning, which are in case of μ_o the total concentration of particles in the gas, whereas μ_1 is the total volume of particles per unit gas volume. For μ_2 instead the definition is not so straightforward, but anyway it is related to the size standard deviation. All the parameters related to the distribution function can be obtained from those 3 parameters, including v_G, σ_{log} and every other different μ_k [79].

In the assumed balances of the moments are accounted the main phenomena which affect the aggregates evolution, that are:

1. Convection: particles move with the gas flow;
2. Thermophoresis: net force acting on particles towards the decreasing temperature;
3. Diffusion: transport due to the concentration gradient;

4. Nucleation: nuclei formation for chemical reactions from gaseous reactants;
5. Coagulation: particles aggregation after collisions;
6. Growth: scavenging of gaseous monomer on particles surface;
7. Fouling: deposition on the reactor walls.

However in the model of Kim and Pratsinis [79] it was not included the contribution related to the particles growth. STR group [83] instead treated the particles growth rate as independent by their diameter, using a correlation derived from the Hertz-Knudsen equation. However in some experimental specific works [84, 85] it is underlined that particle growth and condensation rates are strongly dependent by their size. Therefore, as it wasn't found anything satisfactory enough in the literature, it was obtained ex novo an equation to evaluate the monomer consumption due to the particles growth (R_{gr}), explicit dependent by their size. In fact there were tried two approaches completely different to achieve that expression, but all of them resulted exactly to the same result, reported in Equation 26. The details about its analytical derivation are provided in Section 2.10. Thus probably the Equation 26 should be reliable, which depends on the molecular weight of the monomer (Mw_{mon}), its concentration in the gas (*[mon]*) and $\mu_{2/3}$.

$$R_{gr} = \sqrt{\frac{8\pi RT}{Mw_{mon}}}\left(\frac{3}{4\pi}\right)^{\frac{2}{3}}[mon]\,\mu_{2/3} = K'[mon]\mu_{2/3} \qquad (26)$$

The balances of μ_o, μ_1 and μ_2 are finally expressed as in the following equations:

$$\left(u - K_T\frac{\upsilon}{T}\nabla T\right)\nabla\mu_0 = D\nabla^2\mu_0 + N_{Av}R_{nucl} - \beta_0\mu_0^2 \qquad (27)$$

$$\left(u - K_T\frac{\upsilon}{T}\nabla T\right)\nabla\mu_1 = D\nabla^2\mu_1 + v_0\,N_{Av}\,R_{nucl} + N_{Av}K'\,[mon]\Delta v\,\mu_{2/3} \qquad (28)$$

$$\left(u - K_T\frac{\upsilon}{T}\nabla T\right)\nabla\mu_2 = D\nabla^2\mu_2 + v_0^2\,N_{Av}\,R_{nucl} + \beta_2\mu_1^2$$

$$+ N_{Av}K'[mon]\,\Delta v^2\mu_{2/3} + 2\,N_{Av}K'\,[mon]\Delta v\,\mu_{5/3} \qquad (29)$$

In those equations there are several parameters in principle unknown, except of course the gas velocity (u), the kinematic viscosity (v), the temperature (T), the Avogadro number (N_{Av}) and the nucleation rate (R_{nucl}). Fortunately most of them can be determined theoretically. As already motivated, an important assumption made is that GaN aggregates are in free molecular regime. The first unknown constant is the thermophoretic coefficient (K_T), which is generally assumed between 0 and 1. Anyway for large Knudsen numbers, it can be predicted by the theory describing the motion of a single particle in a temperature gradient [86] and it is equal to 0.55. The particles diffusivity (D) is calculates with the correlation proposed by Lee and Liu [87] and considered explicitly dependent by their geometric mean volume (v_G). Then, the coagulation coefficients (β_0 and β_2) are calculated as proposed by Pratsinis [88] in free molecular regime, dependent by v_G and σ_{log}. The volume of the first stable nucleus (v_0) is instead assumed that corresponding of a sphere with its Lennard Jones diameter. All these theoretical parameters are biased by significant uncertainties, but since the aim of the work is to simulate the GaN deposition profiles rather than to accurately describe the particles size distribution, their estimation can be considered satisfactory enough. This fact is confirmed by an aimed sensitivity analysis.

Finally Δv is the volume increment due to the addition of one GaN unit. Coherently with what experimentally demonstrated [84, 85], the parametric analysis mentioned evidenced that it is a very sensitive variable, because it affects the clusters dimensions. However it can be related to macroscopic properties because the related mass increment (Δm) is known and it is equal to the molecular mass of GaN. If Δv is constant then also the ratio between Δm and Δv it is. This should be thus equal to the average density of the powders ρ_0 and Δv can be calculated as in the Equation 30. Also STR group [83] uses explicitly ρ_0 to evaluate the term related to the particles growth. The Δv resulting for the addition of a

monomeric unit to an aggregate it was calculated assuming a particles density of 4 g/cm^3. This value is qualitative coherent with what usually observed in amorphous solids, whose densities are generally 1.5-2 times lower with respect to those of the corresponding crystalline material. In this particular case the density of the GaN epitaxial layer is indeed 6.15 g/cm^3.

$$\Delta v = \frac{Mw_{GaN}}{N_{Av}\rho_0} \qquad (30)$$

The fitting parameter introduced in the model is the nucleation kinetic constant, taken in a typical range consistent with a collisional constant. Indeed, as explained in Section 5.3.3, its related uncertainty is conspicuous.

2.4.2 Analytical derivation of the growth rate expression

As explained in Section 2.9, it has been necessary to propose a new correlation to predict the particles growth rate, due to the scavenging of the gaseous precursors on their surface. Indeed nothing satisfactory was found in the literature to describe such contribution. However this heterogeneous reactivity is very important in the global kinetics, active during GaN MOVPE, because particles growth consumes part of the reactants, affecting the GaN growth rate on the substrate. This droplets formation has been abundantly documented in the literature [19, 21-28], and its relevance is also underlined by the experimental campaign complementary to this modeling study. For that reason having a good approximation of such phenomenon is a key requisite in order to have a model able to reasonably describe the experimental data. Even if further details are widely provided in Chapter 5, here are anticipated some the main features related to particles growth. The main assumptions on which the derivation is based are:

1. The scavenging phenomenon occurs through the adsorption of gaseous monomeric units on the droplets surface, with the subsequent decomposition to further amorphous GaN;
2. The consumption of one molecule of monomer in the gas, increases the aggregate size by one monomeric unit of volume Δv;
3. The powders growth rate is enhanced with their dimensions increment [refs], hence it is in fact an autocatalytic mechanism;
4. The particles growth is in external diffusive regime;
5. Neglected GaN evaporation from particles surface.

The first approach adopted treats the gas droplets as pseudo gas spherical molecules which collide with monomeric molecules, schematized in Figure 10a. Hence it was carried out with the kinetic gas theory, starting from Equation 23. If considering the collisions between only the particles at fixed diameter d_P, volume v and mass m_P, with the monomers molecule with diameter d_{mon}, and mass m_{mon}, this specific collisional growth rate ($R_{gr}(v)$) can be expressed by Equation 31. Indeed the particles sizes are many times greater respect to those of the monomers, and their velocities are negligible with respect to those of the smaller monomers.

$$R_{gr}(v) = k_{coll}[mon]F(v) = \pi\left(\frac{d_P}{2}\right)^2\sqrt{\frac{8\,k_BT}{\pi\,m_{mon}}}[mon]F(v) \quad (31)$$

The total growth rate is the integral of the growth rates of all the possible particles dimensions. Thus from Equation 31 and the definition of μ_k in Equation 24, is possible to achieve the function of the Equation 32, which is also the correlation in Equation 26.

$$R_{gr} = \left(\frac{3}{4\pi}\right)^{\frac{2}{3}}\sqrt{\frac{8\pi RT}{Mw_{mon}}}[mon]\int_0^\infty v^{\frac{2}{3}}F(v)dv = K'[mon]\mu_{2/3} \quad (32)$$

An alternative approach comes from the Hertz-Knudsen relation (Equation 33), which evaluates the evaporation-condensation rate from a surface. As already pointed out a relation based on this principle has

already been used in the literature [83] to describe particles growth, but the explicit dependence by the particles size was not accounted. P_{mon} is the monomer partial pressure, whereas P_0 is the GaN vapor pressure. Particles growth is considered as a monomer condensation on the droplets external area, as schematized in Figure 10b.

$$R_{gr} = \frac{P_{mon} - P_0}{\sqrt{2\pi Mw_{mon} RT}} \frac{Surface}{Volume} \qquad (33)$$

The total condensation surface dispersed in a unit volume is the integral of the external surface of aggregates of every possible dimension, shown in Equation 34.

$$\frac{Surface}{Volume} = \int_0^{\infty} 4\pi \left(\frac{3}{4\pi}\right)^{\frac{2}{3}} v^{\frac{2}{3}} F(v) dv \qquad (34)$$

Combining Equation 33 with Equation 34, the Equation 35 is obtained. Then if the evaporation of GaN is neglected (P_0=0), such formula becomes identical to Equation 32.

$$R_{gr} = \left(\frac{3}{4\pi}\right)^{\frac{2}{3}} \sqrt{\frac{8\pi RT}{Mw_{mon}}} \left([mon] - \frac{P_0}{RT}\right) \mu_{2/3} \qquad (35)$$

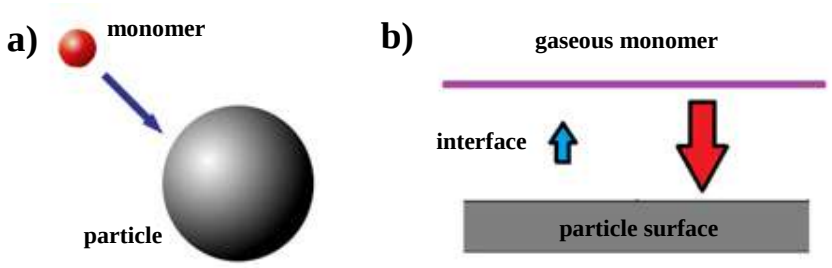

Figure 10: Schematization of a) collision between a monomer unit and a particle; b) monomer evaporation-condensation on a particle surface.

The expression obtained as described above is able to represent the monomer consumption rate if the distribution function (*F(v)*) is known. However in order to predict the effect of the particles growth on their size distribution, the Equation 32 must be implemented in the balances of the

first 3 moments. Basically the addition of a monomeric unit to an aggregate of volume *v*, implies the consumption of a particle with volume *v* and the formation of one with volume $v+\Delta v$. This is shown in the correlations below, where Dg_0, Dg_1 and Dg_2 are the growth contributions to the balances of μ_o, μ_1 and μ_2 respectively. Finally they were added to such balances, resulting to Equation 27, Equation 28 and Equation 29.

$$Dg_0 = N_{Av}K'[mon]\left(\int_0^\infty v^{\frac{2}{3}}F(v)dv - \int_0^\infty v^{\frac{2}{3}}F(v)dv\right) = 0 \qquad (36)$$

$$Dg_1 = N_{Av}K'[mon]\left(\int_0^\infty (v+\Delta v)v^{\frac{2}{3}}F(v)dv - \int_0^\infty v\, v^{\frac{2}{3}}F(v)dv\right)$$
$$= N_{Av}K'[mon]\Delta v\int_0^\infty v^{\frac{2}{3}}F(v)dv \qquad (37)$$

$$Dg_2 = N_{Av}K'[mon]\left(\int_0^\infty (v+\Delta v)^2 v^{\frac{2}{3}}F(v)dv - \int_0^\infty v^2\, v^{\frac{2}{3}}F(v)dv\right)$$
$$= N_{Av}K'[mon]\left(\Delta v^2\int_0^\infty v^{\frac{2}{3}}F(v)dv + 2\Delta v\int_0^\infty v^{\frac{5}{3}}F(v)dv\right) \qquad (38)$$

2.5 Lennard Jones potential

The issues discussed in the first part of this chapter concern the phenomena at the micro scale. However this work is aimed to describe how those kinetic features affect the global performances of the processes analyzed, or in other words the effect at the macro scale. In order to describe the global behavior of those reactors, a reasonable fluid dynamic description should be provided. Indeed also transport phenomena have generally a key role in the systems here studied. Hence good estimations of physical properties as viscosity, thermal conductivity, diffusivities and thermodiffusion coefficients are required, but unfortunately they are not always available in the literature. A very common approach to provide such type of information relies on the Lennard Jones potential [89].

That mathematical model was proposed by Sir John Edward Lennard Jones in 1924 and describes the inter-molecular energies of interaction for atoms or chemical compounds, based on their distance of separation. The equation takes into account the difference between attractive forces (dipole-dipole, dipole-induced dipole, and London interactions) and repulsive forces. Although more accurate potentials exist, the Lennard Jones approach is used extensively in computer simulations because of its computational simplicity. Indeed, in spite of the theoretical critics, that method is a relatively good approximation is often used to describe the properties of gases, and to model dispersion and overlap interactions in molecular models. It is particularly accurate for noble gas atoms and is a good approximation at long and short distances for neutral atoms and molecules. The expression of the Lennard Jones potential (U_{LJ}) is reported in Equation 39 and plotted in Figure 11, as a function of the inter molecular distance (r) and it depends on the collision diameter σ_{LJ} and the characteristic energy ε_{LJ}. The latter is generally expressed in the form of a temperature ε/k, as in the Equation 40.

$$U_{LJ}(r) = 4\varepsilon_{LJ}\left[\left(\frac{\sigma_{LJ}}{r}\right)^{12} - \left(\frac{\sigma_{LJ}}{r}\right)^{6}\right] \qquad (39)$$

$$\varepsilon/k = \frac{\varepsilon_{LJ}}{k_B} \qquad (40)$$

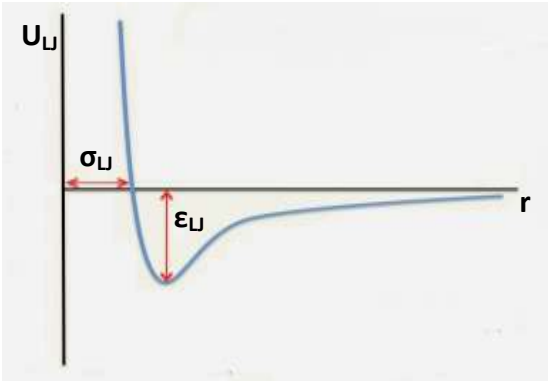

Figure 11: Intermolecular potential function with the Lennard Jones approach.

Knowing the intermolecular interactions in a given mixture, heat capacity and the molecular weights of the species involved, it is possible in

principle to estimate some physical features as viscosity, thermal conductivity, binary diffusivity and thermodiffusion coefficient. In the case of the Lennard Jones approach, is necessary to estimate σ_{LJ} and ε/k. These parameters can be fitted to reproduce experimental data or obtained from accurate quantum chemistry calculations. In the approach herein followed first it was achieved σ_{LJ}, using Le Bas volume contributions [89]. Then it was performed the estimation of the binary diffusion coefficient in H_2 as carrier gas, consistently with the formula proposed by Fuller et al. [89]. After that, such value was imposed equal to the one from the Wilke and Lee formula [89], by means of a simple non-linear equation solution and it was estimated the value of ε/k. This procedure was repeated at different temperature and finally averaged. At this point it is possible to calculate [89] the value of viscosity, thermal conductivity, binary diffusivity and thermal diffusivity factor. The results are computed at different temperatures and mole fractions and fitted in expressions that can be suitably utilized for fluid dynamics simulations.

2.6 Reactors modeling

Once having achieved all the information about the chemical reactivity and the physical properties of the systems in exam, it is possible to provide a description of the macroscopic reactor where the conversion from reactants to products is taking place. The level of approximation selected depends by the geometrical configuration, by the mixing in the gas phase and especially by the aim of the specific type of simulations. Thus several kind of fluid dynamic models of reactors have been developped. Diffusion and thermal diffusion coefficients were calculated from Lennard-Jones parameters.

2.6.1 PSR models

The most simple approximation is that of assuming the system as perfectly mixed, using a PSR representation. This approach is often unable to give a good macroscopic quantitative description, but it is instead very useful to study the micro kinetics. Indeed the main reaction pathways active during the non oxidative conversion of natural gas and during the poly silicon CVD from $SiHCl_3$ have been investigated using PSR models able to describe biphasic homogeneous systems, stationary or time dependent. Hence both gas phase and surface reactivities are accounted, as well as the interphase exchange of active species. Both computational systems have been solved with the Newton-Raphson method using an analytic Jacobian coupled. Such models were also used to provide a basic representation of some simple reaction configurations. Anyway those simulations were focussed in describing the qualitative effect in varying some operative conditions, rather than to give accurate quantitative estimations.

In particular, two different semi-ideal models were used to study methane plasmas. The first (macro-discharge model) is apt to describe the kinetics active in discharges characterized by the formation of a stationary plasma volume, while the second (micro-discharge model) can be used to investigate the kinetics of plasmas that involve the formation of streamers. Both models are based on the assumption that the plasma discharge takes place in a homogenous volume that remains constant during the process, that the plasma volume is perfectly mixed and adiabatic, and that the electron temperature and density are constant when the discharge is active. Also the deposition of coke on the electrodes is accounted. The most important model parameters are the energy absorbed by the discharge (Q_{plasma}), the electron temperature (T_e) and density (n_e), and the plasma volume (V_{plasma}) On this basis, the macro-discharge model can be formulated through a relatively limited set of equations composed by the mass, energy and charge conservation equations [90].

The hypothesis to assume the plasma volume as adiabatic is referred only to the heat exchange. In fact an external electric energy Q_{plasma} is absorbed by the plasma, which activates *NRE* inelastic electron impact reactions. Their rates (r_j) are thus dependent by the Q_{plasma} trough the Equation 41, where the ΔH_j are their reaction enthalpies. Thus, if the electron temperature is known, their desity is calculated by the Equation 41.

$$Q_{plasma} = \sum_{j=1}^{NRE} r_j(n_e, T_e)\Delta H_j V_{plasma} \qquad (41)$$

Furthermore a similar stationary PSR model was also used to investigate the kinetics occurring in Siemens reactors during poly silicon CVD from $SiHCl_3$. On this case the temperatures in the gas and on the substrate were imposed. The primary intent of these simulations was to determine the main reaction pathways active in the typical operative conditions of Siemens reactors as a function of deposition temperature and residence time, neglecting at a first level of approximation transport phenomena.

2.6.2 1D models

A monodimensional fluid dynamic model instead was used to test the predictive capability of the proposed reaction schemes, in the case of poly Si and SiC CVD, by simulating some literature experimental data collected in horizontal reactors. The general layouts of the apparatuses simulated are schematized in Figure 12. Specifically the experiments performed for poly Si were measured in a cold wall rapid thermal chemical vapor deposition (RTCVD) [91], whereas those for SiC deposition in an industrial hot wall reactor built by LPE epitaxial technology [92]. The reactor used for SiC CVD has a reactor chamber height of 7 cm and a subscector dimeter of 10 cm. The reactor used for SiC CVD instead is characterized by a reactor height of 2.5 cm and a 21

cm wide susceptor. Further details can be provided from some reference literature works.

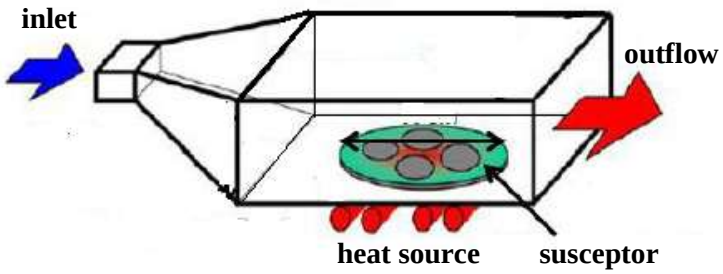

Figure 12: Layout of CVD horizontal reactor used for poly Si and SiC CVD.

Briefly, the computational program solves the mass and energy conservation equations along the flow direction while the mass and energy transfer to the reactor walls, susceptor, and growth surface are solved using boundary layer theory. For the experimental runs considered in the present study the Reynolds number is comprised between 1 and 20, so that the growth is always performed in the laminar regime. The mass and energy transfer coefficients are determined using the Luikov expressions for fully developed flows in rectangular ducts [93]. The surface reaction kinetics is solved in the pseudo steady state approximation (PSSA) together with the homogeneous mass and energy conservation equations, which makes the problem differential algebraic. The numerical integration is performed using the daspk 2.0 solver [94, 95]. This model was validated through the simulations of different CVD deposition processes in previous works [49, 50, 96] made by this research group.

In case of SiC CVD simulations, the temperature profiles in the gas phase and on the substrate were imposed. Such adopted profiles of the deposition surface is expected to be an adequate description of the real temperature distribution on the basis of preliminary calculations that take into account the reactor internal structure and the inductive heating of the susceptor and on the basis of in situ pyrometric of the susceptor temperature profile.

2.6.3 2D models

In case of the non oxidative conversion of methane, some fluid dynamic simulations were performed in order to investigate if and how the removal of the adiabatic and plasma volume conservation hypotheses affect the results obtained with the micro-discharge simulations. The object of such simulations is a pulsed corona discharge, whose typical layout is represented in Figure 13a. The equations considered in the model are the time dependent mass conservation equations in the Maxwell-Stefan formulation, the continuity equation, the Navier-Stokes equations, and the energy conservation equation, accounting for reaction energy changes but neglecting radiative heat transfer. To reduce the computational effort a simplified kinetic scheme, described in Section 3.4.1, was used for the simulations.

The model was implemented in COMSOL Multiphysics 4.1 and integrated in the axial symmetric geometry sketched in Figure 13b. The integration domain has a radius of 3 cm and a height of 1 cm. The discharge region is a coaxial cylinder positioned at the centre of the integration domain. It is assumed that the rates of radical dissociations for electron impacts are constant during the pulse time in all such plasma volume, and evaluated through the Equation 41 for an imposed Q_{plasma}. To favour numerical convergence a buffer volume circumferential to the discharge volume was introduced. It has a cylindrical section with a thickness equal to half of the discharge radius. In this domain, the rates of electronic dissociation processes linearly decrease until zero during the pulse time. Several simulations were performed for different values of the mean diameter d of the discharge region, comprised between 0.1 mm and 1 mm. While the lowest values are consistent with the typical range of streamer diameters reported in the literature, which is 0.1-0.2 mm [1], the highest values can probably be reached at high pulse energies. The boundaries of the integration domain were closed to material and heat

exchanges. The integration structured mesh consisted of about 5000 triangular elements.

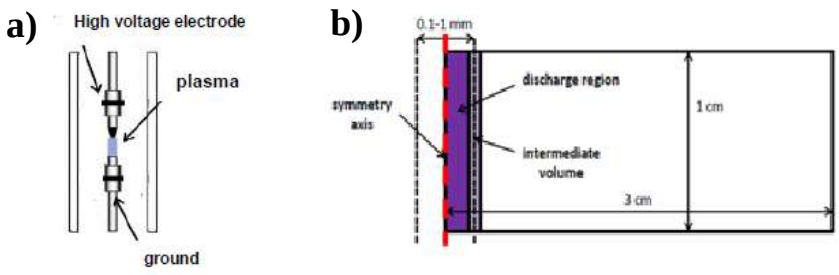

Figure 13: a) scheme of a pulsed corona experimental reactor; b) axial symmetric geometric domain used in fluid dynamic simulations of pulsed corona.

In case of GaN MOVPE 2D fluid dynamic simulations were performed with the purpose to represent the experimental data obtained in a parallel aimed experimental campaign. Those experiments took place in the Sugiyama lab in Tokyo, using an experimental reactor projected for MOVPE (AIX200/4-RFS, AIXTRON), whose configuration is shown in Figure 14. On this case a 1D approximation would not be adequate for a reasonable fluid dynamic description. The main reason is that, as shown in Figure 14, the precursors are fed from different inlets and their mixing is not complete along the reactor height above the substrate. Therefore its geometry was implemented in a stationary 2D program developed by Jensen group in MIT and already tested in several previous works, which also takes into account the surface reactivity [97-103]. In this specific case it was assembled a structured mesh with around 4500 rectangular elements. The numerical solution is computed with the finite element method (FEM) in an iterative way, using an analytical Jacobian. However, as already anticipated in Section 2.4, the program was substantially modified mainly to solve the particles distribution function with the second order method of moments.

The gas flux is assumed in laminar regime because the Reynolds number found in the operative condition tested is less than 100. It was explicitly accounted also the thermophoretic diffusion because it should be significant at the elevated temperature gradients established in the

MOVPE reactor. The material balances are computed after having uploaded the temperature and velocity profiles from a more accurate 3D simulation. This approach should be reasonable because the system is extremely diluted, thus the thermal and velocity profiles are not conditioned by the chemical reactivity. In fact the material balances were not implemented in a 3D geometry too, because the number of chemical species involved in the kinetic mechanism is quite elevated (19 components plus 3 particles moments) and the computational effort would be too onerous. In principle it is also possible to oversimplify the kinetic mechanism and use it in 3D. However from a sensitivity analysis it resulted that the reactivity of several species affects in an appreciable way the GaN deposition profiles. Hence the potential gain in accuracy in the description of the material transport achievable with a 3D model would be widely compensated by a kinetic behavior badly represented, giving finally even worse results. More details about the kinetic mechanism are provided in Chapter 5. In addition the solution of the population balances with the method of moments is resulted to be numerically unstable, due to the autocatalytic nature of particles growth and coagulation. This inconvenient was finally overcome with some numerical expedients added ad hoc in the program to help the convergence, but doing so in a 3D commercial software is hardly feasible. For these reasons it has been chosen to keep a more simplified fluid dynamic description for the material balances, but with an accurate kinetic mechanism.

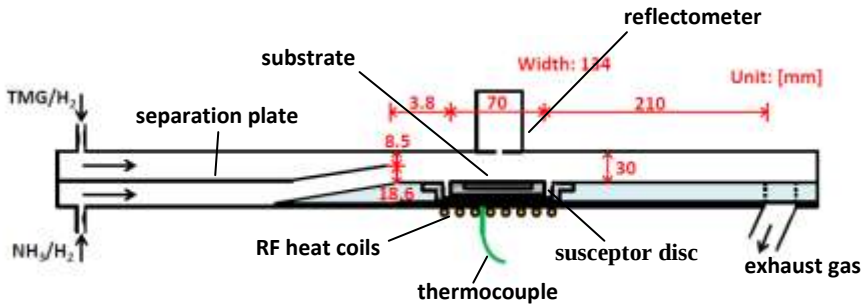

Figure 14: Geometrical configuration of the experimental AIXTRON reactor used for GaN MOVPE in Tokyo.

2.6.4 3D model

Finally, the last kind of fluid dynamic model used during this phd thesis is in a 3D geometry and, as anticipated above, it was aimed to describe the experimental AIXTRON reactor used for GaN MOVPE . Indeed having an accurate representation of the temperature and velocities profiles is essential to achieve a good description of the reaction kinetics, as well as of the resident time of the precursors above the substrate. As already motivated in this model there are not solved the material balances of all the chemical components involved in the kinetic scheme, but it is instead focused only on the fluid dynamics in the gas phase. The only exceptions are constituted by those of H_2 and NH_3, because they are the main constituents of the carrier gas. The stationary equations considered in the model are the time dependent mass conservation equations for such 2 components in the Maxwell-Stefan formulation, the continuity equation, the laminar Navier-Stokes equations, and the energy conservation equation, accounting also the radiative heat transfer. The model was implemented in COMSOL Multiphysics 4.1 and integrated in the 3D geometry sketched in Figure 15, with the dimensions equal to those reported in Figure 14.

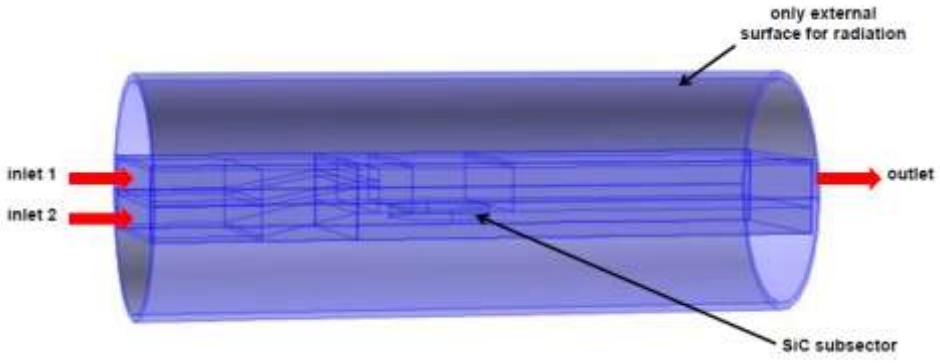

Figure 15: 3D domain used in fluid dynamic simulations of AIXTRON reactor.

The integration structured mesh consisted of about 30000 tetrahedral cells. The domain simulated is the internal part of the reactor, where the GaN growth takes place. However since radiative heat transfer affects considerably the temperature profile, it has been added the surface of the

external cylinder made of inox steel, imposing its temperature equal to 300 K, in order to account the radiative flux between the walls of reactor chamber and such area. The conductive heat flux at the external walls was imposed on their surface and calculated assuming that the gap between that surface and the external cylinder is filled by stagnant hydrogen. Indeed in fact its feed is the minimum to guarantee to be flushed out. Then the substrate temperature was imposed on its surface. In order to validate the model, the temperature profile achieved was compared to that obtained in some fluid dynamics simulations performed by STR group with their software [81] to simulate an identical reactor at the same operative conditions. The resulting profile is in good agreement with that found in that article.

2.7 General methodology developed

In the rest of this chapter, there were described the methods used during this phd thesis. However it was not exactly clarified how those models have been applied, and in which order to investigate the topic of interests. In this last part instead it is provided a global synthesis of how the various theoretical tools were combined together to achieve the final results. In other words it is illustrated the main approach followed during this work. Indeed one of the most important objectives of this phd thesis is to develop a general methodology, useful to investigate the most critical aspects in systems where there is an interaction between some components in a gas phase and an activated surface. Such approach should be extendible to various processes where the chemical reactivity is unknown. The methodology cited is summarized in the following points, applied in the sequence reported.

1. Assembling a preliminary kinetic scheme: a first set of reactions is determined including what already proposed in the literature. Moreover a thermodynamic analysis helps to identify the most

stable intermediates, which may have a significant role in the mechanism. The thermodynamic parameters are theoretically estimated with quantum chemistry methods. After that, additional new classes of conversion routes are hypothesized for the first time and added to the scheme. The gas phase kinetic scheme proposed is then combined with a literature surface mechanism.

2. First theoretical estimation of the kinetic constants: accurate *ab initio* calculations are performed to evaluate the kinetic parameters of the new reactions, based on transition state theory. As already pointed out in Section 2.3, the precision of the computational techniques herein used is higher with respect to those previously utilized in most the earlier articles for the processes object of the present study. Anyway in general the kinetic constants evaluated in various publications are achieved with different methods. Therefore also the gas phase constants taken from the literature are re evaluated in order to avoid comparing reaction pathways using kinetic constants calculated at varied levels of theory. All the reactions are considered as reversible.
3. Micro kinetic analysis: the whole kinetic scheme composed by both the gas phase and the surface mechanisms is tested with a program simulating a simple bi phase PSR reactor model. Other reactions can be added also to the surface mechanism. With a sensitivity analysis it is possible to find the most sensitive reaction pathways and to discard from the mechanism those without any noticeable effect on the global conversion rates. From this analysis is provided a clearer picture of the reaction kinetics, that may also be useful to better explain some macroscopic behavior related to the kinetics. Besides it can be possible in principle also to lump the kinetic mechanism, making it more suitable to be implemented in more complex reactor models.
4. Improvement of the estimation of the kinetic constants: once achieved the final set of reactions, the estimation of the pre

exponential factors is further refined. In this thesis were the 1D hindered rotor approximation and the variational transition state theory. Anyway other techniques can in principle be exploited for an ulterior enhancement of the accuracy, depending by the particular case in exam and by the level of precision desired. After this point the micro kinetic analysis is repeated to check if there are substantial differences due to the more accurate kinetic constants. Then also the effect of the variation of the operative conditions on the reactive behavior is investigated.

5. Inclusion in the model of other types of phenomena: in principle other types of physical behavior may influence the performances of a specific process. Therefore other correlations are proposed and included in the model, with the aim to improve it. For example in the case of GaN MOVPE there were added the population balances of the solid particles produced in the reactor and implemented with a second order method of moments. Then the micro kinetic analysis is repeated again.
6. Macro scale simulations: the transport phenomena in fact heavily influence the performances of real reactors. Thus fluid dynamics models are developed and finally solved including the new proposed mechanism. Diffusion and thermal diffusion coefficients are calculated using the Lennard-Jones approach. The model assumed to describe a particular reactor is selected considering its geometrical configuration, the level of mixing in the gas phase and, most important, the aim of the specific type of simulations.
7. Analysis of the results: the results are compared with some experimental evidences. Some of the previous steps are revised and corrected, till the quality of the predictions are considered enough satisfactory. Finally the model achieved can in principle be utilized to improve the understanding of the system in exam and maybe to propose some criterion to improve it.

The approach described above was applied in principle to all the processes studied during this phd thesis. However it was paid more attention to different topics in each of them, depending on the respective focuses and background of knowledge. The methodology was thus adapted for each case to the specific features of the system under examination, but respecting its main principles. The result of this procedure should not be only a model able to describe the experimental evidences, but especially a useful means to achieve a more complete picture of the phenomena occurring during the process analyzed, with the final aim to provide some useful guidelines to improve the global performances.

CHAPTER 3

Non oxidative conversion of CH_4 in plasmas

The first process on which it was applied the general methodology described in Section 2.7, was the non oxidative valorization of natural gas, described in Section1.2.2. About this topic much research has recently been performed with the intent of understanding its working principles and increasing its efficiency. In the referring article [104] it is possible to find more details.

3.1 State of the art

The non oxidative conversion of natural gas by non thermal plasmas offers a promising route to produce higher value products, such as hydrogen and C2 hydrocarbons. Most of the studies about non oxidative conversion of methane were focused on the correlation between operating parameters of the plasma discharge and process performances. It was thus found that the product distribution is strongly affected by the type of discharge used to sustain the plasma. Summarizing what found in the literature [2-7, 105-130] for several types of experimental reactors by various authors, the increment of the power density in the plasma region brings to a product distribution progressively shifting from ethane, to ethylene and then to acetylene. Anyway if too much energy is supplied, it may result a conspicuous coke deposition at the electrodes, which may

affect the global reactor performances. Of course the specific electric power per unit volume absorbed in a plasma can be in part regulated by changing the electricity fed at the electrodes, but it is also greatly conditioned by the discharge technique utilized. For example it is lower in DBD reactors, whereas in thermal plasmas is much higher.

The underlying motivation of most of the experimental studies mentioned above was to estimate and improve the performances of methane plasma discharges. Different plasma discharges can be compared on the basis of methane conversion, product distribution, methane flow rate, pulse frequency and energy efficiency η_{plasma}, defined as the fraction of the energy supplied to the system used in chemical reactions. As the residual energy is lost into gas heating, the energy efficiency can be estimated as in the Equation 42.

$$\eta_{plasma} = \frac{F_{out}H_{out}(T_{in}) - F_{in}H_{in}(T_{in})}{Q_{plasma}} \qquad (42)$$

Where Q_{plasma} is the electric power supplied, F the inlet and outlet molar flows, and H the molar enthalpies. It is important to point out that the definition of energy efficiency reported above does not include the efficiency of the conversion of the discharge power, which is the total power absorbed by the specific plasma device, into electric power, which is the power of the electromagnetic field that sustains the discharge. This parameter, which is system dependent, should therefore be considered in order to extrapolate the results reported in this study to real processes. It is interesting to point out that some studies on the evaluation of corona plasmas techniques for industrial application have shown that efficiencies for conversion of discharge into electrical energy higher than 90% can be reached through a careful design of the plasma generation apparatus [131]. Considering the criterions listed above, some results achieved by various authors for different type of discharge are summarized in Table 2.

Several kinetic studies [90, 123, 130, 132-136] have been performed on the chemistry of methane plasmas, some of which enriched by a fluid

dynamic model [126, 137-142]. However, though most kinetic parameters are available and IR laser absorption spectroscopy measurements of gas species concentrations [126, 143] have been done, the main reaction mechanism is not yet completely clarified. It is generally agreed that the gas phase is far from the thermodynamic equilibrium [120, 127, 132, 134] and some authors suggest that acetylene yield is higher than the thermodynamic limit [127]. Also, it is agreed that the ionic species reactivity is considerably less important compared to that of the neutral species [132] and that the first step of the reaction mechanism is the formation of radicals by electron impact. Anyway what happens next is still an open discussion. In particular the main reaction pathways, which bring to the formation of the main products, are unknown.

Table 2: Comparison of the energy efficiencies of different atmospheric plasma reactors used for the non oxidative conversion of methane.

Plasma mode	Frequency (Hz)	CH_4 flow rate (mol s^{-1})	Conversion (%)	Main products	Energy Efficiency (%)	Ref
Thermal arc –60 kW	-	0.098 – 0.15	90-100	C_2H_2	40 (est.)	[2]
Thermal arc (Huels)	-	26.45 – 33.2	68	C_2H_2	34	[2]
Gliding Arc	15-20 k	1.1×10^{-3}	40-45	C_2H_2	≈ 10	[105]
Pulsed streamer	55 (90 ns pulse)	7.4×10^{-6}-2.2×10^{-5}	19-41	C_2H_2	6-10	[110]
Pulsed spark	55	7.4×10^{-6}-2.2×10^{-5}	18-69	C_2H_2	6-10	[110]
Spark 5 kV inception	50 (20 ms pulse)	$1\text{-}2\times10^{-5}$	10-65	C_2H_2	27	[3]
Pulsed Corona	9.92k	2.0×10^{-4}	15-45	C_2H_2	51.4	[4]
Pulsed Corona	8.0k	1.0×10^{-4}	15-45	C_2H_2	17.7	[5]
Pulsed Corona	0.1 – 1k	1.6×10^{-3} - 6.4×10^{-3}	5-30	C_2H_2	10 – 32	[6]
DBD 5-9 kV	10 – 40k	4.7×10^{-5}	5-40	C_2H_6	<1	[114]
DBD ac	50	7.4×10^{-6}-2.2×10^{-5}	5-8	C_2H_6 C_2H_4<2%	0.1-0.2	[110]
DBD pulsed dc	50	7.4×10^{-6}-2.2×10^{-5}	6-13	C_2H_6	0.3	[110]
Microwave	2.45G	$0.4 - 1.2\times10^{-1}$	9-13	C_2H_2	≈ 15	[124]
Microwave 40-80 torr	2.45G	$\approx 8\times10^{-4}$	20-80	C_2H_2	50-63	[7]

3.2 Aim of the work and approach

Despite the many kinetic studies, several aspects are however not clear. In particular a simple kinetic analysis shows that the first steps in any non oxidative methane plasma are the following:

E9) $$CH_4 + e \rightarrow CH_3 + H + e$$

G2) $$CH_4 + H \rightarrow CH_3 + H_2$$

P2) $$2CH_3 \rightarrow C_2H_6$$

The maximum energy efficiency of this reaction cycle calculated using Equation 42 at room temperature is only 15%. Any successive reaction, leading for example to C_2H_2, will have the additional energetic cost necessary to decompose C_2H_6, thus further decreasing the energy efficiency. This is however in contrast with experimental results, which report energy efficiencies up to 50%. It is from this apparent failure to explain experimental evidences through a simple model that takes its motivation the present work, which aim is to study the effect of different operating conditions on methane plasmas efficiencies for various types of discharges. The accurate modeling of the kinetics and fluid dynamics active during plasma discharges, in particular when performed at atmospheric pressure and pulsed, is a complex task. Fortunately for the aim of this study, which is that of relating the energy efficiency of the discharge with the gas phase kinetics, several simplifications are possible. More details are provided in Section 2.6.1.

Coherently with the procedure described in Section 2.7 this work started with the proposal of the kinetic mechanism. However on this case most of the reactions are the same of thermal processes with light hydrocarbons, which have been widely studied for decades. Therefore their kinetic constants are already widely reviewed and available in the literature at high precisions. Hence there was no need to re estimate them with new *ab initio* calculations. Also the electronic and ionic reactions were taken from the literature. Summing up the kinetic scheme was assembled after a literature research [90, 123, 130, 132-136] and including also a wide number of reactions coming from the mechanisms active during thermal processes.

Then it was studied the kinetics with the PSR models explained in Section 2.6.1. The gas phase kinetics active in a methane plasma was studied with the double intent of determining which the favored reaction pathways are and of developing a lumped reaction mechanism that may be used for

fluid dynamic simulations. The reaction mechanism was studied through a flux analysis of the micro discharge simulations. The focus on the micro discharge kinetics is determined by the fact that the plasmas most interesting for methane conversion from an industrial standpoint are those operating at atmospheric pressure in non thermal regime, which are best described by the micro discharge model. Anyway it was lately extended also to macro discharges.

Successively those PSR models were then used to study the main macroscopic features for stationary macro discharges and time dependent micro discharges, hence neglecting transport phenomena. The main features of such types of reactors are explained in Section 1.2.1. This approach was already also used to study the kinetics of Diamond Like Carbon deposition in methane plasmas [90]. The aim of such simulations was to explain the effect of the operative conditions on the performances of the reactors from the qualitative point of view. The main focuses were the products distributions and especially the energy efficiency. Anyway the PSR approximation could be quite reasonable to represent a macro discharge reactor, but not so much for micro discharges because, considering the small dimensions of the plasma region, the thermal and material diffusions should not be negligible.

Therefore, in order to test the influence of transport phenomena on the kinetics, a lumped kinetic mechanism was finally inserted in a 2D fluid dynamic model of a pulsed corona atmospheric discharge. The lumped mechanism was achieved during the micro kinetic analysis. More details about the reactor model instead are provided in Section 2.6.3.

3.3 Kinetic scheme

The kinetic scheme adopted in the simulations is reported as supplementary information in the referring article [104]. It involves 30 chemical species including radical, neutral gas components, ions, and

solid carbon deposited on the electrode surface. The considered chemical reactions are 164 and can be classified in five categories: electron impacts, ionic reactions, surface collisions, and radical reactions. The electron impact reactions are promoted by the electric field and lead to the initiation of the kinetic mechanism. Their kinetic parameters were taken from a previous work [134], where they were computed as a function of electronic temperature using a Druyvesteyn electron energy distribution function. Kinetic parameters of ionic reactions have been taken from Tachibana et al. [144], while the rate of the wall reactions through which ions get neutralized was evaluated using the Bohm criterion. Also, it was assumed that the impact of C and C2 on the electrode surface leads to irreversible adsorption, which is consistent with the experimental observation of the formation of carbonaceous deposits on electrode surfaces when exposed to plasmas. The surface flux of C and C2 was calculated using the collisional model with a unary sticking coefficient. The kinetic constants of the radical reactions considered in the model were either taken from the GRI Mech 3.0 [145] or from the literature. All radical reactions were considered reversible. When relevant, pressure dependence was considered using the Troe formalism.

3.4 Results with PSR model

The first set of simulations was performed with two PSR reactor program. Despite the simplicity of the reactor models, those tests were very useful to clarify some of the main features related to the non oxidative valorization of natural gas in plasma.

3.4.1 Micro kinetic analysis

The PSR model was used to investigate the micro kinetics for time dependent micro discharges. In micro-discharges voltage is applied only

for a limited time (10-100 ns) and electron impact reactions are active only in this period. Consequently, the reaction kinetics sensibly changes during the pulse period, as well as temperature and pressure. Therefore, in order to represent the kinetics of a micro-discharge, two different schematizations have been proposed, one valid when the discharge is on and the other one when it is off. The kinetic analysis has been performed using an electronic temperature of 3 eV and a mean absorbed power of 80 kJ. Those results remain valid also for lower and higher absorbed powers (± 30 kJ) and electronic temperatures (± 1 eV), as tested through specific simulations.

The main reactions active during the discharge time are schematized in Figure 16a. The reaction mechanism is started by methane dissociation into active radicals and ions through electron impacts. The analysis of the electron impact processes evidenced, in agreement with Kovacs [132], that the rate of radical dissociation of methane is about one order of magnitude faster than that of ionization. This means that the electric power supplied is mainly exploited for methane homolytic scission. Once generated, radicals undergo propagation and recombination reactions. Radical combinations are exothermic and lead to a significant increase of the gas phase temperature. Since radical combinations and pulse voltage have comparable characteristic times, a significant amount of exothermic heat is produced during the discharge, which affects substantially the energy efficiency as long as it is not exploited for successive chemical reactions. The main reaction paths of methyl and atomic hydrogen, which are the most abundant products of electron impacts, are the following three reactions.

G2) $H + CH_4 \rightarrow CH_3 + H_2$

P1) $CH_3 + H \rightarrow CH_4$

P2) $2CH_3 \rightarrow C_2H_6$

Reaction P1 leads back to the formation of the reactant, and is thus strongly undesired. However, it is one order of magnitude faster with

respect to P2 whereas G2 becomes significant above 1000 K, because of its higher activation energy. The main reaction route of the CH and CH_2 radicals formed through electron impact leads to the production of C_2H_4 through reactions G13^r and G5.

$$\text{G13}^r) \quad CH_2 + H \rightarrow CH + H_2$$
$$\text{G5}) \quad CH + CH_4 \rightarrow C_2H_4 + H$$

The kinetics active when the discharge is off is schematized in Figure 16b. The active reaction pathways are strongly affected by the gas phase temperature since, as shown in Section 3.3.2, the product distribution evolves towards more dehydrogenated hydrocarbons with increasing temperature. The maximum temperature is reached in a characteristic time of 10^{-6} s, when most of CH_3 and H produced by electron impacts are converted to more stable species. When the temperature becomes higher than 1300 K, the following radical propagation reactions get activated:

$$\text{G22}) \quad H + C_2H_6 \rightarrow C_2H_5 + H_2$$
$$\text{P6}^r) \quad C_2H_5 \rightarrow C_2H_4 + H$$
$$\text{G24}) \quad H + C_2H_4 \rightarrow C_2H_3 + H_2$$
$$\text{P10}^r) \quad C_2H_3 \rightarrow C_2H_2 + H$$

First, the residual atomic hydrogen is able to dehydrogenate ethane and ethylene through reactions G22 and G24 and is produced back by reaction P6^r and P10^r, thus forming two distinct catalytic cycles. Then, in a characteristic time comparable with the reverse of the pulse frequency, thermal decompositions become important at about 1400-1500 K. In particular, methane dissociation through the inverse of reaction P1 sensibly enhances the yield of the process. These endothermic reactions exploit the heat produced by radical combinations, thus increasing considerably the energy efficiency of the process. Finally, at elevated temperatures, carbon deposition becomes sensible.

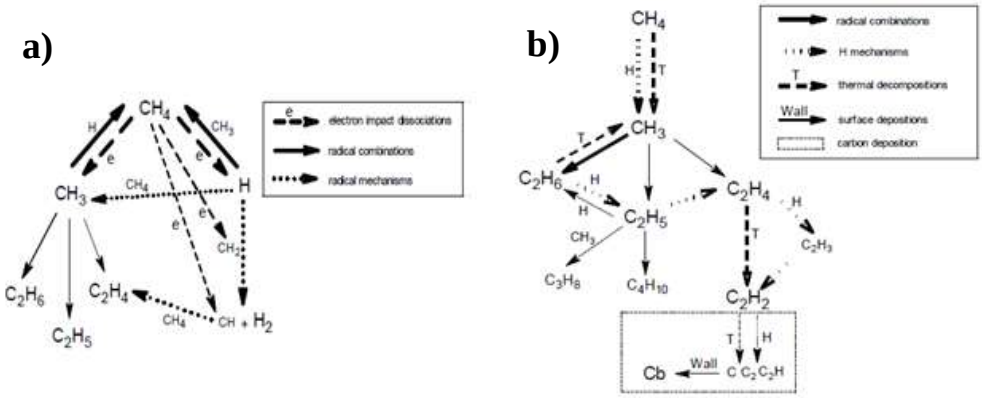

Figure 16: Reaction mechanism active in micro discharges for non oxidative conversion of methane a) during the pulse voltage; b) when discharge is off.

The reaction mechanism reported in Figure 16b allows to explain the reduced experimental energy efficiencies observed in non catalytic micro-discharges operating at low specific powers, such as DBD. In these plasmas power densities are small, so that radical concentrations and therefore gas phase temperatures are limited even after the pulse time. Thus, the residual atomic hydrogen gives the H abstraction reaction G22 rather than G2, forming C_2H_5. The reason is that G22 has an activation energy lower than G2 and that ethane is the most abundant product in those conditions. Once formed the ethyl radical is consumed by the following two reactions, which lead to the formation of higher hydrocarbons:

P8) $$C_2H_5 + H \rightarrow C_2H_6$$

P3) $$C_2H_5 + CH_3 \rightarrow C_3H_8$$

In macro-discharges the recombination kinetics of the atomic hydrogen generated by electron impacts is different. Indeed the inefficient combination with CH_3 (P1) is usually negligible, so that, as explained by Heintze et al. [122], most of H promotes further methane conversion through G2. This is due to the different time dependence of the macro and micro discharge models, which leads to average higher temperatures and lower radical concentrations at parity of absorbed energy for macro discharges.

On the basis of these considerations the overall kinetic scheme can be reduced at a first level of approximation to the set of reactions reported in Table 3, which were then used for the successive CFD simulations.

Table 3: Lumped kinetic mechanism used in fluid dynamic simulations.

	Reaction		Reaction
E16	$CH_4 + e \rightarrow 0.8\ CH_3 + 0.94\ H + 0.13\ H_2 + 0.2\ C_2H_4 + e$	P3	$CH_3 + C_2H_5 \rightarrow C_3H_8$
G2	$CH_4 + H \leftrightarrow CH_3 + H_2$	G19	$C_2H_6 + CH_3 \leftrightarrow C_2H_5 + CH_4$
P1	$H + CH_3 \leftrightarrow CH_4$	G22	$C_2H_6 + H \rightarrow C_2H_5 + H_2$
P2	$CH_3 + CH_3 \leftrightarrow C_2H_6$	P6	$C_2H_4 + H \leftrightarrow C_2H_5$
G6	$CH_3 + CH_3 \rightarrow C_2H_5 + H$	P7	$C_2H_4 \rightarrow C_2H_2 + H_2$
G7	$CH_3 + CH_3 \rightarrow C_2H_4 + H_2$	P8	$C_2H_5 + H \rightarrow C_2H_6$
G24	$C_2H_4 + H \rightarrow C_2H_3 + H_2 \rightarrow C_2H_2 + H + H_2$	G29	$C_2H_5 + C_2H_5 \rightarrow C_4H_{10}$

Further details about how it was made the lumping of some reactions are reported in the referring article [104]. The carbon formation mechanism was not included in the fluid dynamic simulations because in the simulated conditions it is not relevant. Despite such reduction, the reactive behaviour of the system is anyway represented with a reasonable degree of accuracy. This was proved through test simulations performed with the reduced mechanism for different temperatures and residence times in the reaction volume, which evidenced a maximum deviation of 20% of the main reaction products with respect to the predictions of the full mechanism.

3.4.2 Macro and micro discharge models

The PSR models were also used to explain the main macroscopic properties for stationary macro discharges and time dependent micro discharges. The macro discharge simulations were performed parameterizing the specific energy absorbed by the gas and using a volume to surface ratio of 6 cm, an inter electrode distance that, according to our experience, is a reasonable approximation of what would be adopted in microwave and radio frequency plasmas in a pilot or industrial

scale process. Simulations were performed for methane conversions varying between 10 and 90%.

The energy efficiency, calculated for a gas fed at 300 K, is reported in Figure 17a as a function of the specific energy. As it can be observed, the energy efficiency increases significantly with the specific energy up to a maximum of 57.5%. This is associated with the increase of the outlet temperature, shown in Figure 17b, which rises from 900 K to 1800 K, thus indicating a direct correlation between temperature and energy efficiency. The analysis of the reaction fluxes shows that elevated gas temperatures activate methane and ethane decomposition, as well as dehydrogenation processes. Thus the energy lost in gas heating determined by the exothermic radical recombination reactions is recovered by the endothermic reactions that get activated at about 1400 K.

The transition from the low to the high energy efficiency regime is accompanied by a change of the gas phase composition in which the dominant C_2H_x species changes from ethane to acetylene, as shown in Figure 17c. This is consistent with what is known about the thermal conversion of methane into acetylene, which requires high temperatures and has a maximum thermodynamic efficiency of about 70%. It is interesting to observe that the energy efficiency dependence from the specific energy absorbed by the plasma is characterized by the presence of a maximum. This is determined by the fact that at high specific energy the local gas phase temperature becomes sufficiently high to promote a conspicuous carbon deposition at the electrodes.

These simulation results suggest that a critical aspect in obtaining high energy efficiencies in methane conversion is the attainment of a gas phase temperature in the discharge region sufficiently high to activate the thermal methane decomposition mechanism. To test this hypothesis several simulations were performed systematically increasing the temperature of the inlet gases, thus decreasing the temperature gap

necessary to reach the critical reaction temperature. As expected, this lead to a sensible energetic improvement, as shown in Figure 18a. The dependence of the energy efficiency from the pressure is shown in Figure 18b as a function of the absorbed energy. As it can be observed, the maximum energy efficiency attainable increases from 57.5% to 59.1%, and 61.4% decreasing the pressure from 1 to 0.5 and 0.1 atm, respectively. This is determined by less effective radical recombination processes, due to fall off effects, and is consistent with thermodynamic equilibrium predictions.

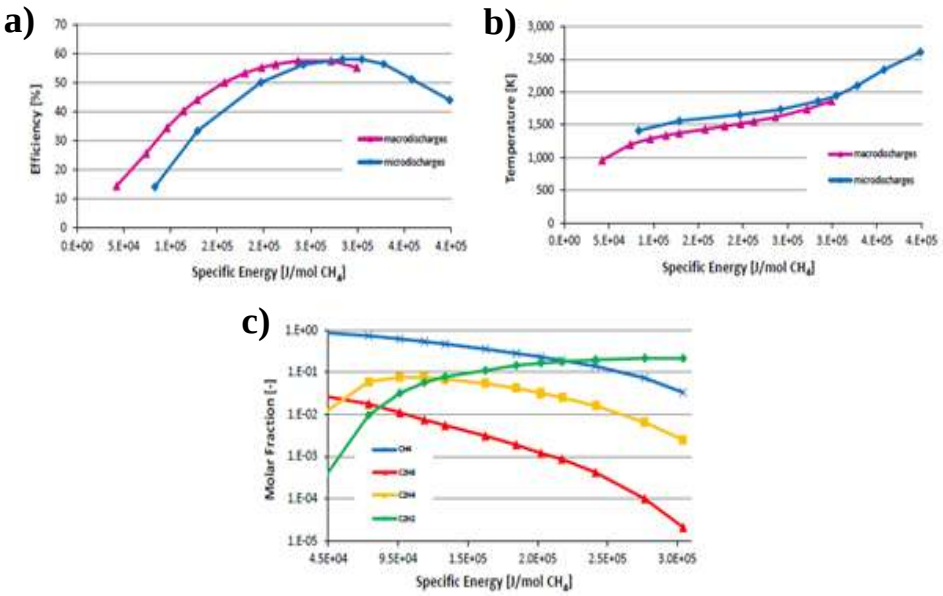

Figure 17: Effect of the specific electric energy supplied on a) energy efficiency; b) temperature in the discharge volume; c) distribution of the main products.

The maximum energy efficiency that can be obtained decreasing the pressure is however limited by the enhancement of carbon formation and deposition reactions. Also, it should be noted that simulations were performed at parity of electron temperature, while a decrease of the pressure is likely to affect its value considerably. Luckily, the model is slightly sensible to the value of the electron temperature as long as it varies by about 1 eV for what concerns the energy efficiency predictions, as discussed in the method section.

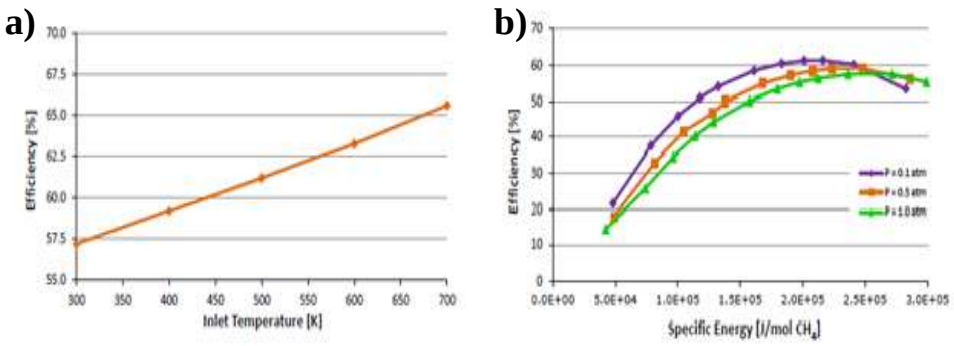

Figure 18: a) Maximum energy efficiency achievable in macro discharge as a function of the inlet gas temperature; b) effect of pressures on energy efficiency for macro-discharges reported as a function of the specific energy.

The energetic behavior of micro discharges is in many ways similar to that observed for macro discharges. For this type of plasmas the geometrical parameters and operating conditions used in the simulations were set equal to those of the atmospheric pulsed corona plasma developed by Zhao et al. [6], which is characterized by relatively high flow rates and energy efficiencies. The calculated energy efficiency is reported in Figure 17a. Comparing the efficiencies of macro and micro discharges, it can be observed that the first ones are higher at low specific energies. As explained in detail in Section 3.4.1, this is due to a different radical kinetics. Increasing the power input, the difference gradually disappears.

It is now interesting to discuss how the predictions of the energetic analysis compare with experimental evidences. Considering the summary of experimental results reported in Table 2, it can be observed that, in agreement with computational predictions, high energy efficiencies are usually associated with the formation of acetylene, while low energy efficiencies are obtained when ethane is the dominant species. Also, it is generally found that DBD discharges, characterized by low energy densities, have energy efficiencies significantly smaller than pulsed corona discharges. It is also interesting to observe that the highest energy efficiencies in pulsed corona reactors have been reported for the point to point configuration, which is characterized by high specific power and

memory effect, thus in agreement with the indications of this study. Finally, both experiment and model indicate that the formation of carbonaceous deposits limits considerably the best performances attainable.

3.5 Results of fluid dynamic simulations

The simulations results lead thus to the conclusion that higher energy efficiencies are possible when the specific energy delivered to the discharge is high. As the power densities reported in Figure 17a are particularly high for micro discharges, it can be argued that it may be difficult to supply the required energy with a single pulse in a pulsed discharge. However, in literature it has been reported that micro discharges are characterized by memory effect [1], which is the tendency to be repeated in the same volume. This way the energy fed to the gas in the second pulse adds to that of the first pulse, as long as the mean residence time in the discharge region is smaller than the discharge repetition frequency. However transport phenomena lead to the dissipation of the exothermic heat released by radical recombination reactions.

Therefore, in order to explain how the global reactor performances are affected by diffusion, some specific fluid dynamic simulations of micro discharges were performed. The model is described in Section 2.6.3 and it is aimed to describe a pulsed corona discharge. In particular it was used the lumped kinetic mechanism reported in Table 3, for a fixed specific energy absorbed by the plasma of 80 kJ/mol CH_4 for three different diameters of 0.1, 0.33, and 1 mm of the plasma channel. The discharge radial dimension was parameterized since its value is usually significantly influenced by the discharge configuration (e.g. point to point vs coaxial) and energy, so that it is system dependent. Simulations were performed in pure methane with initial temperature and pressure of 300 K and 1 bar.

Temperature, conversion, and pressure calculated at the centre of the discharge are reported in Figures 19a, 19b and 19c as a function of simulation time. As radical recombination reactions have characteristic times comparable to the pulse voltage the gas temperature, as well as the pressure, are not constant during the discharge, so that most exothermic reaction heat is released in 10^{-8}-10^{-7} s. As this time is significantly smaller than that of diffusion, in the plasma volume the molar density remains constant while the temperature increases rapidly, with a consequent local pressure enhancement. The maximum pressure is directly proportional to the ratio between final and initial temperatures as in these short times the gas mixture behaves like an adiabatic ideal gas. The situation is similar to the case of an explosive gaseous mixture in the instants that follow the explosion. Successively, a shock wave propagates out of the plasma volume with a velocity comparable to its sound speed. As shown in Figure 19c, the characteristic time of generation of the wave is directly proportional to the discharge radius.

Thermal and mass diffusion become relevant after the pressure wave propagation at characteristic times directly proportional to the discharge area, as shown in Figures 19a and 19b. The increase in temperature that can be observed in Figure 19a with the increase of the simulation time is associated with the conversion of methane into reaction products (mainly C_2H_x, see below), while the increase of the duration of the temperature spike with the diameter of the discharge is determined by the decrease of the ratio of the external area of the simulation volume and the volume itself, which leads in turn to a decrease of the relative dissipation rate of the heat released by the plasma. The discontinuity in the product conversion curve that can be observed at about $2x10^{-8}$ s in Figure 19b is due to the end of the plasma pulse (20 ns), which corresponds in the model to switching off the electron impact processes.

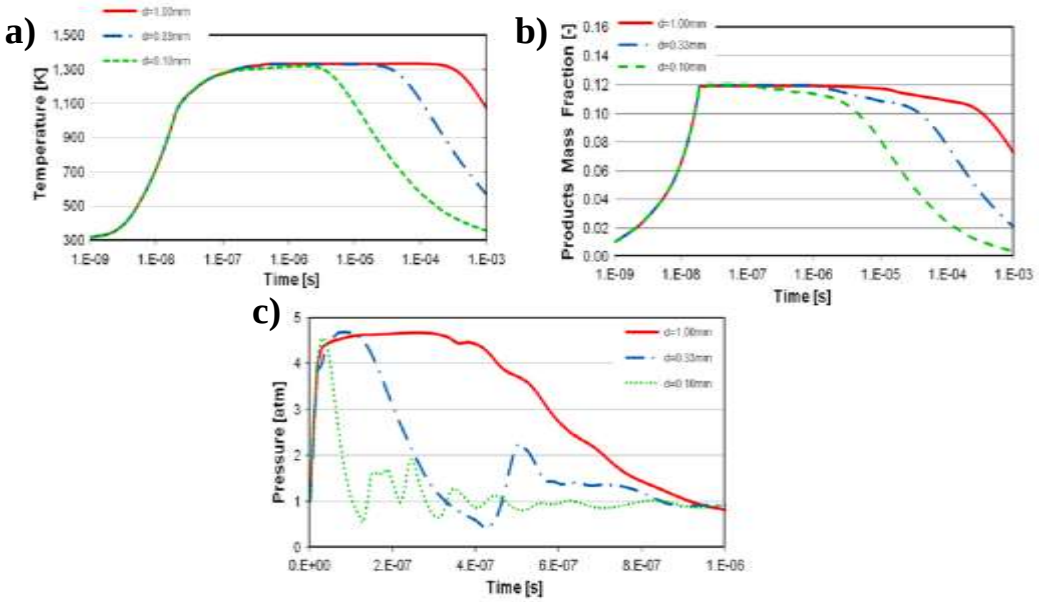

Figure 19: Time dependent profiles in the centre of the plasma volume a) temperature profiles; b) sum of product mass fractions profiles; c) pressure profiles.

The radial evolution of the temperature and pressure profiles during the gas expansion are reported in Figures 20a and 20b for a 0.33 mm discharge. Concentration profiles were not reported since they are similar. As it can be observed, when the pressure equilibrium is reached the volume of reacted gas has augmented proportionally to the ratio between final and initial temperatures, coherently with the ideal gas law used in the simulations. It is interesting to observe that the propagation of the high temperature wave is preceded by a pressure wave, characterized by a maximum located just before the region where the temperature starts increasing abruptly.

Since memory effects may play a role in increasing the energy efficiency by exploiting the heat not dissipated in the discharge volume, it was interesting to test whether this may be the case also when transport is considered. For this purpose some simulations were performed with consecutive 10 kHz pulse voltages.

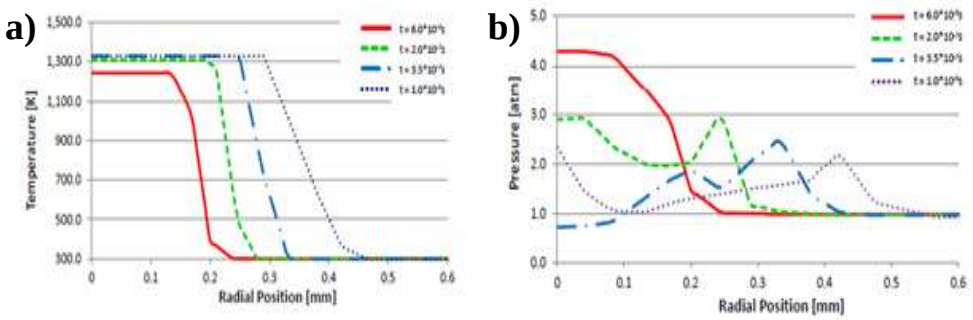

Figure 20: Profiles during adiabatic expansion in a single pulse discharge with a diameter of 0.33 mm at different times a) temperature profiles; b) pressure profiles.

As shown in Figure 21a repeated micro discharges in the same volume give a systematic enhancement of temperature and concentrations profiles of the reacted species. Moreover the composition of the main chemical species produced in the methane plasma is a function of the temperature reached in the reaction zone. For instance the acetylene yield is the highest for the discharge that takes place in the largest volume (1 mm) because of the lower impact of thermal dissipation phenomena.

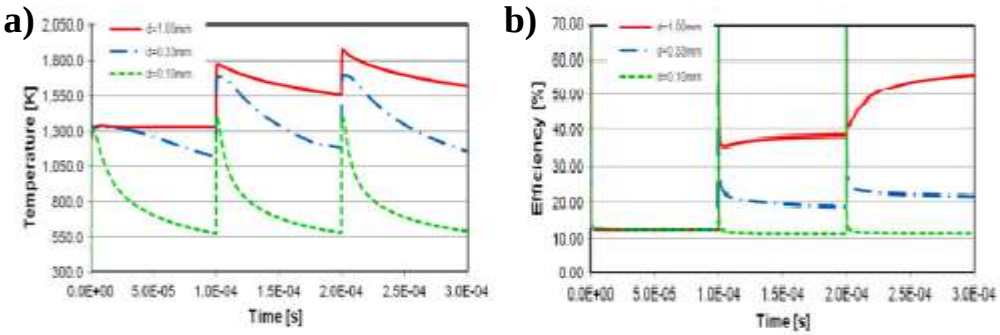

Figure 21: Time evolution in multiple pulse discharges at different diameters a) temperature in the centre of plasma region; b) energy efficiency.

Energy efficiencies were calculated integrating the reaction enthalpy changes over the volume. As found for the adiabatic semi ideal simulations, high energy efficiencies are usually associated with the attainment of high gas phase temperatures. Though the absorbed specific energy is relatively small, the energy efficiency is comparable to that of a highly energetic single pulse. The memory effect improvements are however subject to heat and mass dispersion through diffusion. The highest is the surface to volume ratio (i.e. the smallest the discharge radius), the smallest is the energy efficiency. This indicates that the

transport of the excess heat released by radical recombination reactions has a key effect on the energy efficiency of a pulsed atmospheric discharge.

3.6 Concluding remarks

The main result of this study is the elucidation of the relationship between process parameters and energy efficiency in plasmas used for the conversion of methane to higher value hydrocarbons. It was found that in order to obtain high energy efficiencies it is necessary to reach local gas phase temperatures that are sufficiently high to initiate the thermal decomposition of ethane and methane. This allows to recover the thermal energy lost in exothermic recombination reactions, which would otherwise be dissipated. High energy efficiencies are therefore associated to high specific energies absorbed by the plasma and, given the elevated local temperatures, to the formation of acetylene, which is thermodynamically stable in these conditions. For what concerns atmospheric micro discharges, such as DBD and pulsed corona plasmas, the simulations suggest that the repetition of the discharge in the same plasma volume is beneficial in terms of energy efficiency. This interpretation of energy fluxes gives a realistic explanation of the reason why the highest energy efficiencies for methane conversion in atmospheric plasmas were found in pulsed corona discharges operated in a point to point configuration, which is characterized both by high specific energies and repetition of the discharge in the same volume of space. Also, it is possible to condense the results of this study in the following set of suggestions that may be exploited to increase the energy efficiency in plasma discharges for methane conversion:

1. increase the energy delivered to the discharge, for example, in the case of a pulsed corona plasma, increasing the maximum voltage

of the power generator, the duration of the pulse, or the discharge frequency;

2. try to localize the discharge in a well defined plasma volume;
3. decrease the surface/volume ratio, as this will decrease the extent of carbon deposition;
4. pre-heat the gases, for example using a heat exchanger to recover the exhaust thermal energy.

Another important indication that comes from this study is that the inclusion of energy balance equations when modelling atmospheric pulsed discharges is important in order to capture the reaction kinetics activated by the discharge. This is because, though atmospheric pulsed plasmas are usually considered as non thermal, the simulations clearly indicate that in the discharge volume high temperatures can be easily reached if the absorbed energy is sufficiently high. Heat conduction will then lead rapidly, in the time scale of a few millisecond, to the dissipation of the excess local thermal energy and to the attainment of the uniform average temperature of the gas.

A second result of this study is the analysis of the kinetic mechanism and the proposal of a simplified reaction mechanism. It was found that, for limited absorbed specific energies, macro-discharges are more efficient with respect to micro-discharges because the radical recombination mechanism is different. However such difference is compensated at higher power densities, when the temperature threshold at which dehydrogenation reactions became active is reached.

Finally, the fluid dynamic study of a pulsed corona discharge allowed to confirm the central role played by energy fluxes in this system. It was in fact found that temperature and pressure sensibly increase when the discharge is active in the plasma volume, while the molar gas density remains constant. Successively, mechanical equilibrium is reached through the propagation of a pressure wave in the volume external to the

plasma. The volume to surface ratio (i.e. the diameter) of the discharge affects significantly the performances of the system, since it determines the extent of transport phenomena so that the heat is not dissipated and can be exploited to further chemical reactions, in particular if memory effects are present.

As a final remark, it can be observed that the simulations may lead to the false conclusion that there is not much difference for what concerns the energy efficiency between a non thermal plasma and a thermal process for the conversion of methane to higher hydrocarbons. There is however one important difference between the two processes, which concerns the soot formation mechanism. While in the atmospheric thermal conversion of methane (for example through pyrolysis or the thermal arc) it is well known that soot nucleates abundantly in the gas phase, thus limiting significantly the energy efficiency and posing the problem of its disposal, in non thermal plasmas the high temperature spikes of which it is predicted the formation will be present only for a few millisecond. In these conditions the formation of soot is kinetically limited because of the rapid quenching, so that these processes have indeed the possibility to reach energy efficiencies higher than those possible for thermal processes.

CHAPTER 4

Chemical vapor deposition of Si and SiC

After having studied non oxidative conversion of natural gas in plasmas, the subsequent part of this phd thesis was dedicated to the chemical vapor deposition of epitaxial poly Si and SiC from chlorinated silanes. The general features of those processes are described in Section 1.3.2 for silicon and in Section 1.3.3 for silicon carbide. The global reactions are quite similar, with the difference that in case of SiC is also included the reactivity of light hydrocarbons. Therefore also the kinetic mechanisms hypothesized for the two processes have several common points. For this reason they are presented both in this chapter. Further information can be found in the referring articles for Si [146] and for SiC [147].

4.1 State of the art

Trichlorosilane is actually the most common precursor to deposit silicon in the Siemens process for photovoltaic applications. Moreover the use of this same reactant is also recently emerging as the most promising route in SiC technology, in order to assure both high quality films and high throughput production processes. Despite of this, their gas phase and surface kinetics have both not yet been completely understood.

The description of the reactivity in a Siemens reactor is made particularly complex by the significant interplay between gas phase and surface

chemistry. At the typical elevated temperatures of the growth reactor, the homogeneous decomposition of the precursor is significant and the $SiCl_2$ formed in the gas is believed to be the main source of the adsorbed components on the surface [49, 148-152]. Another gaseous species that heavily influences Si growth is the HCl produced during its deposition, because it is heavily corrosive for the substrate and leads to its etching [153]. Moreover it can also react with the precursor to form $SiCl_4$, which is usually produced at significant yields [8]. Recently [50] in this research group it was combined the available information on the chlorosilane kinetics [100] with ab initio calculations on the kinetics of a chlorinated Si surface [154] to propose a new model potentially able to describe both the growth and etching reactions active during Si deposition from $SiHCl_3$. The detailed surface reaction scheme was combined with a simple gas phase kinetics consisting of the following two reactions:

$$\text{C1)} \qquad SiHCl_3 \rightarrow SiCl_2 + HCl$$

$$\text{C2)} \qquad SiHCl_3 + HCl \rightarrow SiCl_4 + H_2$$

Counter intuitively, it was found that the progress of reaction C2 has a positive impact on the Si deposition rate. In fact, though it leads to a consumption of the precursor, it also removes HCl from the gas phase. This was found to be of extreme importance since the fluid dynamic simulations revealed that, above a critical concentration, HCl etches Si, thus effectively blocking its further growth. These results lead to the conclusions that in case of poly Si CVD, the rate of conversion of HCl into $SiCl_4$ has an important role in Si deposition from $SiHCl_3$.

The gas phase reactivity of chlorosilanes has been the subject of several investigations in the last years [49-55, 149, 155-157], most of which focused on the homolitic dissociation of the chlorinated precursors. An interesting analysis of the chlorosilane gas phase kinetics was performed by Swihart and Carr [51-53], who proposed that the interconversion between the different SiH_xCl_{4-x} gas phase species is promoted by the formation of disilanes, followed by their subsequent thermal dissociation.

The possibility that a radical mechanism may be active has been in general ruled out a priori on the basis that all investigations agree that the fastest dissociation channel for monochlosilanes does not lead to the formation of radicals.

It is instead interesting to point out that several gas phase kinetic mechanisms used to model SiC deposition from chlorosilanes and hydrocarbons [16, 56-58, 158-164] contain a significant number of radical reactions. It must however be observed that the gas phase temperatures of SiC deposition are usually much higher than those of Si deposition from $SiHCl_3$. One of the first models of the gas phase kinetics active during the SiC growth from silanes was developed by Allendorf and co-workers [160], which was more recently updated by Daniellson et al. [158]. The first detailed mechanism involving chlorinated species for SiC epitaxial growth was developed by Veneroni and coworkers in 2006 [16]. It comprised a model of the gas phase and surface chemistry active during the deposition of light hydrocarbons, silane, and either chlorosilanes and/or HCl as chlorinated species. In the last years several other *in silico* approaches were focused on describing the impact on the gas chemistry and growth rate induced by the addition of chlorine precursors. Recently Leone et al. [161] considered the presence of five different silicon precursors (SiH_4, SiH_2Cl_2, $SiHCl_3$, $SiCl_4$ and CH_3SiCl_3) in the gas-phase kinetic scheme allowing to reach a further improvement of our understanding of the SiC growth process.

4.2 Aim of the work and approach

The purpose of the present study is to provide a widespread analysis of the chemical kinetics active during the epitaxial CVD of polycrystalline Si and SiC when chlorine is present in the gas phase. Such analysis is focused on the reaction kinetics and on the effect of the micro kinetics on the global features of the reactors.

Initially the work was focused on poly silicon CVD and it has been only lately extended also to SiC. Thus it was proposed a new Si-H-Cl gas phase mechanism, which takes place during poly Si CVD from trichlorosilane. That reaction scheme was assembled starting from a literature research [49-55, 149, 155-157] and then including other new classes of reactions proposed here for the first time. The second step consisted in the estimation of all the gas phase kinetic constants at the same level of theory. The details about the theoretical methods used for such *ab initio* calculations are provided in Section 2.3. Also the kinetic parameters taken from the literature were here re evaluated because the data reported in the referring articles were achieved with methods less accurate with respect to that used in the present work. Then the homogeneous reactive mechanisms, was combined with a related surface kinetic scheme previously developed by this research group [50].

The gas phase and surface kinetic mechanisms were used to simulate Si deposition through two different reactor models. In the first it is assumed that the reactor is perfectly stirred (PSR). The primary intent of these simulations was to determine the main reaction pathways active in the typical operative conditions of Siemens reactors as a function of deposition temperature and residence time, neglecting at a first level of approximation transport phenomena. Further details are reported in Section 2.6.1. This model was also used to evaluate the effect of some other important operative parameters in Siemens reactors, in order to explain their effect from the qualitative point of view. The second reactor model is 1D and it was used to test the predictive capability of the proposed reaction scheme by simulating experimental data collected in a horizontal reactor [91]. Hence it was accounted a simplified contribution of the transport phenomena. Other related information can be found in Section 2.6.2.

Finally it was also verified whether the new proposed mechanism is also effective for SiC CVD when chlorine is present in the gas phase.

Therefore it was included in a wider kinetic scheme involving further reactions pathways previously evaluated in the literature to describe the Si-H-C [158] reactivity. The surface kinetics was taken from the literature as well [16]. The new set of reactions here estimated instead constitutes the Si-H-Cl sub mechanism. In particular trichlorosilane and ethylene were assumed respectively as the Si and the C precursors. The new global reactive scheme was then tested in 1D simulations, using the same model cited above. The predictions of those simulations were compared with experimental results measured in an industrial reactor [92].

4.3 Kinetic scheme for poly Si CVD

The kinetic scheme used in the simulations is composed by a gas phase and a surface mechanism, with the main focus on the gas phase kinetics. The surface mechanism used for all the simulations is the same developed previously by this research group [50], where some key parameters were fitted over experimental data. However in this work there were added the adsorption reactions on free surface sites for all the radicals considered in this study. It was assumed that radicals stick on free sites with collisional efficiency. The surface kinetic mechanism is summarized in Table 4.

The gas phase mechanism here developed is reported in Table 5. The bulk of the present work consists thus in the extension of the basic scheme proposed by Cavallotti and Masi in 2011 [50], which consisted only of two reactions describing the decomposition of $SiHCl_3$ and its bimolecular conversion to $SiCl_4$. The gas phase kinetic mechanism is the sum of three different sub-mechanisms: the original two-reaction mechanism, a radical chain mechanism introduced here for the first time for chlorosilanes, and the catalytic SiH_xCl_{4-x} inter-conversion mechanism that involves the formation of dimers and that was first proposed by Swihart and Carr [52]. Summing up the three reactions sets are thus the direct route constituted by reactions C1 and C2, the radical pathway constituted by reactions C3-

C18, and the disilane pathway constituted by reactions C19-C26. All those sub mechanisms are able to describe independently the conversion of $SiHCl_3$ into $SiCl_4$, a key aspect of the reactivity of the Siemens process.

Table 4: Surface kinetic mechanism for poly Si CVD[α].

	Reaction	A	α	E_a
S1	$SiHCl_3 + 4\sigma \rightarrow SiCl^* + H^* + 2Cl^*$	$1.1x10^8$	0.5	-3.80
S2	$H^* \rightarrow 0.5H_2 + \sigma$	$2.0x10^{15}$	0	57.10
S3	$H^* + Cl^* \rightarrow HCl + 2\sigma$	$7.1x10^{25}$	0	65.00
S4	$SiCl_2 + 2\sigma \rightarrow SiCl^* + Cl^*$	$3.2x10^{10}$	0.5	0
S5	$SiCl^* \rightarrow Si_b + Cl^*$	$1.0x10^{14}$	0	50.00
S6	$H_2 + 2\sigma \rightarrow 2H^*$	$2.3x10^{11}$	0.5	12.00
S7	$2Cl^* + Si_b \rightarrow SiCl_2 + 2\sigma$	$1.6x10^{24}$	0	65.00
S8	$Cl^* + SiCl^* \rightarrow SiCl_2 + 2\sigma$	$1.6x10^{24}$	0	65.00
S9	$HCl + 2\sigma \rightarrow H^* + Cl^*$	$5.4x10^{10}$	0.5	0
S10	$SiCl_3 + 3\sigma \rightarrow SiCl^* + 2Cl^*$	$2.8x10^{11}$	0.5	0
S11	$SiHCl_2 + 3\sigma \rightarrow SiCl^* + H^* + Cl^*$	$3.2x10^{11}$	0.5	0
S12	$H + \sigma \rightarrow H^*$	$3.2x10^{12}$	0.5	0
S13	$Cl + \sigma \rightarrow Cl^*$	$5.4x10^{11}$	0.5	0

[α] Kinetic constants expressed as $k = A\,T^{\alpha} exp\left(-\frac{E_a}{RT}\right)$ in units consistent with cm, s and mol. All adsorption rate constants expressed in $cm^2/mol/s$ and computed for a surface density of $6.8\ 10^{14}$ sites/cm^2. Activation energies in kcal/mol. The part of the kinetic mechanism constituted by reactions S1-S9 was taken from the literature [50].

As it is well known, at process conditions reaction C1 proceeds fast and rapidly reaches equilibrium, so that the exact value of its kinetic constant is not particularly relevant. It is however here of some interest to compare the value of this kinetic constant with what reported previously in the literature. The present *ab initio* calculations overestimate only by a factor of 2 the experimental $SiHCl_3$ decomposition data of Walker at al. [149], which can be considered as a good agreement given the experimental and computational uncertainties.

Table 5: Gas phase kinetic mechanism for poly Si CVD[β].

	Reaction	Forward			Backward		
		A	α	E_a	A	α	E_a
C1[a]	$SiHCl_3 \rightarrow SiCl_2 + HCl$	$3.2x10^{12}$	0.65	70.4	$4.9x10^{3}$	2.52	14.2
C2[a]	$SiHCl_3 + HCl \rightarrow SiCl_4 + H_2$	$2.2x10^{3}$	2.67	42.6	$6.8x10^{6}$	2.11	60.6
C3	$SiHCl_3 \rightarrow SiCl_3 + H$	$5.9x10^{17}$	-0.75	93.8	$2.5x10^{13}$	0.08	-0.2
C4	$SiHCl_3 \rightarrow SiHCl_2 + Cl$	$3.5x10^{20}$	-1.3	110.4	$3.4x10^{14}$	-0.12	-0.2
C5	$SiCl_4 \rightarrow SiCl_3 + Cl$	$7.0x10^{22}$	-1.96	111.6	$9.0x10^{12}$	0.23	-0.4
C6	$SiH_2Cl_2 \rightarrow SiHCl_2 + H$	$8.7x10^{17}$	-0.7	93.1	$1.4x10^{13}$	0.18	-0.4
C7	$Si_2Cl_6 \rightarrow 2SiCl_3$	$9.5x10^{22}$	-2.15	79	$3.8x10^{11}$	0.25	0.2
C8	$Cl_2HSiSiHCl_2 \rightarrow 2SiHCl_2$	$5.1x10^{23}$	-2.37	77.7	$1.3x10^{12}$	0.17	0.3
C9	$Si_2HCl_5 \rightarrow SiCl_3 + SiHCl_2$	$5.2x10^{23}$	-2.36	78.9	$2.6x10^{11}$	0.43	-0.1
C10	$SiHCl_2 \rightarrow SiCl_2 + H$	$1.3x10^{19}$	-1.25	50.3	$7.2x10^{12}$	0.35	-0.7
C11	$SiCl_3 + HCl \rightarrow SiHCl_3 + Cl$	$7.3x10^{6}$	1.56	9.5	$1.8x10^{11}$	0.74	0
C12	$SiHCl_2 + HCl \rightarrow SiH_2Cl_2 + Cl$	$8.0x10^{6}$	1.63	9.6	$1.2x10^{11}$	0.94	-0.7
C13	$SiCl_3 + SiHCl_3 \rightarrow SiCl_4 + SiHCl_2$	$3.8x10^{4}$	2.66	18	$1.5x10^{5}$	2.57	17.2
C14	$SiHCl_2 + SiHCl_3 \rightarrow SiCl_3 + SiH_2Cl_2$	$5.1x10^{3}$	2.98	6.1	$5.7x10^{3}$	3.04	5.4
C15	$SiCl_3 + HCl \rightarrow SiCl_4 + H$	$1.2x10^{2}$	3.08	11.8	$9.3x10^{9}$	1.47	19
C16	$SiHCl_3 + H \rightarrow SiCl_3 + H_2$	$7.4x10^{8}$	1.6	2.7	$1.3x10^{5}$	2.44	13.9
C17	$SiHCl_2 + HCl \rightarrow SiHCl_3 + H$	$2.4x10^{2}$	3	12	$4.7x10^{9}$	1.48	20.1
C18	$SiH_2Cl_2 + H \rightarrow SiHCl_2 + H_2$	$1.2x10^{9}$	1.62	2.8	$2.2x10^{5}$	2.39	14.8
C19	$Si_2Cl_6 \rightarrow SiCl_2 + SiCl_4$	$1.2x10^{12}$	0.47	48.3	$3.7x10^{1}$	3.03	13
C20	$SiHCl_5 \rightarrow SiCl_2 + SiHCl_3$	$6.1x10^{11}$	0.48	45.5	$4.0x10^{1}$	3.01	12
C21	$Cl_2HSiSiHCl_2 \rightarrow SiCl_2 + SiH_2Cl_2$	$1.3x10^{11}$	0.65	48.4	$1.2x10^{1}$	3.16	15.3
C22	$Cl_3SiSiClH_2 \rightarrow SiCl_2 + SiH_2Cl_2$	$1.2x10^{11}$	0.66	43.4	$4.1x10^{0}$	3.24	9.4
C23	$Cl_3SiSiClH_2 \rightarrow SiHCl + SiHCl_3$	$6.9x10^{10}$	0.62	46.6	$1.6x10^{1}$	2.99	1.8
C24	$Si_2HCl_5 \rightarrow SiHCl + SiCl_4$	$1.5x10^{11}$	0.6	51.0	$1.6x10^{2}$	2.93	4.9
C25	$SiHCl + SiHCl_3 \rightarrow Si_2Cl_4 + H_2$	$1.3x10^{1}$	3.24	8.0	$1.3x10^{4}$	2.36	6.2
C26	$Si_2Cl_4 \rightarrow 2SiCl_2$	$1.4x10^{24}$	-2.92	24.9	$3.7x10^{13}$	-0.23	0.4

[β]Kinetics constants are high pressure limits and are expressed as $k = A\,T^{\alpha} exp\left(-\frac{E_a}{RT}\right)$ in units consistent with cm, s and mol. Activation energies in kcal/mol.

The radical pathway here investigated consists in the set of homolytic decomposition reactions C3-C10 and is complemented by several propagation reactions (C11-C18). Termination reactions are given by the backward C3-C9 reactions. The kinetic constants of dissociation reactions were determined using variational transition state theory as described in Section 2.3. In base of the experience maturated in this research group,

the level of uncertainty of the present calculations should be about a factor of 4, half due to the use of a single reference wave function to determine the PES and half to the treatment of the transitional degrees of freedom in the harmonic approximation. The hindered rotor approximation was instead applied for the reactions C7-C9, involving disilanes to describe the Si-Si torsions. The radical reactions C13-C18 are characterized by a well defined saddle point connecting the reactant and product minima on the PES. In the transition states of reactions C13 and G14, where H or a Cl are transposed between two moieties, the forming and breaking Si-Cl-Si and Si-H-Si bonds are aligned. The respective torsional motions around the reaction coordinate are slightly hindered and were therefore treated as hindered rotors.

The disilanes mechanism considered in this work consists of reactions C19-C26, which is a selection of those proposed by Swihart e Carr [52] to describe disilane reactivity. In fact only the portion of the Swihart and Carr scheme relevant to the $SiHCl_3$ reactivity was considered in the present calculations, in order to limit the complexity of the overall mechanism. The reactions to include were determined through a sensitivity analysis on the original scheme performed in the range of operative conditions relevant for $SiHCl_3$ CVD and considered in this study (see Table 7 in Section 4.4.2). Several tests with the full original mechanism were performed to determine the consistence of the chosen subset of reactions. In all cases the reduced mechanism was able to reproduce the results obtained using the full kinetic mechanism in terms of overall conversion and gas phase composition of the most abundant species with an accuracy of ±10%, which was considered satisfactory. In most of these reactions the transition state is characterized by a bridged structure. In three cases (reactions C20-C22) two parallel transitional states with similar energies are possible. A global reaction rate was there calculated as the sum of that of the two channels. The two transition states located for reaction C20 are reported in Figure 22 to provide an example.

Also, two optical isomers are sometimes possible and were therefore considered in the calculation of the reaction path degeneracy. As found for the radical mechanism, several TSs are characterized by a low vibration corresponding to the rotation around the Si-Si bond. However for these reactions this motion was treated in the harmonic approximation, as its description as a hindered rotation would have lead to the disruption of the bridged structure, and thus easily to the evolution of the reaction towards different wells.

Reactions C25 and C26 involve the formation and consumption of Si_2Cl_4. Similarly to Swihart and Carr [52] in this work only the most stable Si_2Cl_4 isomer was considered, which structure is $Cl_3SiSiCl$. The reason is that isomerization to $Cl_2SiSiCl_2$ is very fast compared to the other reactions, so that it is reasonable to assume chemical equilibrium between the two isomers and that the most stable isomer dominates over the other. It is here important to point out that the products of reaction C25 differ from those proposed by Swihart and Carr. An intrinsic reaction path analysis showed in fact that the addition of H_2 to Si_2Cl_4 leads directly to the formation of SiHCl and $SiHCl_3$, without the formation of a $Si_2H_2Cl_4$ intermediate. The kinetic constant of reaction C26 was determined using variational transition state theory treating the torsional rotation in the hindered rotor approximation.

The kinetic mechanism, reported in Table 5, consists of 26 reversible reactions and involves the following 16 chemical species: H_2, HCl, $SiHCl_3$, $SiCl_4$, SiH_2Cl_2, $SiCl_2$, SiHCl, Si_2Cl_6, Si_2HCl_5, $HCl_2SiSiCl_2H$, $H_2ClSiSiCl_3$, Si_2Cl_4, $SiCl_3$, $SiHCl_2$, H, Cl. The calculated thermodynamic parameters are in quantitative agreement with the experimental data of Chase et al. [165] and of Shuman et al. [157]. Indeed the maximum difference between the calculated reaction enthalpies and entropies and available experimental data are of 1.5 kcal/mol and 1.5 cal/mol/K, respectively, which is within the uncertainties of the experimental and computed data. A comparison between calculated and experimental data is reported in Table 6. Further details about the rotational PESs and inertia

moments, as well as about the optimized structures of the wells and saddle points are provided as supplementary information in the referring article [146].

Table 6: Comparison of estimated thermodynamic parameters with literature data (enthalpies in kcal/mol and entropies in cal/mol/K at 298 K and 1 bar).

	Calculated		Experimental	
Reaction	ΔH_0^R	ΔS_0^R	ΔH_0^R	ΔS_0^R
$SiHCl_3 \rightarrow SiCl_3 + H$	93.2	28.9	93.4[a]	28.4[b]
$SiCl_4 \rightarrow SiCl_3 + Cl$	109.7	35.3	110.1[a]	36.4[b]
$Si_2Cl_6 \rightarrow 2SiCl_3$	78.2	43	79.8[a]	
$H_2 \rightarrow 2H$	105.1	23.6	104.0[b]	23.6[b]
$HCl \rightarrow H + Cl$	103.4	20.7	103.1[b]	22.2[b]
$SiHCl_3 \rightarrow SiCl_2 + HCl$	55.7	36.9	56.2[b]	36.9[b]
$SiH_2Cl_2 \rightarrow SiCl_2 + H_2$	35.9	30.1	36.3[b]	29.9[b]
$SiCl_4 + H_2 \rightarrow SiHCl_3 + HCl$	18.2	9.3	17.7[b]	9.3[b]
$SiHCl_3 + H_2 \rightarrow SiH_2Cl_2 + HCl$	19.8	6.9	19.9[b]	7.0[b]

a) Shuman et al. [157]; b) Chase [165]

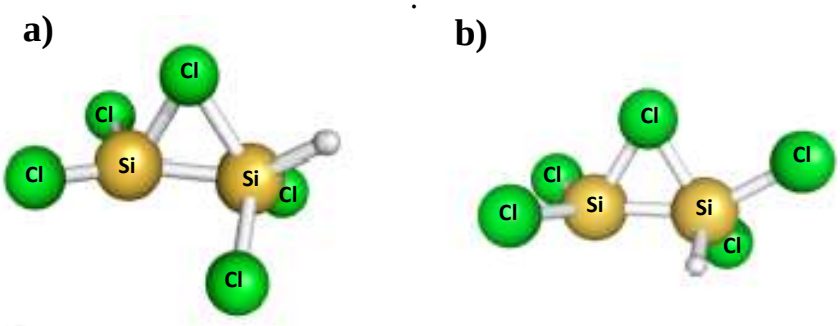

Figure 22: Transition states located for reaction G20: $Si_2HCl_5 \rightarrow SiCl_2 + SiHCl_3$. Two pathways are possible, differentiated by the relative position of the H atom. The dissociation to products takes place directly after the transposition of Cl.

4.4 Results with PSR model for poly Si CVD

The gas phase kinetic mechanism reported in Table 5 and the surface mechanism of Table 6 were embedded in a PSR reactor model and used to study the reaction kinetics. Despite the simplicity of the reactor models, those tests were very useful to clarify some of the main features related to the poly Si CVD in Siemens reactors.

4.4.1 Micro kinetic analysis

The first tests with the PSR model were aimed to determine the most important reaction pathways active in the gas phase. However also the inclusion of the surface kinetics plays a fundamental role since HCl is a by product of the deposition process, so that an increase of the deposition rate corresponds to an increase of the HCl gas phase concentration, which affects considerably the overall reactivity. As mentioned in Section 4.1, a critical aspect of this system is the determination of the rate at which HCl and $SiHCl_3$ are converted to $SiCl_4$ and H_2. A previous study has in fact shown that a lower HCl content in the gas phase allows increasing the Si deposition rate, as etching is decreased [50]. In the present kinetic analysis three possible reaction routes are compared: the concerted pathway we proposed in that previous work (reaction G1-G2), a radical chain mechanism (reaction C3-C18), and the disilane mechanism proposed by Swihart and Carr (reactions C19-C26) [52].

The analysis was carried out using a PSR model, assuming a gas feed composed by hydrogen and trichlorosilane, in the range of operative conditions reported in Table 7, which correspond to typical conditions at which Si is deposited from $SiHCl_3$ in Siemens reactors.

Table 7: Operative conditions used in PSR simulations.

Variable	Operative conditions
Pressure	6 atm
Surface temperature	1173 – 1373 K
Gas temperature	973 – 1173 K
Reactor volume	0.15 m^3
Deposition area	1.5 m^2
Gas feed	10^{-1} - 10^7 slm
Mole fraction $SiHCl_3$	0.4
Bath Gas	H_2

The concentration profiles of $SiHCl_3$ and SiH_2Cl_2 and conversion of $SiHCl_3$, calculated at two surface temperatures (1173 K and 1323 K) with gas phase temperatures 200 K smaller than surface temperatures, are

reported in Figures 23 and 24 as a function of residence time. Simulations were performed using the global mechanism reported in Table 5, a sub mechanism in which the disilane pathway was blocked (the radical mechanism), and a sub mechanism in which the radical pathway was omitted (the disilane pathway).

The first results of these simulations is that for all the considered conditions the concerted mechanism of reactions C1 and C2 is at least one order of magnitude slower than the other two mechanisms. Therefore it will not be further discussed here.

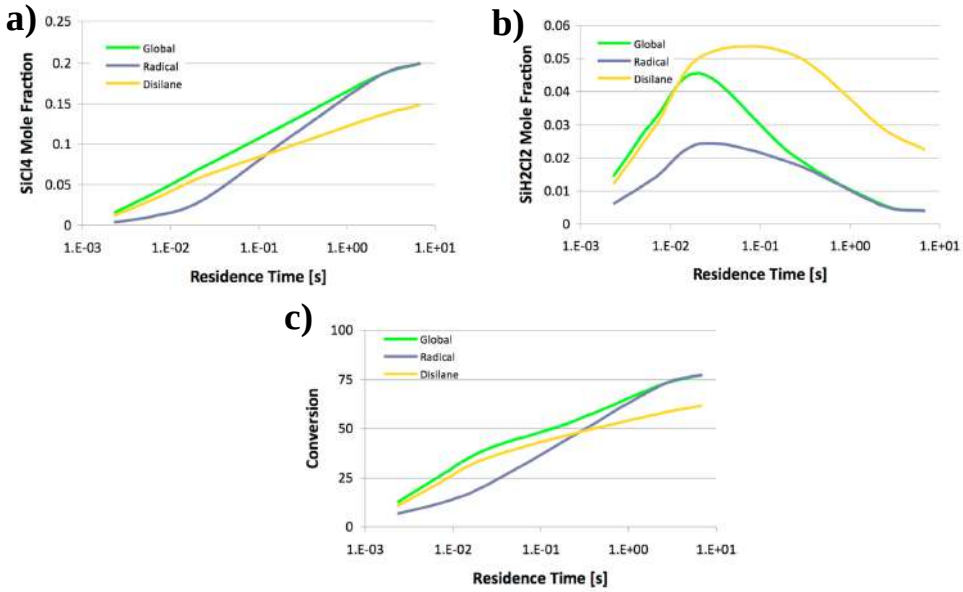

Figure 23: Mole fractions of a) $SiCl_4$; b) SiH_2Cl_2; c) $SiHCl_3$ conversion (percentage) calculated using the PSR model with the operating parameters reported in Table 7 at a gas phase temperature of 1173 K and a surface temperature of 1373 K.

The simulations reveal that at low residence times the dominant reaction route is well described by the disilane mechanism. In these conditions $SiCl_4$ and $Si_2H_2Cl_2$ are produced in similar mole fractions. This can be clearly understood looking at the dominant sequence of reactions. The gas phase reactivity is initiated by the decomposition of $SiHCl_3$ into $SiCl_2$ and HCl through C1 and is followed by the reaction of sylylene with $SiHCl_3$ to form pentachloro disilane ($C20^r$). Once formed Si_2HCl_5 decomposes to form $SiCl_4$ and SiHCl through C24. SiHCl reacts successively fast with $SiHCl_3$ through $C23^r$ to form $H_2ClSiSiCl_3$, which decomposes to SiH_2Cl_2

and $SiCl_2$. The desorption of $SiCl_2$ from the surface or its generation in the gas phase through C1 enhances this reaction loop, which is summarized by the following set of reactions:

C1) $$SiHCl_3 \rightarrow SiCl_2 + HCl$$

C20^r) $$SiHCl_3 + SiCl_2 \rightarrow Si_2HCl_5$$

C24) $$Si_2HCl_5 \rightarrow SiCl_4 + SiHCl$$

C23^r) $$SiHCl_3 + SiHCl \rightarrow H_2ClSiSiCl_3$$

C22) $$H_2ClSiSiCl_3 \rightarrow SiH_2Cl_2 + SiCl_2$$

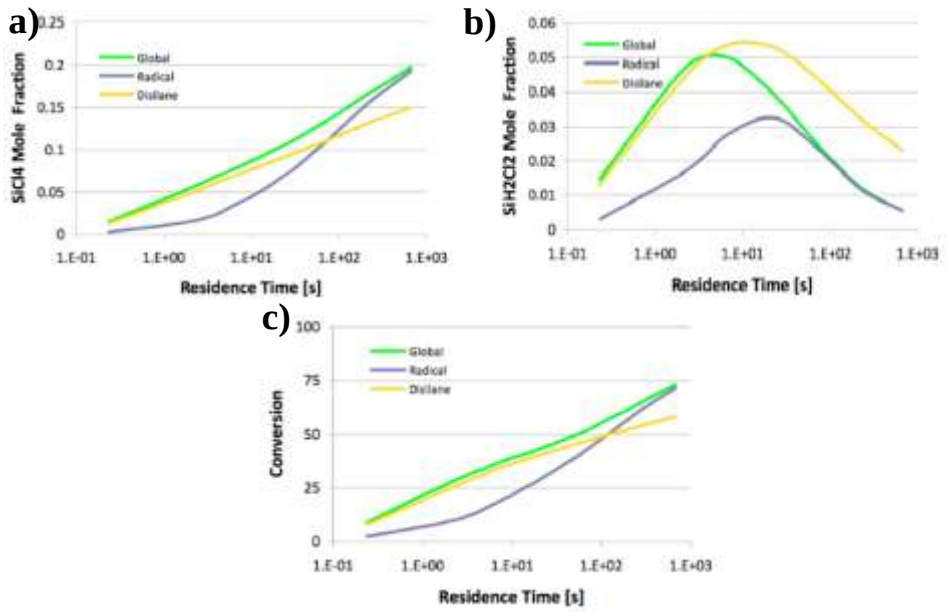

Figure 24: Mole fractions of a) $SiCl_4$; b) SiH_2Cl_2; c) $SiHCl_3$ conversion (percentage) calculated using the PSR model with the operating parameters reported in Table 7 at a gas phase temperature of 973 K and a surface temperature of 1173 K.

As HCl gas phase concentration increases beyond a critical threshold as a result of Si deposition the following set of reactions becomes more and more important, making $SiCl_4$ the dominant product:

C25) $$SiHCl_3 + SiHCl \rightarrow Si_2Cl_4 + H_2$$

C24) $$Si_2Cl_4 \rightarrow 2SiCl_2$$

The reason for this behavior is that reactions C1, C22, and C23^r reach equilibrium, thus effectively limiting the SiH_2Cl_2 formation rate.

Contextually at high residence times the reaction of SiHCl with $SiHCl_3$ becomes sufficiently fast to convert it to Si_2Cl_4, which regenerates $SiCl_2$ and thus efficiently converts SiH_2Cl_2 to $SiCl_4$. It is here important to point out that though this reaction pathway is qualitatively similar to the one already suggested by Swihart and Carr, it is not the same as the present study differs for the explicit consideration of the surface reactivity and for the reactant, which is $SiHCl_3$ and not SiH_2Cl_2, as in their work.

The $SiCl_4$ and SiH_2Cl_2 concentration profiles reported in Figures 24 and 25 clearly show that with the increase of the residence time the radical mechanism becomes dominant. Also in this mechanism the formation of disilanes plays a key role. In fact, the homolytic cleavage of the Si-Si bond requires activation energies at least 15 kcal/mol smaller than those needed for the unimolecular dissociation of chlorinated monosilanes. The initiation of the radical chain occurs in 3 steps, of which the first two (C1 and C20^r) are in common with the disilanes mechanism while the third is the unimolecular decomposition of Si_2HCl_5 into $SiCl_3$ and $SiHCl_2$.

C1) $$SiHCl_3 \rightarrow SiCl_2 + HCl$$

C20^r) $$SiHCl_3 + SiCl_2 \rightarrow Si_2HCl_5$$

C9) $$Si_2HCl_5 \rightarrow SiCl_3 + SiHCl_2$$

The $SiCl_3$ and $SiHCl_2$ radicals so generated can further react through two competitive propagation routes. The first propagation mechanism is active at low HCl concentrations. In these conditions $SiCl_3$ and $SiHCl_2$ react through reactions C13 and C14 with $SiHCl_3$ to form $SiCl_4$ and SiH_2Cl_2:

C13) $$SiHCl_3 + SiCl_3 \rightarrow SiCl_4 + SiHCl_2$$

C14) $$SiHCl_3 + SiHCl_2 \rightarrow SiH_2Cl_2 + SiCl_3$$

With the increase of the residence time, and thus of HCl concentration, the establishment of equilibrium in the set of reactions leading to the formation of SiH_2Cl_2 promotes the initiation of the second propagation route, which is associated to an enhancement of the $SiCl_4$ selectivity:

C10) $$SiHCl_2 \rightarrow SiCl_2 + H$$

C16) $SiHCl_3 + H \rightarrow SiCl_3 + H_2$

The radical chain termination can occur through two distinct routes. The first is radical recombination, favored especially at high gas phase temperatures and pressures. As $SiCl_3$ is the most abundant radical, the homo-molecular reaction $C7^r$ is in general the fastest. However other termination routes are possible. In particular the radical mechanism is terminated by dissociative adsorption of the radicals on the surface, especially through reaction S10, in reactors with a high ratio between the deposition area and the reactor volume and high surface temperatures (or high gas surface gradients), when a high concentration of free sites are present (in the simulated conditions more than 90% of the surface is covered by adsorbed species).

$C7^r$) $SiCl_3 + SiCl_3 \rightarrow Si_2Cl_6$

S10) $SiCl_3 + 3\sigma \rightarrow SiCl^* + 2Cl^*$

The common feature of both mechanisms is the key role played by $SiCl_2$, which is necessary to activate the reactivity through its addition to $SiHCl_3$ to form Si_2HCl_5, the precursor of both the radical chain mechanism and of the disilane reaction pathway. The initiation reaction C9 is conditioned by the concentration of $SiCl_2$ present in the gas phase, which is limited by the attainment of equilibrium in reaction C1 and by the amount of HCl released during silicon deposition. This means that the gas phase and the surface kinetics are strongly inter related. Indeed deposition can proceed only with the consumption of HCl in the gas, but the latter is produced during the deposition itself. Thus also the formation of $SiCl_4$ in the gas requires that the Si growth takes place. The effect of H_2 is instead important for the surface kinetics because it promotes the desorption of HCl from the surface, increasing the fraction of free sites.

The analysis of the simulation results reported in Figures 24 and 25 shows that the kinetics is mostly radical at high residence times, whereas the system is well described by the disilane mechanism at low residence times. The transition between the two mechanisms is determined by the

attainment of equilibrium between SiH_2Cl_2 and $SiHCl_3$ and by the concomitant increase of the Si_2HCl_5 concentration, the initiator of the radical chain. It is also interesting to observe that both in the disilane and in the radical mechanism as the residence time grows the SiH_2Cl_2 formed at low residence times is rapidly converted to $SiCl_4$. The main reaction routes determined from this analysis are summarized in Figures 25a and 25b for the disilane and the radical mechanisms, respectively. The reaction network comprises also surface reactions since, as explained above, the surface and gas phase kinetics are mutually dependent.

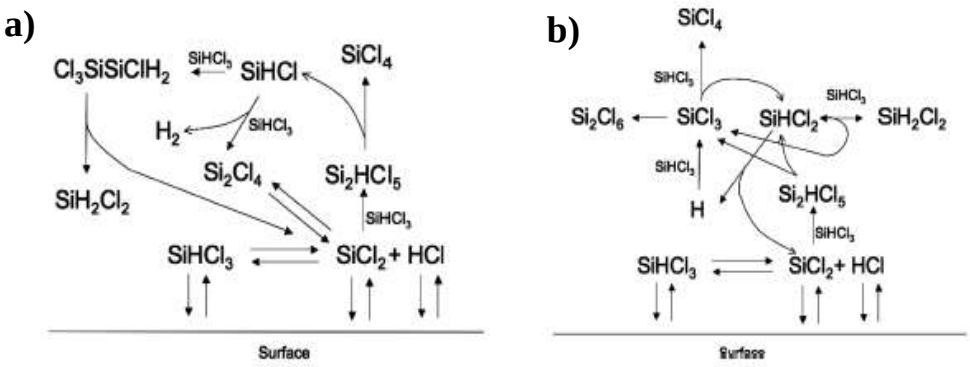

Figure 25: Main reaction pathways in a) disilanes mechanism; b) radicalic mechanism.

The mechanisms discussed above are also confirmed by a sensitivity analysis reported in the referring article [146]. The simulation results indicate that the reactions whose rate is limiting for the formation of $SiCl_4$ are C10 and C13 for the radical mechanism and C23, C24, and C25 for the disilane mechanism. The role of these reactions in the kinetic mechanism is discussed in detail above. It is however important to point out that the absolute values of the sensitivity coefficients are relatively small, which can be ascribed to the fact that the gas phase reacting system is in proximity of thermodynamic equilibrium.

4.4.2 Simulations of growth in Siemens reactors

At a first level of approximation, the simple PSR model introduced in the previous section can be used to study qualitatively deposition in a Siemens reactor, as the turbulent conditions at which these reactors are

operated lead to an almost homogeneous distribution of the reactants in the deposition chamber. Some shortcomings of this approximation are described in a previous work [50]. The typical residence times for these reactors, decreasing significantly between the beginning and the end of the deposition process with the progressive increase of the rod diameter, is comprised between tens and hundreds of seconds. It is thus interesting to complement the results obtained in the previous section with the Si yields and deposition rates computed for the same simulation conditions. The results, sketched in Figures 26, show that with the increase of the residence time the deposition rate decreases and the yield in deposited Si becomes higher. These two parameters are inter related, since an augment of the percentage of deposited Si over the overall Si precursor fed to the reactor leads to an increment of the concentration of HCl in the gas phase, which has the effect of limiting Si deposition because of etching.

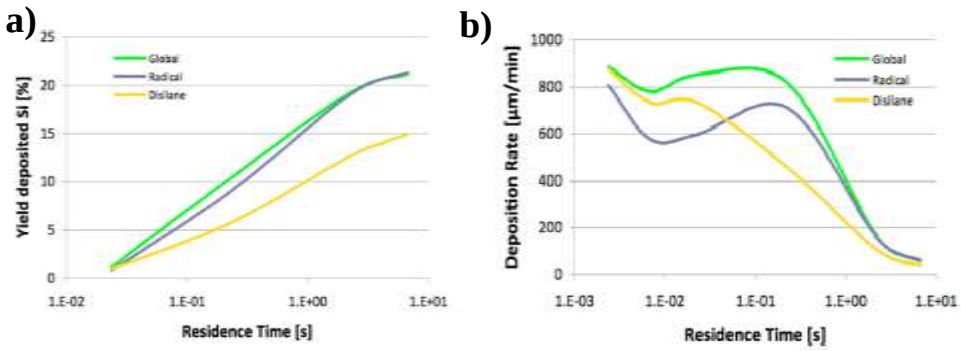

Figure 26: a) Yield in deposited Si, defined as percentage of Si deposited over the total Si fed to the reactor; b) deposition rate calculated using the PSR model with the operating parameters reported in Table 7 at a gas phase temperature of 1173 K. The residence time of the Siemens process vary between tens and hundreds of seconds.

In this context, the analysis of Figures 23 and 24 shows that at higher yield in deposited Si is related to an enhancement of the production of $SiCl_4$. This has a beneficial effect since the production of $SiCl_4$ requires the consumption of an equal amount of HCl, thus decreasing the etching and allowing to proceed with the growth. Finally, the simulations clearly show that in the conditions in which Siemens reactor are operated the radical mechanism prevails over the disilane mechanism.

The sensitivity of the Siemens growth process to the ratio between volume and surface and to the inlet $SiHCl_3$ mole fraction is analyzed in Figures 27. The reference values reported in Table 7 and used to perform most of the simulations correspond to the reactor layout described in a previous study [50] and are representative of growth conditions prevailing at the end of the deposition, when the volume to surface ratio (10 cm in this case) is at a minimum. It should however be pointed out that the reference reactor is quite small, so that surface to volume ratios in real reactors are likely to be much smaller.

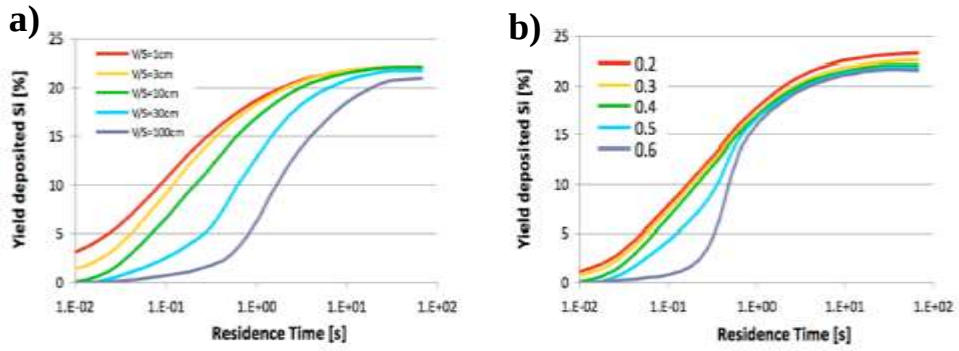

Figure 27: Yield in deposited Si at the same conditions of Figure 27at different a) volume to surface ratio; b) $SiHCl_3$ inlet mole fraction.

The simulation results show that the volume to surface ratio is an important parameter in order to optimize the deposition process, as longer residence times are needed when it increases in order to obtain the same Si yields. This indicates that a modification of the flow rate would help to optimize the deposition process in a Siemens reactor. The sensitivity to the inlet mole fraction of $SiHCl_3$ is less evident, except when $SiHCl_3$ in the inlet becomes about 50% of the inlet mixture, since in this case the decrement of the complementary H_2 concentration starts affecting significantly the surface kinetics.

4.5 Simulations of an experimental horizontal reactor

The simulation of epitaxial deposition in a horizontal reactor was performed using the 1D model. Such model was used to simulate the horizontal reactor used by Angermeier and coworkers [91] to deposit Si

from a $H_2/SiHCl_3$ feed as a function of substrate temperature. The growth rate calculated as a function of temperature is reported in Figure 28 together with the reactor geometric parameters and operating conditions at which the simulations were performed.

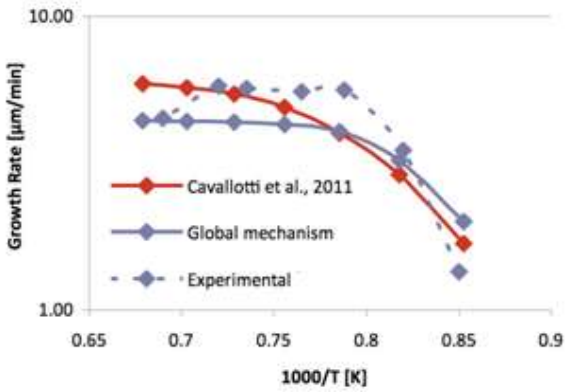

Figure 28: Deposition rate calculated using the horizontal reactor model. The deposition rate data are compared with the experimental data of Angermeier et al.[91] and the results of simulations performed using the simple gas phase kinetic mechanism composed of reactions C1 and C2 [50]. Cold wall horizontal reactor 50 cm long, 7.0 cm high and 19.0 cm wide. $SiHCl_3$ inlet mole fraction 0.137, inlet gas flow rate 5000 sccm.

The growth rate data show that the kinetic model here developed is able to describe the transition to a flat deposition profile that is observed with the increase of the temperature more properly than the previous model developed by this research group [50]. The slight underestimation of the deposition rate that is observed at high temperatures in the diffusion controlled regime and the overestimation observed at low temperatures in the kinetic controlled regime are most likely determined by deficiencies of the fluid dynamic model, rather than to the gas phase kinetics. The analysis of the reaction rates showed that in the diluted conditions in which these reactors operate the disilane mechanism is dominant at low temperatures, while with the enhancement of the temperature, and thus of the reactant conversion, the radical mechanism becomes the fastest. Furthermore also the removal from the substrate of the corrosive HCl released during the growth was found to have a critical role.

4.6 Extension to SiC CVD

The kinetic mechanism here proposed, was then included in a kinetic scheme, aimed to describe the deposition of SiC from trichlorosilane and ethylene. Indeed, even if a hydrocarbon sub mechanism must be added to describe the SiC CVD, the part concerning the Si-H-Cl reactivity should be the same. Further details can be found in the referring article [147], including two other models for N and Al doping.

4.6.1 Kinetic mechanism for SiC CVD

The gas phase e kinetics for SiC is described using a kinetics mechanism composed by two parts: the Si-H-C sub mechanism hypothesized by Danielsson et al. [158], and the Si-H-Cl sub mechanism here proposed and widely described in Sections 4.3 and 4.4. The surface mechanism instead was taken from the work of Veneroni et al. [16]. As the details about such kinetics are reported above or have mostly been published in the literature, it would be redundant to discuss them here explicitly. Anyway most of them are included in the supplementary information file of the referring article [147].

The Danielsson [158] sub mechanism for Si-H-C kinetics has been slightly modified for what concerns the CH_4 and decomposition rate constant, for which the Baulch et al. [166] high pressure data were used. From the same authors [166] were also taken the decomposition rate of C_2H_4 to C_2H_3 and C_2H_2. Furthermore the accurate estimation of Michael et al. was used [166] for the important rate constant for the reaction between CH_4 and H to give CH_3 and H_2, which rules the equilibrium between the two most abundant gas phase chemical species. Differently from Danielsson et al. [158], all the reactions were considered as reversible, with backward rate constants determined using detailed balances, made exception for the hydrogen decomposition rate constant, for which explicit expressions were used for the forward and backward

processes, to correctly account for third body efficiency. For what concerns the Si-H part of the Danielsson mechanism, only the SiH_4 decomposition rate constant was changed and substituted with the 0.1 bar value, calculated by Barbato et al. [57] using RRKM master equation simulations. It is noteworthy that this is the only rate constant of the kinetics mechanism for which the pressure dependence has been explicitly accounted for. A preliminary sensitivity analysis was performed on the rate constants that may be in fall off in the considered operating conditions, notably the CH_4 unimolecular decomposition. Such analysis has shown that the slow down effect given by fall off on decomposition rate constants may impact the simulation results in the first part of the susceptor, in which the temperature changes are most significant. At the highest temperatures instead, after the radical reactions have been initiated, the sensibility to pressure becomes minimal. On the whole, it could be concluded that the pressure dependence of the rate constants should be considered if a quantitative modeling of the growth rate profiles are needed. Anyway if only average growth rate and concentration values are desired, it may then be safely neglected.

The Si-H-Cl sub mechanism originally hypothesized by this research group [16], which was based on the study of Valente et al. [49], has been totally modified with the inclusion of the gas phase Si-H-Cl mechanism proposed in this work to describe the chlorosilanes gas phase reactivity. The mechanism upgrade is likely to lead to a significant enhancement of the gas phase reactivity of chlorinated species, as it contains two different reaction routes, that are significantly faster than those present in the original mechanism. However to the Si-H-Cl sub mechanism in Table 5 there were added other reactions, which were found to be not sensitive in the operative conditions explored for Si CVD. Indeed SiC is growth at very different temperatures and pressures, at highly dilutions in H_2. Their kinetic parameters were taken from the literature, where they were

evaluated with accuracies similar to those calculated in this work. Such new reactions are reported in Table 8.

Table 8: New reactions added to the Si-H-Cl sub mechanism[β].

Reaction	$\log_{10}A$	α	E_a	Ref
$SiH_3Cl \leftrightarrow H_2 + SiHCl$	14.39	0	68.4	[54]
$SiH_2Cl_2 \leftrightarrow SiHCl + HCl$	14.84	0	75.8	[54]
$Si + HCl \leftrightarrow SiCl + H$	14.98	0	13.6	[167]
$Si + H_2 \leftrightarrow SiH_2$	12.08	0.5	0	[16]
$SiH_2Cl_2 \leftrightarrow SiCl_2 + H_2$	13.92	0	77.4	[54]
$SiCl_4 + H_2 \leftrightarrow 2\,HCl + SiCl_2$	7.43	1.94	62.2	[50]

[β] Kinetics constants are high pressure limits and are expressed as $k = A\,T^{\alpha} exp\left(-\frac{E_a}{RT}\right)$ *in units consistent with cm, s and mol. Activation energies in kcal/mol*

As it can be observed, for many reactions the rate constants are explicitly given as forward and backward rate parameters, therefore without enforcing detailed balances. This was done as the rate parameters were calculated using high level first principle calculations, based on CCSD(T) theory [73] with extension to the infinite basis set, so that for some of the rate parameters the backward rate constants estimated from first principles were more accurate than those that could be determined using the available thermodynamic parameters. This is consistent with the recent finding of Danielsson et al. [159] that the predictions of SiC kinetic models may be significantly affected by the choice of the thermodynamic data set used in the calculations.

The surface mechanism used to model the SiC growth is the same described by Veneroni et al. [16]. As it is well described in the original paper it will not be further discussed here, apart for remembering that it was used to model with success the growth measured using two different SiC growth reactors in which growth were performed in different operating conditions. Thus its suitability to simulate different SiC deposition conditions was proved and it was confirmed the consistence of the chemical physical assumptions on the basis of which it was developed.

4.6.2 Simulations of an industrial horizontal reactor

The kinetic mechanism described above was tested to simulate an industrial hot wall reactor suitable for SiC deposition that was built by LPE epitaxial technology. All the data here reported have been published in several different papers in the last years [92, 163, 168-173]. The deposition has been performed at an operating pressure of 0.1 bar, which enhances the gas phase diffusion and limits the gas phase reactivity. The simulations were performed using an imposed temperature profile, which in the case of the study of deposition of SiC at 1600 °C is shown in Figure 29a together with the gas phase temperature computed for a feed of 100 slm of H_2. Further details are provided in Section 2.6.2.

As it can be observed, it was assumed that the inductive heating of the SiC coated graphite susceptor will lead to an almost uniform temperature above the substrates, which will however drop rapidly immediately before and after the deposition zone. Also, it was calculated that the gas phase temperature will be about 30 °C lower than that of the surface, which is determined by the fact that the hot wall above the susceptor is expected to have a temperature that is about 100 °C lower. This will give rise to a limited temperature gradient above the deposition surface that, given also the small height of the reactor, is however not going to affect considerably the diffusion of the precursor through thermal diffusion effects. The growth rate profile calculated for the given temperature profile using the Si-C-H-Cl mechanism for a feed of 100 slm of H_2, 30 sccm of $SiHCl_3$ and 22.5 sccm of C_2H_4 is shown in Figure 29b.

The results reported in Figure 29b show that the agreement between model and experiment is good, though the calculated deposition profile seems to be slightly sharper than that measured experimentally. However, considering the several approximations on which the model is based, and most notably the use of a 1D fluid dynamic model rather than a more proper 2D or 3D model, the results may well be considered as fully satisfactory. An important aspect that was observed while performing a

sensitivity analysis of the growth rate over gas phase mechanism is that the computation of the backward reactions of the hydrocarbon chemistry from detailed balance rather than using the explicit expressions given by Danielsson et al. [158] has a non negligible impact on the growth rate profile, which would be smoother using the Danielsson et al. full kinetic mechanism. The reason is that this change of the gas phase mechanism affects the concentration of methyl, which is the main SiC carbon precursor. Though the difference between the two mechanisms is limited (the deposition profile changes by no more than 20%), this result suggests that some improvement of the hydrocarbon gas phase mechanism may still be possible.

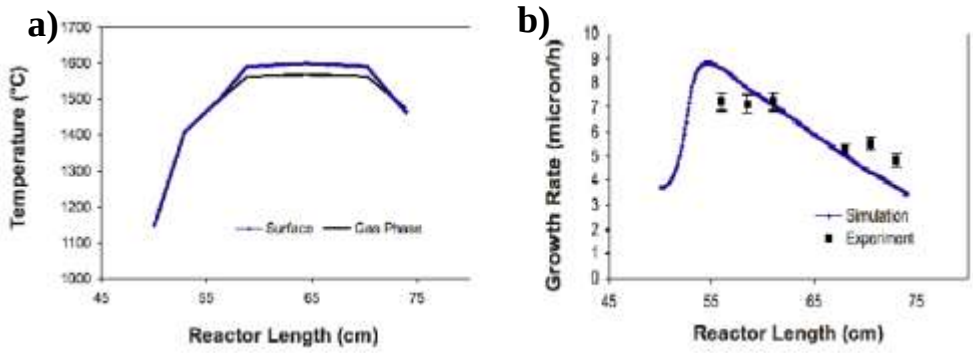

Figure 29: Results calculated using the Si-C-H-Cl mechanism for a feed of 100 slm of H_2, 30 sccm of $SiHCl_3$ and 22.5 sccm of C_2H_4 and substrate temperature of 1600°C a) temperature profiles; b) growth rate experimental and calculated.

In order to test the impact that the inclusion of the new Si-H-Cl mechanism on the gas phase chemistry two different simulations were performed, one with the original mechanism [16] and the other with the updated mechanism. The concentration profiles computed for the main gas phase species are shown in Figures 30 (old mechanism) and 31 (new mechanism). As it can be observed from the comparison of the two sets of results, the differences are significant for some chemical species, while the concentration of some key Si growth precursors, such as $SiCl_2$, is almost untouched. The result is that the impact of the new mechanism on the growth rate is almost negligible with the current model, as the concentration of the key chemical precursor to the film growth, $SiCl_2$, is

not modified. On the other hand it can be observed that the gas phase concentration of many relevant species is considerably changed.

The comparison between the results obtained using the two kinetic models clearly show that the original kinetic model, that lacks the radical and disilane conversion pathways, significantly underestimates the gas phase reactivity. The result is that the $SiHCl_3$ decomposition extent is overestimated by a factor of 3 while the formation of SiH_2Cl_2, SiH_3Cl are underestimated by factors of 20, 30 while the $SiCl_4$ concentration is overestimated by a factor of about 1000. The reason for this behavior is that the original Si-H-Cl gas phase model misses some key reaction pathways for the inter conversion of the main SiH_xCl_{4-x} chlorinated species.

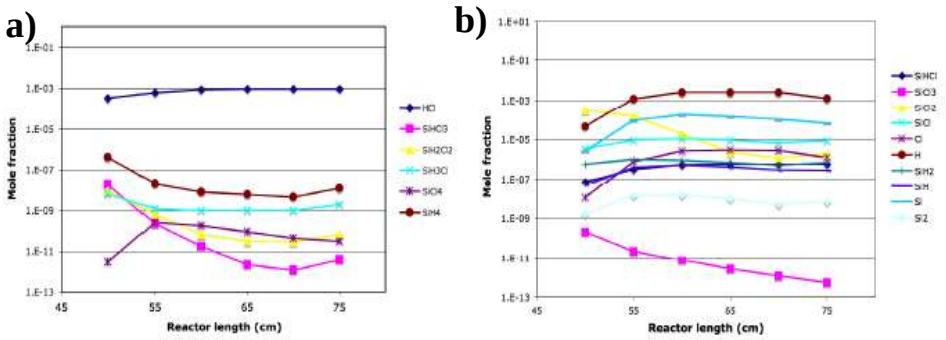

Figure 30: Mole fractions of relevant species calculated above the susceptor for the same conditions of Figure 29 using the old Si-H-Cl mechanism [16] to describe the conversion of the chlorinated precursors.

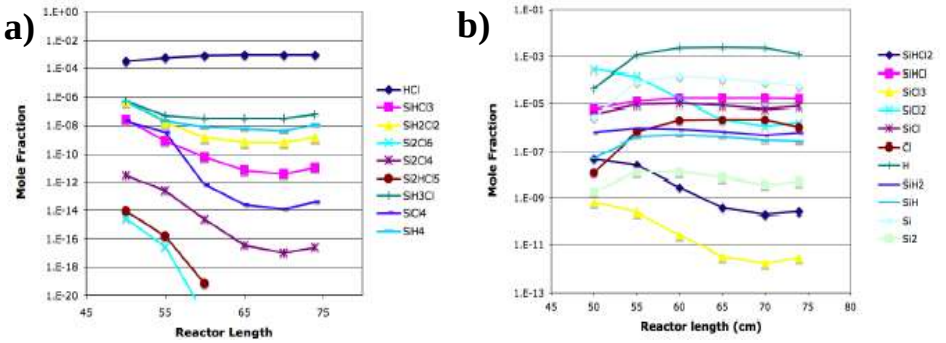

Figure 31: Mole fractions of relevant species calculated above the susceptor for the same conditions of Figure 29 using the new Si-H-Cl mechanism to describe the conversion of the chlorinated precursors.

For the system under consideration in the present study it is however likely that the gas phase enhancement of the gas phase reactivity given by the inclusion of both mechanisms will lead to a gas phase composition governed by the thermodynamic equilibrium. It can in fact be observed that the concentration of the SiH_xCl_{4-x} gas phase species follows the order of abundance predicted by thermodynamic equilibrium for chlorosilanes diluted in H_2: SiH_3Cl> SiH_2Cl_2> $SiHCl_3$ > $SiCl_4$ [ref]. As it can be observed, this is not the case when simulations are performed neglecting the disilane and radical pathways (Figures 30). For what concerns two other key species, SiH_4 and HCl, both mechanisms predict very similar concentrations, indicating that in both cases the reaction kinetics is sufficiently fast to lead to a substantial equilibrium for these chemical species. However those discrepancies would be even more evident when the reactivity is still kinetically controlled, as in the upstream part of the reactor.

The concentrations of the Si radicals and reactive intermediates generated by the decomposition of the $SiHCl_3$ precursor predicted using the two kinetic models is shown in Figures 30b and 31b. As it can be observed, both kinetic schemes predict that the most abundant active species generated in the gas phase are atomic H and Si. However the mechanisms differ in the prediction of the formation of the third most abundant active species, which is predicted to be $SiCl_2$ by the old mechanism and SiHCl by the updated mechanism. This is a relevant finding as according to the present simulations, SiHCl is together with SiCl and $SiCl_2$ an important Si precursor to the growth of SiC. Anyway the main contribution comes from atomic Si, whose inclusion in the film is however ruled by an adsorption/desorption equilibrium that is established at the growth surface. As the growth rate is sensitive to the Si desorption rate, which in the model of Veneroni et al. [16] was determined through fitting to sublimation pressure data, it is suggested that a higher level study of this important reaction and of the surface dynamics of atomic Si may lead to a

better understanding of the SiC growth mechanism. Increasing the rate of the Si desorption rate by a factor of 3 would in fact lead to a quantitative agreement between the simulated and the experimental growth rate profile.

4.7 Concluding remarks

The subject of this study has been the analysis of the gas phase reactivity active during the chemical vapor deposition of Si and SiC from trichlorosilanes. Simulations were performed considering explicitly the surface kinetics using a literature mechanism. In both cases the gas phase kinetics is significantly influenced by the active species produced at the surface during the film growth.

Concerning the gas phase reactivity, the Si-H-Cl sub mechanism was in common for the kinetics of both processes. Two gas phase mechanisms were analyzed in the present work: the disilane mechanism analogue to that proposed by Swihart and Carr [52] and a radical chain mechanism proposed for the first time in this work. The rate constant of the kinetic scheme were determined using conventional and variational transition state theory, with molecular data calculated through *ab initio* simulations.

The simulations revealed that the formation of disilanes as reaction intermediates plays a crucial role in enhancing the gas phase reactivity, both in the disilane and in the radical mechanisms. This is due to their high reactivity, determined by the relatively low Si-Si bond energy and small barriers for Cl and H intramolecular transfers. The disilane mechanism is thus the fastest route for the conversion of $SiHCl_3$ into SiH_2Cl_2, though it is slower with respect to the radical mechanism in describing the formation of $SiCl_4$. The radical mechanism is initiated by the homolytic decomposition of Si_2HCl_5 into $SiCl_3$ and $SiHCl_2$, and is followed by a series of fast propagation reactions. Termination can take

place either in the gas through recombination of radicals or at the surface following the dissociative adsorption of the radical.

The simulations of Si growth in Siemens and in horizontal reactors showed that both the disilane and the radical mechanisms are active during Si deposition from $SiHCl_3$, with the first dominating at low gas phase temperatures and precursor conversion and the second becoming the fastest at high temperatures and conversions. Besides, it was confirmed, as found in a previous study [50], that the formation of $SiCl_4$ in the gas phase has a positive impact on the film growth, as it is associated with the consumption of HCl and thus favors the film growth by removing a most active etching agent. These results indicate that operating Si deposition process in conditions in which the gas phase reactivity is favored (i.e. at high gas phase temperatures) should enhance the precursor conversion and the film growth rate, though at the expense of an increased production of tetrachlorosilane.

The new mechanism was also included in a kinetic scheme, which describes the SiC CVD. The predictions of the model are in good agreement with experimental data collected in an industrial reactor produced by the LPE company [92]. The inclusion of the radical and disilane mechanisms in the SiC deposition model enhances considerably the gas phase reactivity, so that the gas phase composition approaches now the thermodynamic limit. However, as the operative conditions are completely different with respect to those for Si CVD, the product distributions totally change. SiH_3Cl is thus predicted to be the chlorosilane by product that is formed in the gas phase in the highest concentration, followed by SiH_2Cl_2, $SiHCl_3$ and $SiCl_4$. SiHCl is predicted to be among the most abundant chemical species that are present in the gas phase, though the main precursor to the film growth is atomic Si. Those simulations predict that the surface kinetics of atomic Si can influence the SiC deposition profile, so that it is suggested that its surface reactivity should be investigated in higher detail in successive works.

To conclude, the kinetic schemes here proposed may be used as valuable tools to model the epitaxial poly Si and SiC deposition process in any CVD reactor.

CHAPTER 5

Metal organic vapor phase epitaxy of GaN

The final part of this research is dedicated to the GaN MOVPE. The general features of that process are described in Section 1.3.4. This work is in collaboration with the groups of prof. Sugiyama and prof. Shimogaki in the University of Tokyo. During this thesis there were spent 6 months there to allow a more direct interaction. The modeling part was combined with an aimed experimental campaign, performed mainly by prof. Momose and lately also by Y. Suzuki, in Sugiyama laboratories. The results presented in this chapter will be included in a related article to be submitted soon.

5.1 State of the art

GaN attracts great interest because of its several applications in optoelectronic, high power and high frequency devices. The preferred industrial method to produce such material is metal organic vapor phase epitaxy (MOVPE), using ammonia and trimethyl gallium as gaseous precursors. However the deposition mechanism of GaN has not yet been clarified and the operative condition of the process are actually based on the trial and error approach. Thus the study of this aspect can potentially lead to relevant improvements in the GaN production.

At the typical operative conditions for the GaN growth, it is generally agreed that deposition is in external diffusive regime [19, 25, 27, 28, 59, 174-179], because at those elevate substrate temperatures (1200-1400 K), the surface decompositions are generally very fast. Therefore transport phenomena have a fundamental role in determining the film growth rate, as also underlined in some recent studies by Sugiyama et al. [177-179]. It is agreed that $Ga(CH_3)_3$ undergoes various chemical reactions with ammonia in the gas phase that bring to the formation of the direct deposition precursor. This is the chemical component that is directly adsorbed on the substrate, where it is then decomposed to solid GaN. However the nature of such important specie has not yet been clarified.

Another critical aspect is related to the generation of solid GaN particles in the gas phase [19, 21-28]. Those droplets are formed in the typical operative conditions of GaN MOVPE and are mainly flowed towards the cold walls in the downstream part of the reactor, due to the thermophoretic effect. This side reactivity is strongly undesired because those powders scavenge part of the precursors, limiting the deposition rate. Moreover if they drop on the substrate, the quality of the film will be affected for the inclusion of additional defects to the crystalline layer and for the possible attainment of preferential growing areas. Also the exact composition and structure of such particles, as well as the reaction intermediates which lead to their generation are still open questions.

With the purpose to understand more about the gas phase reactivity, several experimental investigations with mass spectroscopic analysis have been carried on [69, 180-183]. Anyway it is difficult to obtain definitive conclusions because during this analysis part of the $Ga\text{-}CH_3$ bonds are easily dissociated, due to the ionization [183, 184]. It was found that room temperature it is formed a Lewis acid-base adduct between NH_3 and $Ga(CH_3)_3$, but such specie is rapidly decomposed completely between 400 and 500 K, thus indicating a very low thermal stability. Also dimeric clusters like $(CH_3)_4Ga_2(NH_2)_2$ or $(CH_3)_4Ga_2NH$ have been observed, with

maximum concentrations at around 700 K, but then their signals drop at higher temperatures. Glockling and Strafford [183] also detected the trimeric compound $Ga_3(CH_3)_9$, but other authors didn't confirm it in later studies. Unfortunately it is still not clear what happens at substrate temperatures above 1000 K, which are the typical operative conditions of the process.

Of course if it is not even known exactly what it is formed in the gas above the substrate, it is difficult to make certain assumptions about the chemical reactivity, and many works have been dedicated to such delicate task [26, 27, 59-69], mostly based on DFT *ab initio* calculations. Nowadays the kinetic mechanism most commonly adopted to model the gas phase kinetics in GaN MOVPE was proposed by Hirako et al. [59]. Those authors assembled their kinetic scheme by collecting the reactions proposed by several different authors, with kinetic constants evaluated using DFT methods. Then they proposed other reactions, assuming the parameters taken from analogue reactions. In alternative they estimated the parameters of some elementary reactions with the kinetic gas theory, or by applying the transition state theory, but without giving further details concerning those calculations.

Several models aimed to describe the GaN growth [27, 28, 81, 82, 185-187] have been developed. However the correlations used mostly relies on fitting parameters obtained from wide experimental data. Recently the program developed by STR group [81, 82], was used in a collaboration project with AIXTRON to reproduce some experimental data obtained in a planetary reactor by Dauelsberg et al. [25, 175]. Such commercial software uses the kinetic scheme proposed by Hirako et al. [59] and a model based on the method of moments with several fitting correlations to describe particles dynamics [83]. The experiments were achieved mainly by rotating the wafer, hence averaging the growth rate, but in some cases the rotation was stopped, achieving generally a reasonable agreement between simulations and experiments. However, as pointed out

by those authors [25], the deposition rates in those conditions are mainly dominated by the transport phenomena and in some cases are affected by particle nucleation. Thus the agreement should be due mainly to an accurate fluid dynamics description and to a good fitting in the droplets generation model, rather than to an exact understanding of the chemical reactivity involved.

5.2 Aim of the work and approach

This research is aimed to investigate the reaction kinetics active during GaN MOVPE. In particular the main focuses are the chemical reactivity that leads to the formation of the direct deposition precursor, the mechanism of particles generation and their related behavior, as well as the effect of material and thermal diffusions on the reactor performances. This study has been performed through both a theoretical analysis and an experimental investigation. In particular, in the present thesis has been carried on the modeling part. The final model developed should be able also to reproduce the experimental results.

5.2.1 Experimental section

As explained above, in this work the modeling part was combined with some aimed experiments. As this thesis is focused on the modeling aspects, here it is provided just a general description of the experimental procedure adopted, but further details will be provided in the incoming article. The experiments were obtained using a single wafer horizontal reactor (AIX200/4-RFS, AIXTRON), whose configuration is shown in Figure 32. The wafer for GaN deposition is conventionally placed atop a rotating disc to ensure the uniformity of the film thickness. On the other hand with such configuration it is difficult to retrieve information about the kinetics from the experimental results. Therefore with the purpose to achieve indication more suitable for a study of the chemical reactivity,

after growing a standard template, the rotation was intentionally stopped during the main growth.

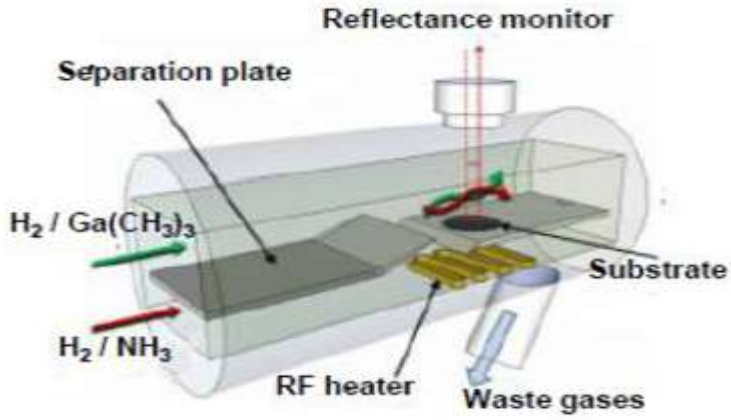

Figure 32: Schematization of the experimental reactor used for GaN MOVPE.

The resulting GaN thicknesses are not constant on the growing surface, hence it is confirmed the importance of the gas phase phenomena. As can be seen in the example in Figures 33, the growth profiles evidence a consistent qualitative variation along the flow direction, whereas the deviation along the perpendicular direction seems considerably less important, even if still appreciable. Hence, concerning the diffusion of fresh reactants from the lateral edges of the reactor at lower temperatures, from Figure 33b it can be inferred that probably it is not completely negligible. Anyway this effect should be less significant with respect to the diffusion of the Ga precursors from the top section of the reactor towards the substrate and to their consumption along the flow direction.

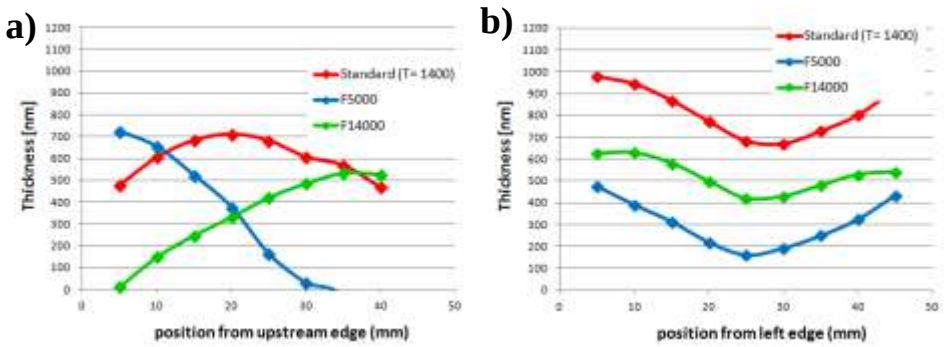

Figure 33: Deposition profiles at different total flow rates a) along the flow direction; b) perpendicular to the flow direction.

Those trends seem to confirm what concluded in other studies [19, 25, 27, 28, 59, 174, 175, 177], which supposed that the deposition is in external diffusive regime. The experimental growth profiles are affected by an uncertainty of about 20%.

The effects of several operative parameters were evaluated by assuming a referring experiment and then changing the variables of interest with respect to those of such experiment, but keeping constant all the other ones. The operative conditions of the standard experiment are reported in Table 9.

Table 9: Operative conditions for the standard experiments.

Variable	Operative conditions
Substrate temperature	1400 K
Flow rate upper channel	3.5 slm
Flow rate lower channel	6.5 slm
Total pressure	200 mbar
$Ga(CH_3)_3$ pressure	$6.9x10^{-2}$ mbar
NH_3 pressure	50 mbar

Finally it is noteworthy to point out that in the experimental conditions explored, it is usually observable a conspicuous amount of powders on the GaN film surface, especially in the downstream part, as shown in the example reported in Figures 34.

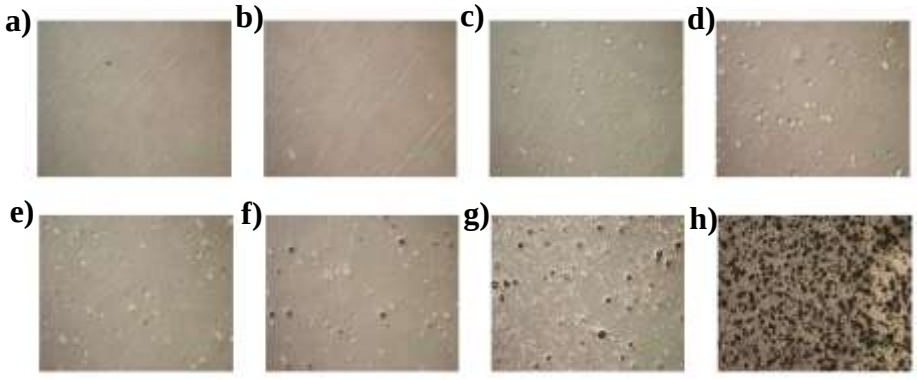

Figure 34: Surface morphologies at different positions from the upstream edge of the substrate for the experiment at total flow rate of 14 slm: a) 0.5 cm; b) 1.0 cm; c) 1.5 cm; d) 2.0 cm; e) 2.5 cm; f) 3.0 cm; g) 3.5 cm; h) 4.0 cm.

5.2.2 Modeling approach

The experiments described above have been the main basis for the theoretical investigation, object of the last part of this phd thesis. The methodology described in Section 2.7 was applied also for this specific case. The first part was dedicated to the proposal of the kinetic mechanism. The main assumption is that the deposition was considered in external diffusive regime, as motivated in the previous sub section. Therefore the surface mechanism assumed is the simplest as possible, which consists in hypothesizing that the decomposition of the direct deposition precursor to GaN on the activated surface is immediate. Indeed the rate determining step of such reactivity is the diffusion of the active species towards the substrate.

The gas phase kinetic scheme instead is much more complex. The starting point was a related literature research, focusing on the theoretical works about the reaction kinetics in GaN MOVPE [26, 27, 59-69], but also on the spectroscopic experiments [69, 180-183]. The hypothesis of the chemical species involved in the mechanism was made considering those previously proposed in the literature, but then additional other compounds were supposed. The same consideration is valid also for the elementary chemical reactions. Furthermore a preliminary thermodynamic analysis was performed in order to identify the most stable intermediates, which may have a significant role in the gas phase mechanism. Such analysis was used as a support for the proposal of the reactions to be included in the kinetic scheme. Indeed, considering that even molecules with 3 Ga atoms were detected in the spectroscopic experiments [183], with geometrical structures not defined, the number of chemical components involved may be very elevated and subsequently the related reaction paths may become countless. The thermodynamic parameters of all the possible reactants were evaluated through *ab initio* calculations, as explained in Section 2.3. Obviously also all the transition states were then treated at the same level of theory. Anyway it is important to point out that the

kinetic constants here calculated are generally more accurate with respect to those reported in the previous works [26, 27, 59-69] because calculated with more advanced techniques. Besides some of these results were also compared with the same parameters evaluated appositely at the CCSD(T)/aug-cc-pVTZ level [73], finding a maximum discrepancy in the activation energies of around 1 kcal/mol.

After having assembled the new kinetic scheme, a sensitivity analysis was performed, in order to identify the main reaction pathways active during GaN MOVPE. However, as already specified, material and thermal diffusions have a dominant role in the kinetics of the process. Indeed reagents start mixing just before reaching the substrate and stay in the growth area for a very limited time (less than 1 s), undergoing a huge temperature gradient. Hence there is no much sense in a micro kinetic analysis, but the main reaction routes were identified directly with a 2D schematization of the central section of the reactor. The details about this model are provided in Section 2.6.3.

Another important aspect of this work was the description of particle formation. Indeed solid GaN powders are conspicuosly formed above the disc and cannot be treated simply as the other gas components. For this purpose the FORTRAN program for the 2D simulations was substantially modified with the addition of equations based on the second order method of moments. Such model is described in Section 2.4, but it worth remind that the correlations found in the literature [79] were partially modified. In particular it was obtained a new analytical expression to predict the terms related to the scavenging of reagents from the particles surface.

The fluid dynamics was represented in a very accurate way, developing a stationary model with a 3D geometry, taking into account also the radiative heat exchange. However for obvious computational limits, the material balances of all the chemical species and of the three moments were instead solved in 2D, assuming the temperature and velocitiy profiles estimated with the 3D idealization. The fluid dynamic 3D model

is discussed in Section 2.6.4. Then, in order to understand if the reaction kinetics or the transport phenomena are predominant in determining the deposition profiles, an aimed sensitivity analysis was performed. Finally the global model developed was validated with the experimental results.

5.3 Kinetic scheme

The kinetic scheme used in the simulations is composed not only by a gas phase and a surface mechanism, but also by a particle growth model. However the nature of the key chemical components involved in the formation of the direct deposition precursor, as well as that of the direct deposition precursor itself, and that of the species which promotes particles nucleation and growth are not known a priori. This was clarified through a thermodynamic analysis reported in Section 5.3.1. In the following sub section instead is presented the gas phase kinetic scheme.

As already explained above, the surface reactivity assumed is very basic. Once adsorbed on the substrate the direct deposition precursor is immediately converted to crystalline GaN. Other reactions involved in the surface kinetics are thus the adsorption of the direct deposition precursor on the thin film, but also those of the dimers and radicals, that are immediately converted on the surface. Basically the latter ones are in fact radical terminations on the surface. It was assumed that those species stick on free sites with collisional efficiency. Hence the parameters of all the adsorption reactions were calculated with the kinetic gas theory.

The particles growth model describes the droplets evolution after their formation. The mathematical aspect of such model are described in Section 2.4, but there are not explained exactly the nature of the interactions between the aggregates and the precursors in the gas phase. This is instead discussed in Section 5.3.3.

5.3.1 Thermodynamic analysis

As explained above, the first preliminary step before assembling the gas phase kinetic scheme was a thermodynamic analysis. Several chemical components were considered, including various possible isomers. Here are described the most remarkable results. In Figure 35 is shown the temperature variation of the mole fractions of the most stable molecules in the gas phase. There were assumed initial composition and pressure equal to those of the referring experiment, listed in Table 9.

As it can be noted the concentration of $Ga(CH_3)_3$ is not reported, because it is very unstable, even at room temperature. Its conversion is thus regulated only by kinetic limitations. The $Ga\text{-}CH_3$ bonds are gradually substituted by the more stable $Ga\text{-}NH_2$. Anyway also the formation of Ga-H bonds is favored with respect to $Ga\text{-}CH_3$, hence this type of species may be generated as reaction intermediates. Such assumptions were also suggested in the thermodynamic analysis performed by Timoshkin et al. [65] based on the results of DFT *ab initio* calculations. Then, also the Lewis acid-base adducts were considered in this analysis. At low temperatures $Ga(CH_3)_3{:}NH_3$ is more stable with respect to $Ga(CH_3)_3$, but this is not true since temperature raise above 450-500 K. This is consistent with what demonstrated in the spectroscopic experiments [69, 180-183], where it was observed that the Lewis acid-base adducts start decomposing in that temperature range.

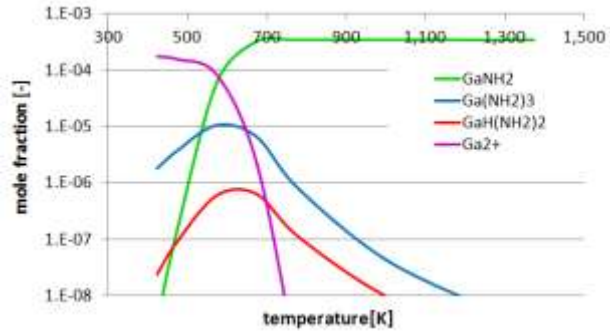

Figure 35: Mole fractions of the most stable molecules in the gas phase of GaN MOVPE reactors, calculated for different temperatures at the thermodynamic equilibrium, assuming the operative conditions reported in Table 9.

Another conclusion that can be inferred from this thermodynamic analysis concerns the direct deposition precursor. Indeed at the very high temperatures (1200-1400 K) in the proximity of the substrate, the unstable components should tend to be rapidly decomposed to the most stable ones. As the deposition is in external diffusive regime, the concentration of the direct deposition precursor must be enough to justify the experimental growth profile. Therefore it cannot be an unstable molecule. In Figure 35 is shown that since above 600 K the specie most stable in the gas is $GaNH_2$, while the thermodynamic concentrations of all the other ones become soon negligible. Thus it was supposed that such component is the direct deposition precursor, as already hypothesized by this research group [60].

Then it is possible to get information also about the particles generation mechanism. In the literature it is generally postulated that the aggregates are formed and grow through a simple polymerization mechanism [24, 26, 28, 59, 63, 66], proposed by Mihopoulos [26]. In other words it is assumed that there are no substantial differences from the reactive point of view between the various molecules with more than 1 Ga atom. The thermodynamic analysis instead revealed that the molecular structures of the most stable compounds with 2 Ga atoms are completely different with respect to those with 3 Ga atoms. Hence also their related physical properties change completely. In Figure 35 is shown that the molecules with more than 1 Ga atoms (generally named Ga_2+) are the most stable below 600 K. However the kinetic analysis made lately revealed that Ga-CH_3 substitutions with Ga-NH_2 are activated at higher temperatures. Therefore, considering the focus of this work, it would be not useful investigating the behavior at room temperature, but it is rather important to understand what happened since 600-700 K, where the first Ga-NH_2 bonds start to be formed in MOVPE reactors.

In the conditions of interest the kind of poly Ga molecules most stable is that reported in Figure 36a. Something similar was already postulated in

other theoretical studies [60, 61]. It is characterized by a planar 6 atoms ring with 3 Ga atoms, similar to that of aromatic hydrocarbons. That specie is much more stable with respect to any other with 2 Ga atoms. Hence it was supposed that such meta stable compound is the precursor of powders generation in the gas, or in other words the first stable particle nucleus. Of course also several different molecular structures were hypothesized, but they were proved to be much more unstable.

Concerning the species with 2 Ga atoms instead there were found two different possible configurations, with comparable stabilities at the operative conditions of interest. The first one is represented in Figure 36b, and it is a Lewis acid-base complex resulting by the addition of 2 molecules with 1 Ga atom. If compared with the $Ga(CH_3)_3$:NH_3 adduct discussed above, it is more stabilized from the energetic point of view because there are 2 acid base bonds. Anyway it is still entropically disfavored and it decomposes at high temperatures, even if higher with respect to those of $Ga(CH_3)_3$:NH_3. The other possible structure instead, shown in Figure 36c, comes from the molecules of Figure 36b through an ammonia elimination. The specie of Figure 36c is more stable at higher temperatures.

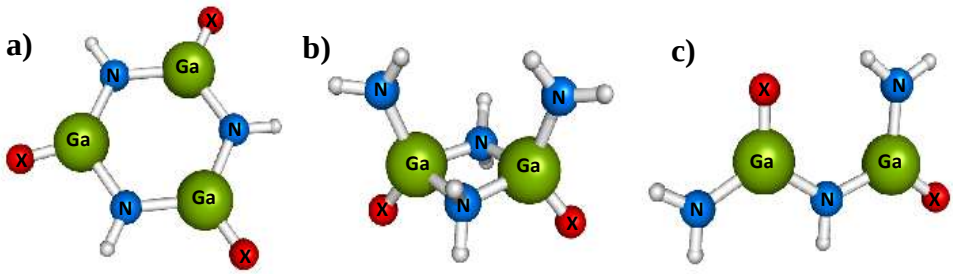

Figure 36: Structures of the most stable dimers and trimers, with X that can be CH_3, NH_2 or H a) first stable nucleus; b) Lewis acid base adduct; c) dimer after ammonia elimination.

Anyway in the operative conditions of interest, both the dimers presented here in principle may have a determinant role in the kinetic mechanism of particles formation. Furthermore those structures are both consistent with what found in some previous spectroscopic analysis [69, 180-183].

Therefore both the structures were initially taken in consideration for the kinetic mechanism discussed in the following sections.

5.3.2 Gas phase kinetic scheme

After having achieved indication about the chemical components which may be significantly involved in the gas phase kinetics, it was investigated how those molecules can react. The final kinetic scheme is reported in Table 10. It is important to point out that in assembling the final scheme, there were frequent drawbacks with some sensitivity tests, which have been essential for this task. Some of the reactions were taken from the literature [59-62, 64], but re evaluated at the higher level of theory used in this study. Other ones were hypothesized by similarity with those in the literature, on the basis of what suggested by the thermodynamic analysis. Finally other conversion routes were proposed here for the first time. The torsions around the Ga-CH_3 bonds were all treaded as 1D unhindered rotors, because their rotational PESs are characterized by hindrance potentials lower than 1 kcal/mol. In Table 10 are reported only the elementary reactions found to have a role not negligible in the global gas phase kinetics. Anyway other reactions were previously taken in consideration and then discharged because not relevant, thus they are not further discussed here.

The first class of reactions introduced was ammonia condensations [59-61, 64, 67-69], J35-J39,J41,J43. One example of transition state is reported in Figure 37a. As already pointed out in previous studies [60, 67-69], those reactions in principle, take place in 2 steps. The first is the formation of Lewiss acid-base adducts, like $Ga(CH_3)_3{:}NH_3$, at lower energies, without any energetic barrier. Then the second step is the elimination of a molecule of CH_4, characterized by *tight* transition states. However as explained above the complex is very unstable above 500 K and it is rapidly decomposed. Thus the rate of such reactions can be calculated neglecting the formation of the adduct, and then evaluating the

reaction rate as that of a bimolecular process using the conventional transition state theory [60]. Such approximation was verified a posteriori and it was confirmed that adduct generation is not relevant. Besides also the H_2 condensations [62], J40 and J42 were treated with the same approach, because they are conceptually quite similar, even if on those cases there are not formed any intermediate adducts.

The radical substitutions with H and NH_2 [60], J44-J47 and J53-J57 occur in a similar way of ammonia condensations. Indeed it is initially formed a radicalic adduct and then is eliminated another radical to form a more stable compound. The second step is characterized by a *loose* transition state. Such reactions were initially calculated with the kinetic gas theory. Then the estimations of H substitutions were refined using the variational transition state theory because it was found with a successive sensitivity analysis that those reactions are very sensitive. The estimation of NH_2 substitutions instead was not refined because those reactions are not so sensitive.

Possible reaction routes for the production of the direct deposition precursor, which is $GaNH_2$, passes forcibly through some kind of decompositions. One example is constituted by homolytic dissociations [60], J16-J21 and J63-J64. Their *loose* transition states were evaluated with the variational transition state theory. Then there were here hypothesized for the first time H scissions J48-J52 and J58, and eliminations reactions, J22-J25, whose transition states are well defined saddle points. Also those reactions can lead to the formation of $GaNH_2$. As it can be noticed, in case of $GaHCH_3NH_2$ (reactions J22-J23), in spite CH_4 elimination would bring to more stable products, it is less kinetically favored than that of NH_3. In general ammonia elimination was found to be an important element in the gas phase kinetics of GaN MOVPE, also for more complex molecules.

Table 10: Gas phase kinetic mechanism for GaN MOVPE[β].

	Reaction	A	α	E_a
J1	$Ga_2NHCH_3(NH_2)_3 + GaCH_3(NH2)_2 \rightarrow$ nuclei + $2NH_3$	$4.0x10^{11}$	0.5	0
J2	$Ga_2NHCH_3(NH_2)_3 + GaH(NH2)_2 \rightarrow$ nuclei + $2NH_3$	$4.0x10^{11}$	0.5	0
J3	$Ga_2NHCH_3(NH_2)_3 + Ga(NH2)_3 \rightarrow$ nuclei + $2NH_3$	$4.0x10^{11}$	0.5	0
J4	$Ga_2NHH(NH_2)_3 + GaCH_3(NH2)_2 \rightarrow$ nuclei + $2NH_3$	$4.0x10^{11}$	0.5	0
J5	$Ga_2NHH(NH_2)_3 + GaH(NH2)_2 \rightarrow$ nuclei + $2NH_3$	$4.0x10^{11}$	0.5	0
J6	$Ga_2NHH(NH_2)_3 + Ga(NH2)_3 \rightarrow$ nuclei + $2NH_3$	$4.0x10^{11}$	0.5	0
J7	$Ga_2NHH_2(NH_2)_2 + GaCH_3(NH2)_2 \rightarrow$ nuclei + $2NH_3$	$4.0x10^{11}$	0.5	0
J8	$Ga_2NHH_2(NH_2)_2 + GaH(NH2)_2 \rightarrow$ nuclei + $2NH_3$	$4.0x10^{11}$	0.5	0
J9	$Ga_2NHH_2(NH_2)_2 + Ga(NH2)_3 \rightarrow$ nuclei + $2NH_3$	$4.0x10^{11}$	0.5	0
J10	$2GaH(NH_2)_2 \rightarrow Ga_2NHH_2(NH_2)_2 + NH_3$	$4.7x10^{-2}$	2.87	-16.53
J11	$Ga_2NHH_2(NH_2)_2 + NH_3 \rightarrow 2GaH(NH_2)_2$	$6.0x10^{-2}$	3.11	-12.06
J12	$GaCH_3(NH_2)_2 + Ga(NH_3)_3 \rightarrow Ga_2NHH_2(NH_2)_2 + NH_3$	$4.7x10^{-2}$	2.87	-16.53
J13	$Ga_2NHH_2(NH_2)_2 + NH_3 \rightarrow GaCH_3(NH_2)_2 + Ga(NH_3)_3$	$4.7x10^{-2}$	3.12	-11.49
J14	$GaH(NH_2)_2 + Ga(NH_3)_3 \rightarrow Ga_2NHH(NH_2)_3 + NH_3$	$4.7x10^{-2}$	2.87	-16.53
J15	$Ga_2NHH(NH_2)_3 + NH_3 \rightarrow GaH(NH_2)_2 + Ga(NH_3)_3$	$4.2x10^{-2}$	3.1	-11.54
J16	$Ga(CH_3)_3 \rightarrow GaCH_3 + 2CH_3$	$9.0x10^{16}$	0	79.00
J17	$Ga(CH_3)_2NH_2 \rightarrow GaNH_2 + 2CH_3$	$1.2x10^{27}$	-3.2	81.40
J18	$GaCH_3(NH_2)_3 \rightarrow GaNH_2 + CH_3 + NH_2$	$1.9x10^{18}$	-0.59	81.66
J19	$Ga(NH_2)_3 \rightarrow GaNH_2 + 2NH_2$	$3.8x10^{18}$	-0.81	95.40
J20	$GaH(NH_2)_2 \rightarrow GaNH_2 + NH_2 + H$	$3.2x10^{16}$	-0.4	87.60
J21	$GaCH_3HNH_2 \rightarrow GaNH_2 + CH_3 + H$	$4.0x10^{24}$	-2.6	79.94
J22	$GaCH_3HNH_2 \rightarrow GaNH_2 + CH_4$	$2.2x10^{11}$	0.79	70.63
J23	$GaCH_3HNH_2 \rightarrow GaCH_3 + NH_3$	$5.3x10^{12}$	0.21	63.10
J24	$GAH(NH_2)_2 \rightarrow GaNH_2 + NH_3$	$6.0x10^{12}$	0.2	60.82
J25	$GANH_2 + NH_3 \rightarrow GAH(NH_2)_2$	$4.7x10^{0}$	3.52	39.74
J26	$CH_3 + NH_3 \rightarrow NH_2 + CH_4$	$2.5x10^{3}$	2.9	14.60
J27	$NH_2 + CH_4 \rightarrow CH_3 + NH_3$	$1.1x10^{3}$	3.2	10.92
J28	$CH_4 + H \rightarrow CH_3 + H_2$	$4.0x10^{3}$	3.2	8.75
J29	$CH_3 + H_2 \rightarrow CH_4 + H$	$6.5x10^{3}$	2.7	8.86
J30	$H + NH_3 \rightarrow NH_2 + H_2$	$5.8x10^{4}$	2.8	10.27
J31	$NH_2 + H_2 \rightarrow NH_3 + H$	$2.5x10^{2}$	3.2	5.15
J32	$C_2H_6 \rightarrow 2CH_3$	$1.8x10^{21}$	-1.24	90.82
J33	$2CH_3 \rightarrow C_2H_6$	$3.5x10^{13}$	0	0
J34	$CH_3 + H \rightarrow CH_4$	$1.6x10^{32}$	-6	4.14

J35	$Ga(CH_3)_3 + NH_3 \rightarrow Ga(CH_3)_2NH_2 + CH_4$	$2.57x10^{0}$	3.39	14.59
J36	$Ga(CH_3)_2NH_2 + NH_3 \rightarrow GaCH_3(NH_2)_2 + CH_4$	$2.9x10^{-1}$	3.84	20.99
J37	$GaCH_3(NH_2)_2 + NH_3 \rightarrow Ga(NH_2)_3 + CH_4$	$6.1x10^{-1}$	3.49	24.93
J38	$GaCH_3 + NH_3 \rightarrow GaNH_2 + CH_4$	$8.3x10^{1}$	3.25	18.09
J39	$GaCH_3HNH_2 + NH_3 \rightarrow GAH(NH_2)_2 + CH_4$	$2.0x10^{0}$	3.48	21.70
J40	$Ga(NH_2)_3 + H_2 \rightarrow GaH(NH_2)_2 + NH_3$	$1.8x10^{7}$	1.28	29.49
J41	$GaH(NH_2)_2 + NH_3 \rightarrow Ga(NH_2)_3 + H_2$	$2.6x10^{1}$	3.16	23.06
J42	$GaCH_3(NH_2)_2 + H_2 \rightarrow GaCH_3HNH_2 + NH_3$	$1.7x10^{5}$	1.83	28.36
J43	$GaCH_3HNH_2 + NH_3 \rightarrow GaCH_3(NH_2)_2 + H_2$	$2.9x10^{0}$	3.48	19.25
J44	$GaH(NH_2)_2 + NH_2 \rightarrow Ga(NH_2)_3 + H$	$7.1x10^{4}$	2.33	-2.00
J45	$Ga(NH_2)_3 + H \rightarrow GaH(NH_2)_2 + NH_2$	$4.4x10^{12}$	0.15	7.10
J46	$GaCH_3(NH_2)_2 + H \rightarrow GaH(NH_2)_2 + CH_3$	$4.7x10^{11}$	0.78	0.71
J47	$Ga(CH_3)_2NH_2 + H \rightarrow GaCH_3HNH_2 + CH_3$	$5.0x10^{11}$	0.82	0.35
J48	$Ga(CH_3)_2NH_2 + H \rightarrow GaCH_3 + CH_3 + NH_3$	$1.4x10^{8}$	1.61	6.41
J49	$GaCH_3(NH_2)_2 + H \rightarrow GANH_2 + CH_3 + NH_3$	$2.3x10^{7}$	1.69	2.90
J50	$Ga(NH_2)_3 + H \rightarrow GaNH_2 + NH_2 + NH_3$	$6.3x10^{7}$	1.69	4.42
J51	$GaH(NH_2)_2 + H \rightarrow GaNH_2 + NH_2 + H_2$	$2.8x10^{9}$	1.6	2.51
J52	$GaCH_3HNH_2 + H \rightarrow GANH_2 + CH_3 + H_2$	$1.6x10^{-4}$	5.8	0.03
J53	$GaCH_3 + NH_2 \rightarrow Ga(CH_3)_2NH_2 + CH_3$	$2.6x10^{12}$	0.5	0
J54	$Ga(CH_3)_2NH_2 + NH_2 \rightarrow GaCH_3(NH_2)_2 + CH_3$	$1.9x10^{12}$	0.5	0
J55	$GaCH_3(NH_2)_2 + NH_2 \rightarrow Ga(NH_2)_3 + CH_3$	$9.5x10^{11}$	0.5	0
J56	$GaCH_3HNH_2 + NH_2 \rightarrow GaH(NH_2)_2 + CH_3$	$9.5x10^{11}$	0.5	0
J57	$GaCH_3 + NH_2 \rightarrow GaNH_2 + CH_3$	$9.5x10^{11}$	0.5	0
J58	$GaNH_2 + H \rightarrow Ga + NH_3$	$9.6x10^{8}$	1.23	6.73
J59	$Ga + NH_3 \rightarrow GANH_2 + H$	$1.7x10^{5}$	2.65	22.31
J60	$Ga + H \rightarrow GaH \rightarrow GaNH_2$	$1.8x10^{14}$	0.19	0
J61	$Ga + NH_2 \rightarrow GaNH_2$	$1.2x10^{14}$	0.19	0
J62	$Ga + CH_3 \rightarrow GaCH_3$	$1.3x10^{14}$	0.19	0
J63	$GaNH_2 \rightarrow Ga + NH_2$	$2.7x10^{26}$	-3.65	93.22
J64	$GaCH_3 \rightarrow Ga + CH_3$	$1.8x10^{26}$	-3.51	68.63

[β]Kinetics constants are high pressure limits and are expressed as $k = A\,T^{\alpha} exp\left(-\frac{E_a}{RT}\right)$ *in units consistent with cm, s and mol. Activation energies in kcal/mol*

As discussed in the previous section, the particles generation is promoted by the formation of the first stable nuclei with 3 Ga atoms, shown in Figure 36a. Of course, before it is necessary to form molecules with 2 Ga atoms. For the first time in this study, dimerizations J10-J15 were supposed to occur in 2 steps like ammonia condensation, and in fact their PESs are conceptually very similar. In Table 10 there are reported only the most sensitive ones. In the first step there is the formation of the

Lewis acid-base adducts reported in Figure 36b. Then the compounds in Figure 36c are formed through ammonia eliminations. Their activation energies are even negative because their *tight* transition states come after the formation of the adducts at lower energies and the transitions states are stabilized by acid-base interactions as well, as shown in Figure 37b. There were also tested the eliminations of CH_4 and H_2, but there were found energy barriers that are more than 20 kcal/mol higher. Therefore the latter paths were neglected.

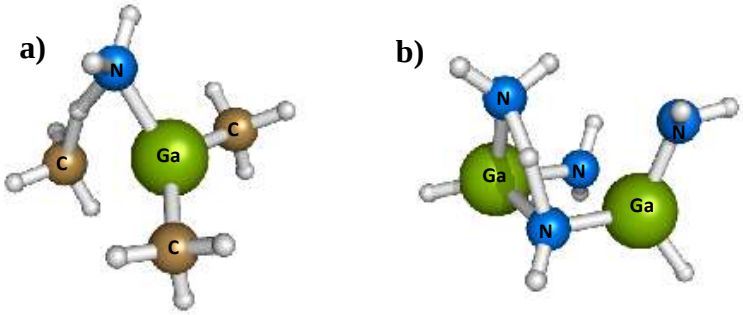

Figure 37: Structures of the transition states related to a) $Ga(CH_3)_3 + NH_3 \rightarrow Ga(CH_3)_2NH_2 + CH_4$; b) $2GaH(NH_2)_2 \rightarrow Ga_2NHH_2(NH_2)_2 + NH_3$.

5.3.3 Reactivity between particles and gas precursors

In this section is clarified the nature of the interactions between the particles formed after nucleation and the precursors in the gas phase. As explained in the previous sections, the first aggregates formed are supposed to be molecules like those in Figure 37a. The evaluation of the nucleation rate constant is a complex task. The generation of the first stable nuclei, occurs through the formation of unstable dimers with a subsequent addition of another molecule with 1 Ga atom. Anyway, as it was demonstrated that CH_3 and H_2 eliminations are kinetically disfavored. Consequently those 2 steps should take place through 3 NH_3 eliminations, hence the particles nucleation precursors must have at least two amino groups, and their generic formula is $GaX(NH_2)_2$, with X that can be H, CH_3 or NH_2. This novel type of mechanism seems to find

partial confirm with what experimentally found in a study on $[H_2GaNH_2]_3$ in supercritical ammonia [188]. Indeed, though the operative conditions are totally different with respect to those in GaN MOVPE, that study underlies the importance of ammonia eliminations in the production of poly imidogallane.

The nucleation might pass through the formation of a metastable complex with 3 Ga atoms, resulting from the reaction between a dimer and $GaX(NH_2)_2$, which at high temperatures is very unstable and should rapidly decompose. To be converted to the first stable nucleus such complex needs to release two ammonia molecules. This act could occur in many ways because that big molecule has many internal positional degrees of freedom. Besides it is not known a priori if the starting dimers are like those in Figure 37b or those in Figure 37c. Several researches of the transition state have been carried out and it seems that the rate determining step of that reaction is the collision between the dimer and $GaX(NH_2)_2$, rather than the subsequent complicate reactive steps. Therefore that reaction should be barrierles and estimable with a reasonable approximation with the kinetic gas theory. The value adopted to better fit the experimental data and reported in Table 10 (J1-J9) is indeed in that typical range. The uncertainty may be of one order of magnitude, but due to the complexity of those molecules and of the strong long range interactions involved, most probably it won't be possible to achieve a much more accurate prediction by applying the very time consuming variational transition state theory. Besides the PESs of this type of collisions are strongly conditioned by long range Ga-N intermolecular interactions and this further complicate that task.

Some tests made lately have evidenced that at the conditions of interest, the concentrations of the dimers like those in Figure 37c are one order of magnitude higher with respect to those of the analogue dimers like in Figure 37c. Moreover the eventual nucleation of the later would be more complex because it would be necessary to eliminate one additional NH_3

with respect to the former. Therefore it was hypothesized that the dimers kinetically relevant for the nucleation mechanism are those like in Figure 37c.

Finally once clarified the aspects concerning nucleation, it is also necessary to provide more information about particles growth. It is assumed that the droplets surface behave exactly as the substrate and the reactor walls. Thus $GaNH_2$ can be agglomerated in the powders as amorphous GaN through a deposition supposed in external diffusive regime. This hypothesis seems reasonable because simulations revealed that nucleation takes place at high temperatures above the substrate (above 800-900 K), whereas what exactly happens after, in the downstream, is not of interest for this research. Moreover there was also included the radicals terminations on the particles surface, still exactly as on the substrate. Summing up the gaseous monomer for the droplets growth it was assumed to be $GaNH_2$ as in the case of the film deposition.

5.4 Analysis on the reaction kinetics

After having assembled the kinetic scheme, the following step included in the general procedure developed should be a micro kinetic analysis, in order to clarify the most significant conversion pathways. However, as motivated in Section 5.2.2, here the analysis on the reaction kinetics was made directly with the 2D model. The main reaction routes resulting from this analysis were then compared with those found by Hirako et al. [59] because their kinetic scheme is actually the most used to model the kinetics in GaN MOVPE.

5.4.1 Main reaction pathways in the gas

The referring operative conditions for the kinetic analysis were those of the standard experiment, reported in Table 9. Anyway some tests were also made by changing some operative parameters in the range explored

in the parallel experimental campaign. A scheme representing the main reaction pathways is represented in Figure 38.

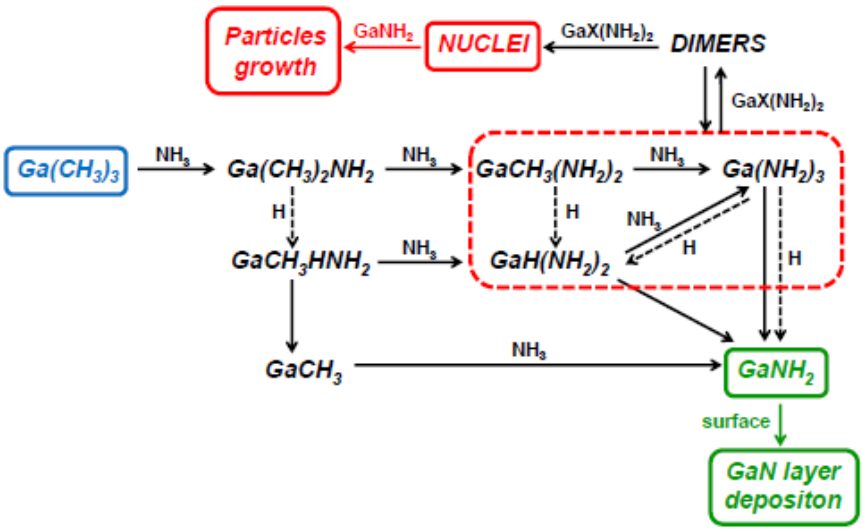

Figure 38: Main reaction pathways active in the gas phase during GaN MOVPE.

The Ga-CH_3 bonds of the $Ga(CH_3)_3$ fed are gradually substituted by the more stable Ga-NH_2 mainly through ammonia condensations, even though also NH_2 substitutions give a not negligible contribution. Anyway those reactions don't end with the first one, but proceed in principle till $Ga(NH_2)_3$, as also inferred by Ikeda et al. [64], as well as by this research group [60]. In parallel also Ga-H formations occur in a significant way above the substrate, with comparable reactions rate of those of ammonia condensations. Those reactions are very important because the resulting intermediates $GaXHNH_2$, can be decomposed through ammonia eliminations and finally generate the direct deposition precursor $GaNH_2$. Ammonia eliminations are indeed the main ways to form it. However the rate determining steps of this mechanism are ammonia condensations and H substitutions. The latter are in fact radical propagations. Instead H_2 condensations were found to be considerably slower with respect to H substitutions because their activation energies are quite elevated (around 30 kcal/mol). In fact it was also tried to include other hydrogenated species in the scheme reported in Table 10, but the deposition and particle formation rates changed only very slightly. Hence it was considerate not

enough to justify an increased complexity of the reaction mechanism. One example of possible reaction pathway that brings to the formation of $GaNH_2$ is constituted by the reactions set reported below. Anyway other analogue conversion routes are possible, as it can by noticed in Figure 39. Then a further secondary contribution is given by the $Ga(NH_2)_3$ decompositions.

J35) $$Ga(CH_3)_3 + NH_3 \rightarrow Ga(CH_3)_2NH_2 + CH_4$$

J46) $$Ga(CH_3)_2NH_2 + H \rightarrow GaCH_3HNH_2 + CH_3$$

J39) $$GaCH_3HNH_2 + NH_3 \rightarrow GaH(NH_2)_2 + CH_4$$

J24) $$GaH(NH_2)_2 \rightarrow GaNH_2 + NH_3$$

In Figure 39b is reported the 2D concentration profile of $GaNH_2$ at the operative conditions of the standard experiment, whereas those of the hydrogenated species that promote its formation are in Figures 39c and 39d. It is interesting to compare them with the temperature profile in Figure 39a. As it can be expected the concentration of $GaNH_2$ is the highest in the proximity of the substrate, whereas the other species are decomposed in the lower part of the reactor. This is explained by the fact that it is necessary to overcome a temperature threshold to activate chemical mechanisms as NH_3 eliminations, H substitutions (due to the formation of radicals) and NH_3 condensations. Then the concentration of $GaNH_2$ decreases in the downstream part because of its scavenging due to the particles growth.

The particles nucleation instead is possible only after the formation of species like $GaX(NH_2)_2$. Therefore the initial steps are at least 2 ammonia condensations. After that the dimers like those in Figure 36c can be produced through the reactions J10-J15. It was found that those reactions are very fast, hence the concentration of the dimers are regulated by their thermodynamic equilibrium with $GaX(NH_2)_2$. In the final kinetic scheme there are included only the most sensitive dimerizations, in order to limit the computational effort. In Figure 39e is reported the profile of the most abundant dimer. As it can be noticed dimers are formed above the

substrate because it is necessary to reach a temperature threshold to activate the formation of $GaX(NH_2)_2$.

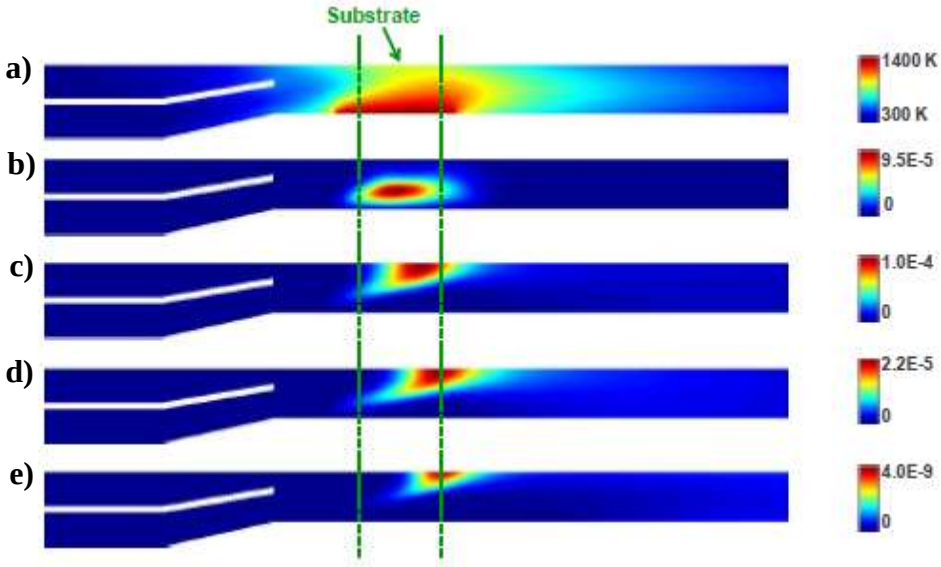

Figure 39: Temperature and mole fractions in the gas phase at the conditions reported in Table 9 a) temperature; b) $GaNH_2$; c) $GaCH_3HNH_2$; d) $GaH(NH2)_2$; e) $Ga_2NHH_2(NH_2)_2$.

5.4.2 Particles generation dynamics

After the formation of dimers, they reacts with another $GaX(NH_2)_2$ molecule in a collisional way to generate the first stable nuclei. A possible particles nucleation pathway results from following reactions.

J10) $$2GaH(NH_2)_2 \leftrightarrow Ga_2NHH_2(NH_2)_2 + NH_3$$

J8) $$Ga_2NHH_2(NH_2)_2 + GaH(NH_2)_2 \rightarrow Ga_3N_3H_6 + 2NH_3$$

As it can be deduced the presence of ammonia inhibits dimerizations, because they are regulated by the thermodynamic equilibrium. On the other hand, higher ammonia concentrations enhance the generation of $GaX(NH_2)_2$, which are the first nucleation precursors. In other words the increment of NH_3 concentration should slow down the nucleation rate, but nucleation should start before. In the operative conditions considered here, the second effect is predominant, thus NH_3 enhances particles formation. The subsequent growth of the solid aggregates is promoted with the contextual scavenging of $GaNH_2$. As explained in Section 2.4.2,

this is an auto catalytic mechanism, enhanced with the increment of the particles dimensions. Such mechanism is partially limited by the droplets fouling on the reactor walls, driven by thermophoretic forces and by the aggregates coagulation, which reduce their total external surface, available for $GaNH_2$ adsorption.

In Figures 40 are reported the profiles of μ_o, μ_1 and μ_2. The moments in that figure are dimensionless rearranged as mole fractions (M_k) through the Equation 43, where N_{Av} is the Avogadro number, Δv the volume increment due to the addition of one GaN unit and C_{gas} the total gas concentration.

$$M_k = \frac{\mu_k}{N_{Av}\,\Delta v^k C_{gas}} \qquad (43)$$

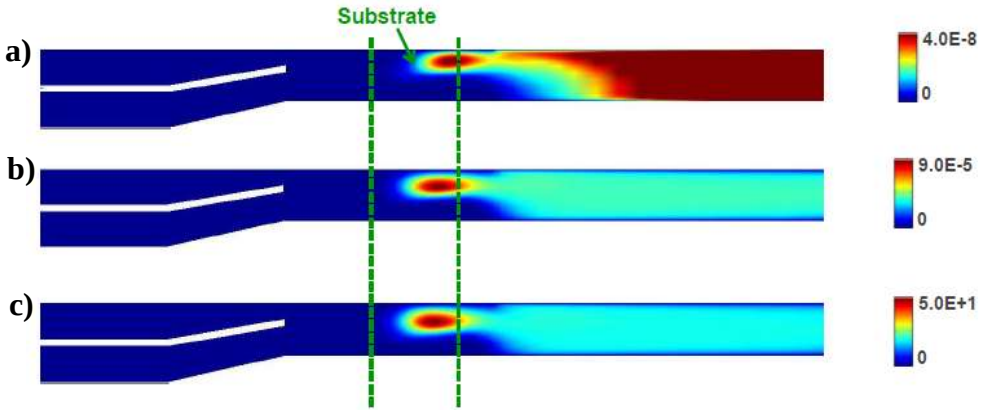

Figure 40: Profiles of the first 3 moments of the particles distribution function expressed as in the Equation 43 at the conditions reported in Table 9 a) M_0; b) M_1; c) M_2.

These solutions have been cut off for the introduction of a temperature threshold (750 K) below it the reactions involving particles have been blocked, in order to help the numerical convergence. Thus the results considerably beyond the downstream edge of the substrate are unreliable. Anyway the region of interest should be reasonably represented. The average molar diameter, in Figure 41a, is around 8 nm, corresponding to an average number of monomeric units per aggregate of around 10^4. The massive average diameter, in Figure 41b, is instead around 70 nm, corresponding to $5x10^6$ monomeric units. This doesn't mean that there are

not present in significant amount also bigger particles, with diameters greater than 100 nm or 1 μm, because σ_{log} is around 2 (log-normal distribution). This is coherent with previous researches, where there were found particles dimensions mainly in the nano scale above the substrate [28]. Most of powders are formed in the upper section and tend to go mostly towards the colder walls for thermophoresis, but part of them moves towards the substrate for Brownian diffusion. The coagulation tends to increase their dimensions, but also to reduces σ_{log} because the most favored collision are those between the small but fast aggregates and the big ones. In the standard experimental condition most of powders are generated in the downstream part of the substrate, while the upstream is less affected by their presence.

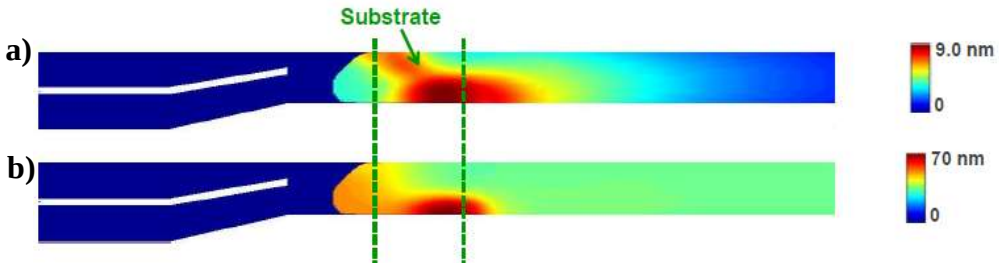

Figure 41: Profiles of the mean particles diameters at the conditions reported in Table 9 a) molar averaged; b) massive averaged.

5.4.3 Comparison with the most used literature mechanism

The kinetic mechanism here proposed was compared with what previously hypothesized in the literature. In particular the kinetic scheme actually most commonly adopted to model the gas phase kinetics in GaN MOVPE was hypothesized by Hirako et al. [59]. Of course also all the reactions proposed by those authors were initially considered in the kinetic analysis described in Section 5.4.1. Anyway it is important to underline that the computational method used in this study is much more accurate. Furthermore the reactions included in the scheme of Hirako et al. were calculated with different DFT techniques, because taken from several previous literature works. Therefore the parameters of the most

sensitive reactions indicated by those authors were re estimated using the computational method adopted in this research. In Figure 42 there are shown the discrepancies between the mechanism here proposed and that by Hirako et al.

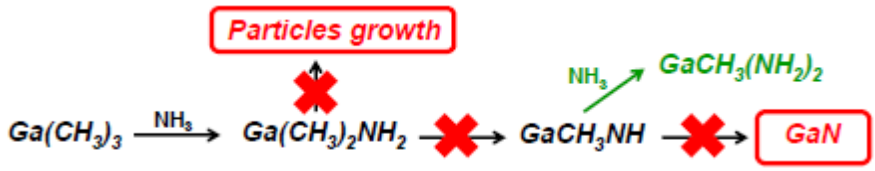

Figure 42: Kinetic analysis of the main reaction pathways in the most cited literature mechanism [59] to describe the gas phase reactivity in GaN MOVPE.

The first main difference concerns the direct deposition precursor. Indeed also Hirako et al. [59] assumed the deposition in external diffusive regime for temperatures higher than 750 K, but they postulated another direct deposition precursor, that is gaseous GaN. This assumption was not supported by any other kind of investigations. As explained in Section 5.3.1, from a thermodynamic analysis it was demonstrated that the most stable gas precursor above the substrate is $GaNH_2$. It was also compared with gaseous GaN through the reaction J65, and it was found that such reaction is extremely disfavored at the typical operative conditions of GaN MOVPE. Therefore the presence of GaN in the gas phase, which has a triplet ground state [68], should be negligible at the typical operative conditions of GaN MOVPE. An alternative candidate to be the direct deposition precursor was the gaseous atomic Ga, suggested by Shäfer et al. [181] on the basis of experimental spectroscopic analysis. Here it was found instead that also that specie is less stable than $GaNH_2$. This result seems in contradiction with the experimental evidences, but it should be pointed out that such kind of analysis is considerably affected by the strong ionization which partially dissociates a consistent part of the Ga-CH_3 bonds [183, 184]. Moreover if the signal of Ga is compared with that of $Ga(CH_3)_2$ at low temperatures, that should be due to the ionization of the initial $Ga(CH_3)_3$, the former is about two order of magnitude lower. Thus it is not enough to justify a deposition in external diffusive regime.

J65) $$GaNH_2 \rightarrow GaN + H_2$$

As evidenced in Figure 42, the first step of both the mechanisms is in common, which is the first ammonia condensation of $Ga(CH_3)_3$. What happens next instead is completely different. Indeed Hirako et al. [59] postulated a decomposition of $Ga(CH_3)_2NH_2$ to the more unstable $GaCH_3NH$, through the reaction J66. Also this reaction was taken in consideration in the initial kinetic scheme and it was re evaluated with the more accurate method used in this study. It was found with respect to the calculation of Hirako et al. [59] an activation energy 30 kcal/mol higher. This result confirms what previously calculated by Mondal et al. [68], which evaluated the transition state of the same reaction using different techniques, included various CCSD(T) estimations, finding an activation energy around 76 kcal/mol. This means that the reaction J66 is very much slower than how hypothesized by Hirako et al. and probably it should not take place in a significant way.

J66) $$Ga(CH_3)_2NH_2 \rightarrow GaCH_3NH + CH_4$$

Another critical point is that in such mechanism it is not considered the possibility to form more stable species from $GaCH_3NH$, like for instance $Ga(CH_3)_2NH_2$. Moreover the reaction J66 is assumed as irreversible. Here it was thus hypothesized a possible addition with ammonia J67, and it was scanned its PES. Such reaction was proved to be barrierless, consequently it should be very fast because it is close to the collisional limit, and then NH_3 concentration in the gas is elevated. The consequence is that if even J66 occurred in a significant way, the resulting $GaCH_3NH$ wouldn't be enough to be converted to the unstable gaseous GaN through J68, as supposed by Hirako et al., because it would rather react with NH_3 through J67.

J67) $$GaCH_3NH + NH_3 \rightarrow GaCH_3(NH_2)_2$$

J68) $$GaCH_3NH \rightarrow GaN + CH_4$$

Finally also the mechanism of powder formation here proposed is different with respect to that included in the kinetic scheme by those authors, who assumed it as a simple polymerization. Among the various divergences, in the present kinetic scheme $Ga(CH_3)_2NH_2$ is not a promoter of particles formations. Indeed the conversion to the first stable nucleus requires 3 NH_3 eliminations and this is possible only if in the initial reactants with 1 Ga atom there are at least 2 NH_2 groups. Anyway this is already widely discussed and motivated in previous sections and it would be redundant to report further details here.

In conclusion the analysis reported above evidences that the reaction pathways proposed by Hirako et al. [59] are extremely both kinetically and thermodynamically disfavored. Therefore other effective reaction pathways should rather take place in a much more significant way.

5.5 Comparison between the effects of kinetics and diffusion

As already pointed out in previous sections, the deposition is not only ruled by the reaction kinetics. Indeed the conditions in the MOVPE reactors are very far from being homogeneous. Therefore material and thermal diffusions have also a critical effect on the global performances of the process. However it is not clear exactly which of the two contributions is the most important among kinetics and fluid dynamics. The understanding of this aspect is very important for planning the eventual solutions that can be adopted with the aim to improve the optimization of the operative conditions. An aimed sensitivity analysis was thus carried on in order to provide indications about such point.

A fundamental feature is the mixing of the precursors and it should be checked whether it is complete or not above the substrate. Indeed NH_3 and $Ga(CH_3)_3$ are fed in two separate inlets and stay in the zone of interest for characteristic times lower than 1 s. In Figure 43a is evidenced that for the standard experiment, the mixing of ammonia is in fact

complete before to reach the substrate. Thus $GaNH_2$ and GaN particles (in Figure 40b and Figures 41) are generated when this process is already complete. Hence such phenomenon should not affect the resulting deposition profile. Observing instead the sum of the concentrations of the species with 1 Ga atom in Figure 43b it can be noticed that such mixing is slower with respect to the ammonia one. This is due to the lower diffusivities associated to the Ga precursors, further enhanced by thermophoresis. Consequently the growth rate should be limited by the diffusion of the group III reactants from the top part of the reactor towards the hot susceptor.

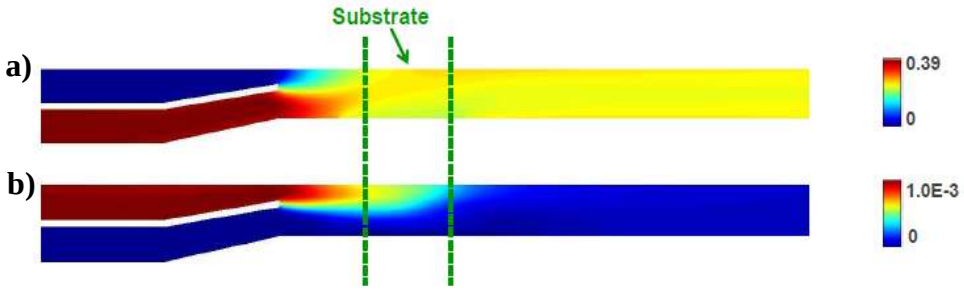

Figure 43: Mixing profiles at the conditions reported in Table 9 a) NH_3 mole fraction; b) sum of the mole fractions of the species with 1 Ga atom.

The conclusion mentioned above was further confirmed by a sensitivity analysis in which the diffusivities of all species with 1 Ga atom were increased by 30%, with the only exception of the direct deposition precursor, $GaNH_2$. Such result is reported in Figure 44 (blue line). Hence it is clear that the diffusion coefficients are sensitive parameters because the mixing is not complete at the upstream edge of the substrate. However in the same figure is also shown that also the correct estimation of the kinetic constants of some key reactions is fundamental. In the plot is reported only the effect of a decrement by 10 times of all the H substitutions J44-J47 (purple line), but also other reactions, like ammonia condensations are very sensitive. The reason is that it is necessary to overcome a temperature threshold to activate the conversion of the reactants to $GaNH_2$. Then, since the residence time above the substrate is very low, the chemical reactivity is still in a kinetically controlled regime.

Furthermore, as underlined in Section 5.4, also particles generation gives a dramatic undesired contribution by scavenging the active species from the gas phase. Also this side conversion is in a kinetically controlled regime. In Figure 44 (green line) is evidenced that the solid droplets start affecting the deposition profile only in the downstream part of the susceptor, where they started to be formed, as shown in Figures 41. Indeed that curve reported in the plot is achieved without including the particles formation mechanism.

What stated above is qualitatively valid also at different operative conditions in the experimental operative range explored. The difference is just that the deposition profiles shift along the flow direction or change in their absolute values coherently with the reactivity and the diffusivities in the specific case. Besides, also Dauelsberg at al. [25] made similar considerations at different operative conditions, finding in some cases growth profiles ruled mainly by diffusion and in other cases affected by the particles generation kinetic. Hence, summing up, the main finding of the sensitivity analysis described above is that both kinetics and fluid dynamics have a key role in the typical operative conditions in GaN MOVPE reactors.

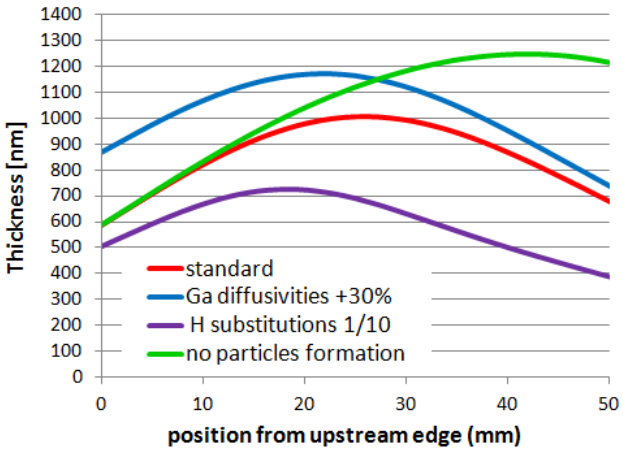

Figure 44: Sensitivity analysis on GaN deposition profiles at the conditions reported in Table 9, achieved by changing the diffusivities, the pre exponential factors of H substitutions or by not including the particles generationn mechanism.

5.6 Validation with the experimental results

Finally here the results of the simulations are compared with the experiments. In Figures 45 is showed the substrate temperature dependence. Indeed in the experiments reported there, the only condition changed from the standard experiment was the substrate temperature, decreased respectively to 1300 K (T1300) and to 1200 K (T1200). The other operative parameters are instead equal to those reported in Table 9 in all this experimental data. In decreasing the temperature, the formation of the particles precursors $GaX(NH_2)_2$ are delayed, in particular the activated ammonia condensations (20-25 kcal/mol as activations enegies). On the other hand also the reactions that lead to the production of $GaNH_2$ are slowed down. The trend is reasonably well represented.

What actually simulations are not able to explain is why in the extreme left edge of the growth profile in the standard experiment at 1400 K, the deposition rate is lower with respect to that at 1300 K. Observing the particles 2D profiles in Figures 42 it seems that the droplets formation should not affect the physical properties in that part of the reactor during the standard experiment. It should be instead mainly dominated by the diffusion of the precursors towards the subscector, which should be enhanced at higher temperatures. Consequently the only reasonable explanation may be a significant etching of part of the GaN film at 1400 K. This is coherent with what found in previous literature experiments [22, 189-191], where it was proven a conspicuous sublimation of the GaN layer at elevated substrate temperatures, with apparent activation energy of 83 kcal/mol [190]. Besides, the presence of a consistent etching at the standard conditions was confirmed by some aimed additional experiments. Hence, with the aim to qualitatively check if the experimental trend would be more reasonable represented by accounting also the etching rate, the curve at 1400 K has been arbitrary shifted of 300 nm in Figure 45c. Apparently including a desorption mechanism in the model would sensibly improve the model predictions from the

quantitative point of view. Thus further studies are required in this direction. The absolute values of the simulated results reported in this section are thus higher with respect to the experimental values probably because the etching is not considered. The eventual desorption of $GaNH_2$ from the substrate may eventually also increase its scavenging on the particles surface, hence further enhancing also the autocatalytic growth mechanism.

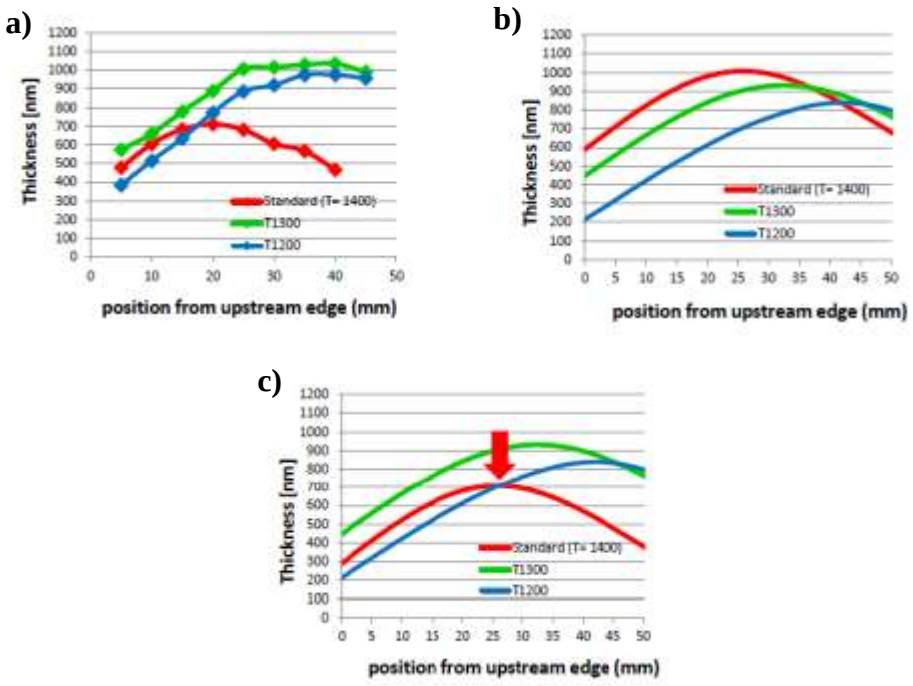

Figure 45: Effect of the substrate temperature on the deposition profiles a) experimental; b) simulated; c) with the simulated curve at 1400 K shifted of 300 nm for a possible etching mechanism.

In the experiments reported in Figures 46 it was changed only the total flow rate from 10 slm (Standard) to 5 slm (F5000) and 14 slm (F14000), keeping the flows distributions constant. Excepting the absolute discrepancy probably due to the sublimation mentioned above, there is a good agreement between simulation and experiments. The flow rate influences mainly the residence time above the substrate and consequently the starting point of chemical reactions, which are in kinetically controlled regime. Besides also the diffusion of group III sources from the upper part of the reactor towards the growth area and a little the temperature profile are conditioned by the flow rate.

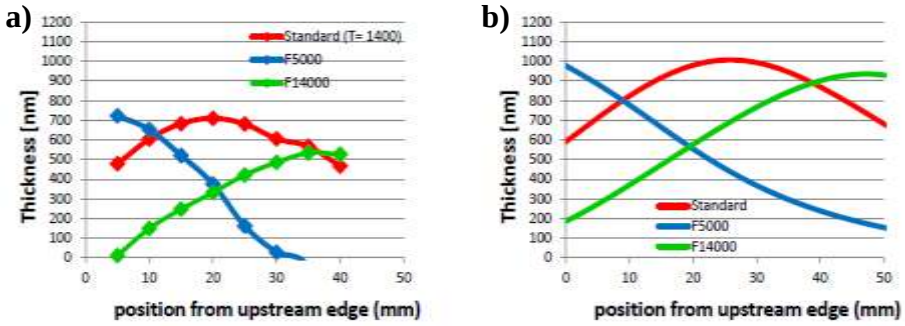

Figure 46: Effect of the flow rate on the deposition profiles a) experimental; b) simulated.

In Figures 47 is represented the dependence by the partial pressure of the inlet $Ga(CH_3)_3$, that was varied from $6.9x10^{-2}$ mbar (Standard) to $3.9x10^{-2}$ mbar (PIII20) and $9.8x10^{-2}$ mbar (PIII50). Experiments show that the curves are not exactly proportional to that parameter as it can be guessed a priori. Simulations are not able to predict this discrepancy, but probably shifting the curves consistently with the GaN desorption rate might explain it. Then, though a general reasonable agreement, observing the trends there is a slight difference between simulations and experiments. However, considering the level of accuracy of the methods used here to calculate the kintic constants and the particles growth, as well as the lack of the GaN desorption mechanism, the model predictions seems acceptable.

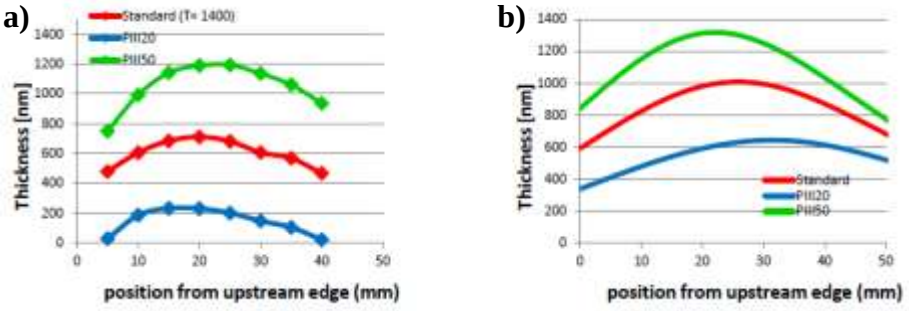

Figure 47: Effect of the $Ga(CH_3)_3$ initial partial pressure on the deposition profiles a) experimental; b) simulated.

Finally in Figures 48 is represented the dependence of the total pressure, changed from 200 mbar (Standard) to 100 mbar (P100) and 280 mbar

(P280). Anyway in order to keep constant the residence time above the substrate, also the total flow rates were modified accordingly. Specifically it was varied from 10 slm (Standard) to 5 slm (P100) and 14 slm (P280). Apart that the difference in the particles generation should be a little less enhanced, probably for the same reason explained for the results in Figure 47, the description is in quite good agreement. The effect is partly due to a variation of the main kinetics and partly to the diffusion enhanced at low pressures. Thus though the residence time was kept constant, the curve at lower pressure is shifted towards the upstream because of the enhanced material transports. The inclusion of an etching mechanism would probably compensate part of the discrepancies because the sublimation is enhanced at lower pressures. Furthermore some sensitive reactions may be in fall off regime.

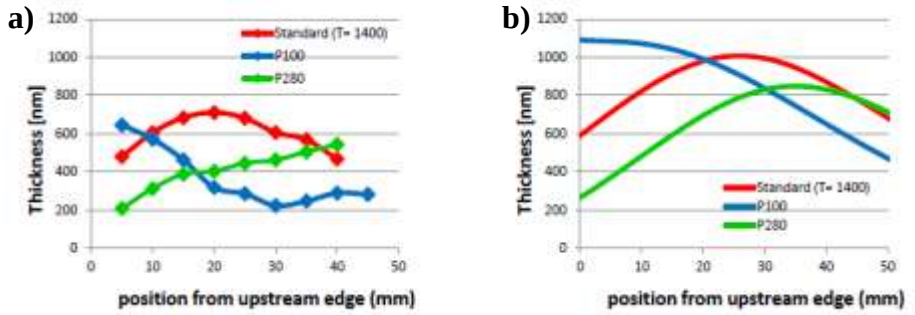

Figure 48: Effect of the total pressure on the deposition profiles a) experimental; b) simulated.

5.7 Concluding remarks

In this work it was proposed a novel kinetic mechanism to describe the reaction kinetics active during the GaN MOVPE. The level of accuracy of the *ab initio* calculations here performed is much higher with respect to those previously used in the literature and further new conversion pathways were added in the kinetic scheme. The assumptions here adopted are also supported by a thermodynamic analysis and are coherent with what found in some earlier spectroscopic experiments. With the inclusion in the gas phase kinetics of new set of elementary reactions and

chemical species, as well as with a more accurate estimation of the kinetic constants, the present mechanism was proved to be more realistic than what previously suggested in the literature.

It is assumed that $GaNH_2$ is the direct deposition precursor because it is the most stable gaseous molecule above the substrate. It was demonstrated that other hypothesis reported in the literature instead are not able to justify the growth profiles in external diffusive regime. Indeed those unstable compounds would be rapidly decomposed at the high temperatures above the substrate. The conversion of the initial $Ga(CH_3)_3$ to $GaNH_2$ occurs in several steps involving the gradual substitution of the $Ga\text{-}CH_3$ bonds with the more favored $Ga\text{-}NH_2$ and Ga-H, as well as the ammonia eliminations here proposed.

Then also the nucleation was treated in a different way than in the literature. Here it is not approximated the particle growth as a simple polymerization because the molecular structures of the most stable oligomers with different number of Ga atoms changes completely. Consequently their related physical properties and chemical reactivity are not similar. It was suggested in this research that the first stable nucleus is produced after 3 ammonia eliminations from species like $GaX(NH_2)_2$, with X that can be H, CH_3 or NH_2. From thermodynamic evaluations resulted that such key oligomer should have a planar geometry whose kernel is a ring composed by 3 Ga and 3 N atoms, with a structure in some way analogue to those of the aromatic hydrocarbons. The dimers instead are much more unstable intermediates, whose concentrations are regulated by the thermodynamic equilibrium.

Anyway the gas phase reactivity was not the only object of this research. Indeed a fluid dynamic representation of the AIXTRON reactor was developed. Then particles formation and growth were described using a model based on the second order method of moments. Also such model was improved from what previously proposed, by including a new correlation to keep into account explicitly the size dependence of the

aggregates growth rate. That expression was achieved analytically using two different approaches, obtaining the same result. The growth mechanism found on this way is in fact auto catalytic.

An aimed sensitivity analysis carried on in this study, showed that both the transport phenomena and the kinetics have a key role in determining the global performances of the MOVPE reactors. Indeed the mixing of the group III precursor is not complete above the substrate, thus its diffusion towards the hot susceptor limits the deposition rate. On the other hand also the chemical reactivity is in a kinetically controlled regime because it is required to overcome a temperature threshold to activate the reactions that lead to the $GaNH_2$ production. Moreover also the particles nucleation is kinetically controlled as well.

The model here developed is able to explain the experimental evidences with prediction in general good agreement, consistently with the level of precision of the *ab initio* calculations and the uncertainties in the correlations of the method of moments adopted. Besides, also using a 2D model to solve the material balances may have partially affected the simulations results. However in order to achieve a better quantitative representation, it is necessary to include also some correlations able to predict the sublimation of the GaN from the substrate. From a qualitative analysis explained above, the latter phenomenon is able to explain most of the discrepancies between the simulations and the experimental data.

CHAPTER 6

Conclusions

In this phd thesis it was developed a general methodology to clarify the kinetics at different scales in bi phase systems characterized by an interaction between a gas and an activated solid surface. Such method implies the formulation of advanced kinetic mechanisms composed only by elementary reactions. Their parameters are estimated through accurate quantum chemistry *ab initio* calculations, based on the transition state theory. The precision of the techniques applied here is higher with respect to classical DFT, used in the literature to describe the same type of processes, because the latter presents conspicuous uncertainties especially in the activation energies. Besides the micro kinetics, it was also evaluated the effect of fluid dynamics on the global performances of the reactor. Indeed transport phenomena could be fundamental in determining the behavior at the macro scale. Such approach was successfully applied to describe four different systems of interest from the industrial point of view. Therefore the methodology here proposed was resulted to be a useful tool to optimize the operative conditions for various types of processes with a subsequent improvement of their global performances.

The first part of the work was dedicated to the non oxidative valorization of natural gas through non thermal plasmas. The simulations are consistent with the results reported in the literature, that have demonstrated the possibility to achieve elevated acetylene yields with energy efficiencies comparable with those of thermal processes.

Moreover one of the main findings of this study is that the temperature evolution in the plasma volume plays a key role in determining the system reactivity and its energy consumption. Among the conclusions of this study are included a set of guidelines that may be useful to improve the energy efficiency of plasma methane conversion.

Then it was studied the silicon CVD from trichlorosilane. A micro kinetic analysis revealed that a radical chain mechanism, never proposed before in the literature, should be predominant in the gas phase of industrial Siemens reactors. Furthermore it was pointed out a strong inter relation between the reactivity in the two phases because of the consumption of the corrosive HCl in the gas, produced during the deposition. Thus operating Si CVD in conditions in which the gas phase reactivity is favored (i.e. at high gas phase temperatures) should enhance the precursor conversion and the film growth rate, though at the expense of an increased production of tetrachlorosilane. The new proposed conversion pathways have lately been proved to be effective also during SiC growth, evidencing good agreement between simulations and experiments. However, as the operative conditions are completely different with respect to those in Si CVD, the product distribution totally changes. Those simulations predict that the surface kinetics of atomic Si can influence the SiC deposition profile.

Finally this research was also focused on GaN MOVPE. Such project was in cooperation with two research groups in the University of Tokyo and part of the phd thesis was spent there. A reasonable good agreement between simulations and experiments was achieved. With the hypothesis proposed it has been possible to clarify various phenomena that take place in the reactor during the film growth, focusing in particular on kinetics and diffusion. Thus the model can potentially be used as a means to achieve higher growth rates, as well as to reduce the powders drop on the substrate.

Bibliography

[1] A.A. Fridman, Plasma chemistry, Cambridge University Press, Cambridge ; New York, 2008.
[2] J.R. Fincke, R.P. Anderson, T. Hyde, B.A. Detering, R. Wright, R.L. Bewley, D.C. Haggard, W.D. Swank, Plasma thermal conversion of methane to acetylene, Plasma Chem Plasma P, 22 (2002) 105-136.
[3] S. Kado, Y. Sekine, T. Nozaki, K. Okazaki, Diagnosis of atmospheric pressure low temperature plasma and application to high efficient methane conversion, Catal Today, 89 (2004) 47-55.
[4] S.L. Yao, E. Suzuki, N. Meng, A. Nakayama, A high-efficiency reactor for the pulsed plasma conversion of methane, Plasma Chem Plasma P, 22 (2002) 225-237.
[5] S.L. Yao, A. Nakayama, E. Suzuki, Methane conversion using a high-frequency pulsed plasma: Important factors, Aiche Journal, 47 (2001) 413-418.
[6] G.B. Zhao, S. John, J.J. Zhang, L.N. Wang, S. Muknahallipatna, J.C. Hamann, J.F. Ackerman, M.D. Argyle, O.A. Plumb, Methane conversion in pulsed corona discharge reactors, Chem Eng J, 125 (2006) 67-79.
[7] A.I. Babaritsky, S.A. Diomkin, V.K. Givotov, V.G. Makarenko, S.A. Nester, V.A. Rusanov, A. Fridman, Non-equilibrium approach to methane conversion into acetylene in microwave discharge, in: Kurchatov Institute of Atomic Energy, 1991.
[8] P. Woditsch, W. Koch, Solar grade silicon feedstock supply for PV industry, Sol Energ Mat Sol C, 72 (2002) 11-26.
[9] W.O. Filtvedt, A. Holt, P.A. Ramachandran, M.C. Melaaen, Chemical vapor deposition of silicon from silane: Review of growth mechanisms and modeling/scaleup of fluidized bed reactors, Sol Energ Mat Sol C, 107 (2012) 188-200.
[10] B. Hazeltine, C. Fero, Q. W., Advancements in the commercial production of polysilicon Photovoltaic World, 3 (2010).
[11] L. Fabry, K. Hesse, Crystalline Silicon Feedstock Preparation and Analysis, in: G.P. Willeke, E.R. Weber (Eds.) Advances in Photovoltaics, Vol 1, pp. 185-261.
[12] M. Willander, M. Friesel, Q.U. Wahab, B. Straumal, Silicon carbide and diamond for high temperature device applications, J Mater Sci-Mater El, 17 (2006) 1-25.
[13] D. Crippa, M. Masi, D.L. Rode, Silicon epitaxy, Academic Press, San Diego, CA, 2001.
[14] T. Kimoto, A. Itoh, H. Matsunami, Step-controlled epitaxial growth of high-quality SiC layers, Phys Status Solidi B, 202 (1997) 247-262.

[15] H. Pedersen, S. Leone, O. Kordina, A. Henry, S. Nishizawa, Y. Koshka, E. Janzen, Chloride-Based CVD Growth of Silicon Carbide for Electronic Applications, Chem Rev, 112 (2012) 2434-2453.
[16] A. Veneroni, M. Masi, Gas-phase and surface kinetics of epitaxial silicon carbide growth involving chlorine-containing species, Chem Vapor Depos, 12 (2006) 562-568.
[17] P. Gibart, Metal organic vapour phase epitaxy of GaN and lateral overgrowth, Reports on Progress in Physics, 67 (2004) 667-715.
[18] S.C. Jain, M. Willander, J. Narayan, R. Van Overstraeten, III-nitrides: Growth, characterization, and properties, J. Appl. Phys., 87 (2000) 965-1006.
[19] I.M. Watson, Metal organic vapour phase epitaxy of AlN, GaN, InN and their alloys: A key chemical technology for advanced device applications, Coord. Chem. Rev., 257 (2013) 2120-2141.
[20] S. Nakamura, S.J. Pearton, G. Fasol, The blue laser diode : the complete story, 2nd updated and extended ed., Springer, Berlin ; New York, 2000.
[21] J. Han, M.H. Crawford, R.J. Shul, J.J. Figiel, M. Banas, L. Zhang, Y.K. Song, H. Zhou, A.V. Nurmikko, AlGaN/GaN quantum well ultraviolet light emitting diodes, Appl Phys Lett, 73 (1998) 1688-1690.
[22] C.H. Chen, H. Liu, D. Steigerwald, W. Imler, C.P. Kuo, M.G. Craford, M. Ludowise, S. Lester, J. Amano, A study of parasitic reactions between NH3 and TMGa or TMAI, J Electron Mater, 25 (1996) 1004-1008.
[23] F. Nakamura, S. Hashimoto, M. Hara, S. Imanaga, M. Ikeda, H. Kawai, AlN and AlGaN growth using low-pressure metalorganic chemical vapor deposition, J Cryst Growth, 195 (1998) 280-285.
[24] J.R. Creighton, W.G. Breiland, M.E. Coltrin, R.P. Pawlowski, Gas-phase nanoparticle formation during AlGaN metalorganic vapor phase epitaxy, Appl Phys Lett, 81 (2002) 2626-2628.
[25] M. Dauelsberg, D. Brien, R. Pusche, O. Schon, E.V. Yakovlev, A.S. Segal, R.A. Talalaev, Investigation of nitride MOVPE at high pressure and high growth rates in large production reactors by a combined modelling and experimental approach, J Cryst Growth, 315 (2011) 224-228.
[26] T. Mihopoulos, Ph.D. Thesis, Nat Prod Lett, (1999).
[27] M. Sugiyama, S. Yasukochi, T. Shioda, Y. Shimogaki, Y. Nakano, Examination of intermediate species in GaN metal-organic vapor-phase epitaxy by selective-area growth, in: Physica Status Solidi C: Current Topics in Solid State Physics, Vol 7, No 7-8, Wiley-V C H Verlag Gmbh, Weinheim, 2010.
[28] J.R. Creighton, G.T. Wang, M.E. Coltrin, Fundamental chemistry and modeling of group-III nitride MOVPE, J Cryst Growth, 298 (2007) 2-7.
[29] M.J. Frisch, G.W. Trucks, H.B. Schlegel, G.E. Scuseria, M.A. Robb, J.R. Cheeseman, G. Scalmani, V. Barone, B. Mennucci, G.A. Petersson, et al. Gaussian 09 (Revision A.1) Gaussian Inc. Wallingford CT in, 2009.
[30] H.J. Werner, P.J. Knowles, G. Knizia, F.R. Manby, M. Schutz, P. Celani, T. Korona, R. Lindh, A. Mitrushenkov, G. Rauhut, K.R. Shamasundar, T.B. Adler, R.D. Amos, A. Bernhardsson, A. Berning, D.L. Cooper, M.J.O. Deegan, A.J. Dobbyn, F. Eckert, E. Goll, C. Hampel, A. Hesselmann, G. Hetzer, T. Hrenar, G. Jansen, C. Koppl, Y. Liu, A.W. Lloyd, R.A. Mata, A.J. May, S.J. McNicholas, W. Meyer, M.E. Mura, A. Nickla, D.P. O'Neill, P. Palmieri, D. Peng, K. Pfluger, R. Pitzer, M. Reiher, T. Shiozaki, H. Stoll, A.J. Stone, R. Tarroni, T. Thorsteinsson, M. Wang, Molpro, in, 2012.

[31] M.S. Gordon, M.W. Schmidt, Theory and Applications of Computational Chemistry: the first forty years, Elsevier, Amsterdam, 2005.
[32] T. Helgaker, P. Jørgensen, J. Olsen, Molecular electronic-structure theory, Wiley, Chichester ; New York, 2000.
[33] C.D. Sherrill, H.F. Schaefer, The configuration interaction method: Advances in highly correlated approaches, in: P.O. Lowdin, J.R. Sabin, M.C. Zerners, E. Brandas (Eds.) Advances in Quantum Chemistry, Vol 34, 1999, pp. 143-269.
[34] C. Møller, M.S. Plesset, .Note on an Approximation Treatment for Many-Electron Systems, Physical Review, (1934).
[35] R.J. Bartlett, COUPLED-CLUSTER APPROACH TO MOLECULAR-STRUCTURE AND SPECTRA - A STEP TOWARD PREDICTIVE QUANTUM-CHEMISTRY, J Phys Chem-Us, 93 (1989) 1697-1708.
[36] P. Hohenberg, W. Kohn, Inhomogeneous Electron Gas, Physical Review, 136 (1964).
[37] W. Kohn, L.J. Sham, Self-Consistent Equations Including Exchange and Correlation Effects, Physical Review (1965).
[38] A.D. Becke, A NEW MIXING OF HARTREE-FOCK AND LOCAL DENSITY-FUNCTIONAL THEORIES, Journal of Chemical Physics, 98 (1993) 1372-1377.
[39] C.T. Lee, W.T. Yang, R.G. Parr, Development of the Colle-Salvetti correlation-energy formula into a functional of the electron density, Physical Review B, 37 (1988) 785-789.
[40] Y. Zhao, D.G. Truhlar, The M06 suite of density functionals for main group thermochemistry, thermochemical kinetics, noncovalent interactions, excited states, and transition elements: two new functionals and systematic testing of four M06-class functionals and 12 other functionals, Theoretical Chemistry Accounts, 120 (2008) 215-241.
[41] W.S. Ohlinger, P.E. Klunzinger, B.J. Deppmeier, W.J. Hehre, Efficient Calculation of Heats of Formation, J Phys Chem A, 113 (2009) 2165-2175.
[42] G.A. Petersson, M.A. Allaham, A COMPLETE BASIS SET MODEL CHEMISTRY .2. OPEN-SHELL SYSTEMS AND THE TOTAL ENERGIES OF THE 1ST-ROW ATOMS, Journal of Chemical Physics, 94 (1991) 6081-6090.
[43] G.P.F. Wood, L. Radom, G.A. Petersson, E.C. Barnes, M.J. Frisch, J.A. Montgomery, Jr., A restricted-open-shell complete-basis-set model chemistry, Journal of Chemical Physics, 125 (2006).
[44] J. Pfaendtner, X. Yu, L.J. Broadbelt, The 1-D hindered rotor approximation, Theoretical Chemistry Accounts, 118 (2007) 881-898.
[45] A.L.L. East, L. Radom, Ab initio statistical thermodynamical models for the computation of third-law entropies, Journal of Chemical Physics, 106 (1997) 6655-6674.
[46] H. Eyring, The Activated Complex in Chemical Reactions, Journal of Chemical Physics, 3 (1935) 107-115.
[47] F. Jensen, Introduction to computational chemistry, 2nd ed., John Wiley & Sons, Chichester, England ; Hoboken, NJ, 2007.
[48] R. Clausius, Ueber die Art der Bewegung, welche wir Wärme nennen, Annalen der Physik, (1857) 353-379.
[49] G. Valente, C. Cavallotti, M. Masi, S. Carra, Reduced order model for the CVD of epitaxial silicon from silane and chlorosilanes, J Cryst Growth, 230 (2001) 247-257.

[50] C. Cavallotti, M. Masi, Kinetics of SiHCl3 Chemical Vapor Deposition and Fluid Dynamic Simulations, J Nanosci Nanotechno, 11 (2011) 8054-8060.
[51] M.T. Swihart, R.W. Carr, Thermochemistry and thermal decomposition of the chlorinated disilanes Si2HnCl6-n,n=0-6 studied in ab initio molecular orbital methods, J Phys Chem A, 101 (1997) 7434-7445.
[52] M.T. Swihart, R.W. Carr, On the mechanism of homogeneous decomposition of the chlorinated silanes. Chain reactions propagated by divalent silicon species, J Phys Chem A, 102 (1998) 1542-1549.
[53] M.T. Swihart, R.W. Carr, Ab initio molecular orbital study of the thermochemistry and reactions of the chlorinated disilenes and their isomers (Si2HnCl4-n), J Phys Chem A, 102 (1998) 785-792.
[54] M.D. Su, H.B. Schlegel, An Ab-Initio Mo Study of the Thermal-Decomposition of Chlorinated Monosilanes, Sih4-Ncln (N = 0-4), J Phys Chem-Us, 97 (1993) 9981-9985.
[55] S.P. Walch, C.E. Dateo, Thermal decomposition pathways and rates for silane, chlorosilane, dichlorosilane, and trichlorosilane, J Phys Chem A, 105 (2001) 2015-2022.
[56] A. Fiorucci, D. Moscatelli, M. Masi, Homoepitaxial silicon carbide deposition processes via chlorine routes, Surf Coat Tech, 201 (2007) 8825-8829.
[57] A. Barbato, C. Seghi, C. Cavallotti, An ab initio Rice-Ramsperger-Kassel-Marcus/master equation investigation of SiH4 decomposition kinetics using a kinetic Monte Carlo approach, Journal of Chemical Physics, 130 (2009).
[58] L.S. Hong, Y. Shimogaki, Y. Egashira, H. Komiyama, STUDY OF THE REACTION OF SI2H6 IN THE PRESENCE OF C2H2 IN SYNTHESIS OF SIC FILMS BY LPCVD USING A MACRO MICROCAVITY METHOD, J Electrochem Soc, 139 (1992) 3652-3659.
[59] A. Hirako, K. Kusakabe, K. Ohkawa, Modeling of reaction pathways of GaN growth by metalorganic vapor-phase epitaxy using TMGa/NH3/H-2 system: A computational fluid dynamics simulation study, Jpn J Appl Phys 1, 44 (2005) 874-879.
[60] D. Moscatelli, C. Cavallotti, Theoretical investigation of the gas-phase kinetics active during the GaN MOVPE, J Phys Chem A, 111 (2007) 4620-4631.
[61] D. Sengupta, S. Mazumder, W. Kuykendall, S.A. Lowry, Combined ab initio quantum chemistry and computational fluid dynamics calculations for prediction of gallium nitride growth, J Cryst Growth, 279 (2005) 369-382.
[62] H. Tokoi, A. Ohtake, K. Tago, K. Watanabe, T. Mishima, Development of GaN Growth Reaction Model Using Ab Initio Molecular Orbital Calculation and Computational Fluid Dynamics of Metalorganic Vapor-Phase Epitaxy, J Electrochem Soc, 159 (2012) D270-D275.
[63] K. Nakamura, O. Makino, A. Tachibana, K. Matsumoto, Quantum chemical study of parasitic reaction in III-V nitride semiconductor crystal growth, J Organomet Chem, 611 (2000) 514-524.
[64] Y. Ikeda, N. Ohmori, N. Maida, M. Senami, A. Tachibana, Theoretical Study of Gallium Nitride Crystal Growth Reaction Mechanism, Jpn J Appl Phys, 50 (2011).
[65] A.Y. Timoshkin, H.F. Bettinger, H.F. Schaefer, DFT modeling of chemical vapor deposition of GaN from organogallium precursors. 1. Thermodynamics of elimination reactions, J Phys Chem A, 105 (2001) 3240-3248.

[66] A.Y. Timoshkin, H.F. Bettinger, H.F. Schaefer, DFT modeling of chemical vapor deposition of GaN from organogallium precursors. 2. Structures of the oligomers and thermodynamics of the association processes, J Phys Chem A, 105 (2001) 3249-3258.
[67] K. Matsumoto, A. Tachibana, Growth mechanism of atmospheric pressure MOVPE of GaN and its alloys: gas phase chemistry and its impact on reactor design, J Cryst Growth, 272 (2004) 360-369.
[68] B. Mondal, D. Mandal, D. Ghosh, A.K. Das, Computational Study on the Growth of Gallium Nitride and a Possible Source of Oxygen Impurity, J Phys Chem A, 114 (2010) 5016-5025.
[69] J.R. Creighton, G.T. Wang, Kinetics of metal organic-ammonia adduct decomposition: Implications for group-III nitride MOCVD, J Phys Chem A, 109 (2005) 10554-10562.
[70] M. Derudi, D. Polino, C. Cavallotti, Toluene and benzyl decomposition mechanisms: elementary reactions and kinetic simulations, Physical Chemistry Chemical Physics, 13 (2011) 21308-21318.
[71] D. Polino, C. Cavallotti, Fulvenallene Decomposition Kinetics, J Phys Chem A, 115 (2011) 10281-10289.
[72] D. Polino, A. Famulari, C. Cavallotti, Analysis of the Reactivity on the C7H6 Potential Energy Surface, J Phys Chem A, 115 (2011) 7928-7936.
[73] K. Raghavachari, G.W. Trucks, J.A. Pople, M. Headgordon, A 5TH-ORDER PERTURBATION COMPARISON OF ELECTRON CORRELATION THEORIES, Chem Phys Lett, 157 (1989) 479-483.
[74] D.E. Woon, T.H. Dunning, Gaussian- basis sets for use in correlated molecular calculations. 5. Core-valence basis-sets for Boron through Neon Journal of Chemical Physics, 103 (1995) 4572-4585.
[75] J.M.L. Martin, Ab initio total atomization energies of small molecules - Towards the basis set limit, Chem Phys Lett, 259 (1996) 669-678.
[76] S. Fascella, C. Cavallotti, R. Rota, S. Carra, Quantum chemistry investigation of key reactions involved in the formation of naphthalene and indene, J Phys Chem A, 108 (2004) 3829-3843.
[77] S. Fascella, C. Cavallotti, R. Rota, S. Carra, The peculiar kinetics of the reaction between acetylene and the cyclopentadienyl radical, J Phys Chem A, 109 (2005) 7546-7557.
[78] D. Ramkrishna, Population balances : theory and applications to particulate systems in engineering, Academic Press, San Diego, CA, 2000.
[79] K.S. Kim, S.E. Pratsinis, MANUFACTURE OF OPTICAL WAVE-GUIDE PREFORMS BY MODIFIED CHEMICAL VAPOR-DEPOSITION, Aiche Journal, 34 (1988) 912-921.
[80] F. Di Muzio, M. Masi, S. Carra, Modeling of aerosol deposition of titania thin films, Mater Chem Phys, 66 (2000) 286-293.
[81] E.V. Yakovlev, R.A. Talalaev, Y.N. Makarov, B.S. Yavich, W.N. Wang, Deposition behavior of GaN in AIX 200/4 RF-S horizontal reactor, J Cryst Growth, 261 (2004) 182-189.
[82] R.A. Talalaev, E.V. Yakovlev, S.Y. Karpov, Y.N. Makarov, On low temperature kinetic effects in metal-organic vapor phase epitaxy of III-V compounds, J Cryst Growth, 230 (2001) 232-238.

[83] A.N. Vorob'ev, S.Y. Karpov, M.V. Bogdanov, A.E. Komissarov, O.V. Bord, A.I. Zhmakin, Y.N. Makarov, Numerical study of SiCCVD in a vertical cold-wall reactor, Computational Materials Science, 24 (2002) 520-534.
[84] A. Hirsikko, L. Laakso, U. Horrak, P.P. Aalto, V.M. Kerminen, M. Kulmala, Annual and size dependent variation of growth rates and ion concentrations in boreal forest, Boreal Environ Res, 10 (2005) 357-369.
[85] T. Yli-Juuti, T. Nieminen, A. Hirsikko, P.P. Aalto, E. Asmi, U. Horrak, H.E. Manninen, J. Patokoski, M. Dal Maso, T. Petaja, J. Rinne, M. Kulmala, I. Riipinen, Growth rates of nucleation mode particles in Hyytiala during 2003-2009: variation with particle size, season, data analysis method and ambient conditions, Atmos Chem Phys, 11 (2011) 12865-12886.
[86] R.K. Talbot, R.W. Cheng, D.R. Schefer, J. Willis, Thermophoresis of particles in a heated boundary layer, Journal of Fluid Mechanics, 101 (1980) 737-758.
[87] K.W. Lee, B.Y.H. Liu, On the Minimum Efficiency and the Most Penetrating Particle Size for Fibrous Filter, Journal of the Air Pollution Control Association, (1980) 377.
[88] S.E. Pratsinis, Simultaneous Nucleation, Condensation, and Coagulation in Aerosol Reactors, J Colloid Interf Sci, 124 (1988) 416-427.
[89] B.E. Poling, J.M. Prausnitz, J.P. O'Connell, The properties of gases and liquids, 5th ed., McGraw-Hill, New York, 2001.
[90] C. Cavallotti, M. Masi, S. Carra, Modeling plasma-assisted deposition of diamond-like carbon films, J Electrochem Soc, 145 (1998) 4332-4341.
[91] D. Angermeier, R. Monna, A. Slaoui, J.C. Muller, Modeling and analysis of the silicon epitaxial growth with SiHCl3 in a horizontal rapid thermal chemical vapor deposition reactor, J Electrochem Soc, 144 (1997) 3256-3261.
[92] G. Condorelli, M. Mauceri, G. Pistone, L.M.S. Perdicaro, G. Abbondanza, F. Portuese, G.L. Valente, D. Crippa, F. Giannazzo, F. La Via, Thin SiC-4H Epitaxial Layer Growth by Trichlorosilane (TCS) as Silicon Precursor with Very Abrupt Junctions, in: A. Suzuki, H. Okumura, T. Kimoto, T. Fuyuki, K. Fukuda, S. Nishizawa (Eds.) Mater Sci Forum, 2009, pp. 127-130.
[93] A.V. Luikov, Heat and Mass transfer, Mir, Moscow, 1980.
[94] P.N. Brown, A.C. Hindmarsh, L.R. Petzold, USING KRYLOV METHODS IN THE SOLUTION OF LARGE-SCALE DIFFERENTIAL-ALGEBRAIC SYSTEMS, Siam Journal on Scientific Computing, 15 (1994) 1467-1488.
[95] P.N. Brown, A.C. Hindmarsh, L.R. Petzold, Consistent initial condition calculation for differential-algebraic systems, Siam Journal on Scientific Computing, 19 (1998) 1495-1512.
[96] M. Masi, C. Cavallotti, G. Radaelli, S. Carra, Kinetics of indium phosphide epitaxial growth using metal organic precursors, Crystal Research and Technology, 32 (1997) 1125-1136.
[97] S. Banerjee, J.V. Cole, K.F. Jensen, Nonlinear model reduction strategies for rapid thermal processing systems, Ieee Transactions on Semiconductor Manufacturing, 11 (1998) 266-275.
[98] T.P. Merchant, J.V. Cole, K.L. Knutson, J.P. Hebb, K.F. Jensen, A systematic approach to simulating rapid thermal processing systems, J Electrochem Soc, 143 (1996) 2035-2043.
[99] K.F. Jensen, T.G. Mihopoulos, S. Rodgers, H. Simka, CVD simulations on multiple length scales, 1996.

[100] A. Barbato, C. Cavallotti, Challenges of introducing quantitative elementary reactions in multiscale models of thin film deposition, Phys Status Solidi B, 247 (2010) 2127-2146.
[101] C. Cavallotti, M. Nemirovskaya, K.F. Jensen, A multiscale study of the selective MOVPE of AlxGa1-xAs in the presence of HCl, J Cryst Growth, 248 (2003) 411-416.
[102] C. Cavallotti, E. Pantano, A. Veneroni, M. Masi, Multiscale simulation of silicon film growth, Crystal Research and Technology, 40 (2005) 958-963.
[103] M. Masi, V. Bertani, C. Cavallotti, S. Carra, Towards a multiscale approach to the growth of silicon films by chemical vapor deposition, Mater Chem Phys, 66 (2000) 229-235.
[104] S. Ravasio, C. Cavallotti, Analysis of reactivity and energy efficiency of methane conversion through non thermal plasmas, Chem Eng Sci, 84 (2012) 580-590.
[105] A. Indarto, J.W. Choi, H. Lee, H.K. Song, Effect of additive gases on methane conversion using gliding arc discharge, Energy, 31 (2006) 2986-2995.
[106] A. Indarto, N. Coowanitwong, J.W. Choi, H. Lee, H.K. Song, Kinetic modeling of plasma methane conversion in a dielectric barrier discharge, Fuel Process Technol, 89 (2008) 214-219.
[107] S. Kado, K. Urasaki, Y. Sekine, K. Fujimoto, T. Nozaki, K. Okazaki, Reaction mechanism of methane activation using non-equilibrium pulsed discharge at room temperature, Fuel, 82 (2003) 2291-2297.
[108] S.S. Kim, H. Lee, J.W. Choi, B.K. Na, H.K. Song, Kinetics of the methane decomposition in a dielectric-barrier discharge, J Ind Eng Chem, 9 (2003) 787-791.
[109] S.S. Kim, H. Lee, J.W. Choi, B.K. Na, H.K. Song, Methane conversion to higher hydrocarbons in a dielectric-barrier discharge reactor with Pt/gamma-Al2O3 catalyst, Catal Commun, 8 (2007) 1438-1442.
[110] X.S. Li, A.M. Zhu, K.J. Wang, X. Yong, Z.M. Song, Methane conversion to C-2 hydrocarbons and hydrogen in atmospheric non-thermal plasmas generated by different electric discharge techniques, Catal Today, 98 (2004) 617-624.
[111] J. Lu, Z.H. Li, Conversion of natural gas to C(2) hydrocarbons via cold plasma technology, J Nat Gas Chem, 19 (2010) 375-379.
[112] M. Mlotek, J. Sentek, K. Krawczyk, K. Schmidt-Szalowski, The hybrid plasma-catalytic process for non-oxidative methane coupling to ethylene and ethane, Appl Catal a-Gen, 366 (2009) 232-241.
[113] G. Scarduelli, G. Guella, I. Mancini, G. Dilecce, S. De Benedictis, P. Tosi, Methane Oligomerization in a Dielectric Barrier Discharge at Atmospheric Pressure, Plasma Process Polym, 6 (2009) 27-33.
[114] Y. Yang, Direct non-oxidative methane conversion by non-thermal plasma: Experimental study, Plasma Chem Plasma P, 23 (2003) 283-296.
[115] K. Thanyachotpaiboon, S. Chavadej, T.A. Caldwell, L.L. Lobban, R.G. Mallinson, Conversion of methane to higher hydrocarbons in AC nonequilibrium plasmas, Aiche Journal, 44 (1998) 2252-2257.
[116] A.A. Ghorbanzadeh, N.S. Matin, Methane conversion to hydrogen and higher hydrocarbons by double pulsed glow discharge, Plasma Chem Plasma P, 25 (2005) 19-29.

[117] C.L. Gordon, L.L. Lobban, R.G. Mallinson, Ethylene production using a Pd and Ag-Pd-Y-zeolite catalyst in a DC plasma reactor, Catal Today, 84 (2003) 51-57.
[118] S.L. Yao, A. Nakayama, E. Suzuki, Methane conversion using a high-frequency pulsed plasma: Discharge features, Aiche Journal, 47 (2001) 419-426.
[119] H. Lee, H. Sekiguchi, Plasma-catalytic hybrid system using spouted bed with a gliding arc discharge: CH(4) reforming as a model reaction, Journal of Physics D-Applied Physics, 44 (2011) 274008.
[120] S.I. Gritsinin, P.A. Gushchin, A.M. Davydov, E.V. Ivanov, I.A. Kossyi, M.A. Misakyan, Conversion of methane in a coaxial microwave torch, Plasma Phys Rep+, 35 (2009) 933-940.
[121] W. Cho, Y.C. Kim, S.S. Kim, Conversion of natural gas to C(2) product, hydrogen and carbon black using a catalytic plasma reaction, J Ind Eng Chem, 16 (2010) 20-26.
[122] M. Heintze, M. Magureanu, M. Kettlitz, Mechanism of C-2 hydrocarbon formation from methane in a pulsed microwave plasma, J. Appl. Phys., 92 (2002) 7022-7031.
[123] J. Huang, S.L. Suib, Dimerization of Methane through Microwave Plasmas, J Phys Chem-Us, 97 (1993) 9403-9407.
[124] M. Jasinski, M. Dors, J. Mizeraczyk, Production of hydrogen via methane reforming using atmospheric pressure microwave plasma, J Power Sources, 181 (2008) 41-45.
[125] C. Marun, S.L. Suib, M. Dery, J.B. Harrison, M. Kablaoui, Effect of dielectric constant, cavities in series, and cavities in parallel on the product distribution of the oligomerization of methane via microwave plasmas, J Phys Chem-Us, 100 (1996) 17866-17872.
[126] J. Ropcke, L. Mechold, X. Duten, A. Rousseau, A time resolved laser study of hydrocarbon chemistry in H-2-CH4 surface wave plasmas, Journal of Physics D-Applied Physics, 34 (2001) 2336-2345.
[127] C.S. Shen, D.K. Sun, H.S. Yang, Methane coupling in microwave plasma under atmospheric pressure, J Nat Gas Chem, 20 (2011) 449-456.
[128] J.Q. Zhang, Y.J. Yang, J.S. Zhang, Q. Liu, K.R. Tan, Non-oxidative coupling of methane to C-2 hydrocarbons under above-atmospheric pressure using pulsed microwave plasma, Energ Fuel, 16 (2002) 687-693.
[129] M. Mozetic, A. Vesel, D. Alegre, F.L. Tabares, Destruction of methane in low-pressure, electrodeless radio frequency plasma on quartz walls, J. Appl. Phys., 110 (2011) 053302.
[130] S.Y. Savinov, H. Lee, H.K. Song, B.K. Na, A kinetic study on the conversion of methane to higher hydrocarbons in a radio-frequency discharge, Korean J Chem Eng, 21 (2004) 601-610.
[131] H. Winands, K.P. Yan, S.A. Nair, G. Pemen, B. van Heesch, Evaluation of corona plasma techniques for industrial applications: HPPS and DC/AC systems, Plasma Process Polym, 2 (2005) 232-237.
[132] T. Kovacs, Methane Conversion: a Case Study for Simplification of Plasma Chemistry Models by the Omission of Charged Species, Plasma Chem Plasma P, 30 (2010) 207-212.
[133] Y.A. Mankelevich, M.N.R. Ashfold, J. Ma, Plasma-chemical processes in microwave plasma-enhanced chemical vapor deposition reactors operating with C/H/Ar gas mixtures, J. Appl. Phys., 104 (2008) 113304.

[134] M. Masi, C. Cavallotti, S. Carra, Different approaches for methane plasmas modeling, Chem Eng Sci, 53 (1998) 3875-3886.
[135] D.I. Slovetskii, Y.A. Mankelevich, S.D. Slovetskii, T.V. Rakhimova, Mathematical modeling of the plasma-chemical pyrolysis of methane, High Energ Chem+, 36 (2002) 44-52.
[136] Y. Yang, Direct non-oxidative methane conversion by non-thermal plasma: Modeling study, Plasma Chem Plasma P, 23 (2003) 327-346.
[137] C. De Bie, T. Martens, J. Van Dijk, J.J.A.M. Van der Mullen, A. Bogaerts, Description of the Plasma Chemistry in an Atmospheric Pressure Ch(4) Dielectric Barrier Discharge Using a Two Dimensional Fluid Model, 4th International Congress on Cold Atmospheric Pressure Plasmas: Sources and Applications, Proceedings, (2009) 13-16.
[138] C. De Bie, T. Martens, J. van Dijk, S. Paulussen, B. Verheyde, S. Corthals, A. Bogaerts, Dielectric barrier discharges used for the conversion of greenhouse gases: modeling the plasma chemistry by fluid simulations, Plasma Sources Science & Technology, 20 (2011) 024008.
[139] C. De Bie, B. Verheyde, T. Martens, J. van Dijk, S. Paulussen, A. Bogaerts, Fluid Modeling of the Conversion of Methane into Higher Hydrocarbons in an Atmospheric Pressure Dielectric Barrier Discharge, Plasma Process Polym, 8 (2011) 1033-1058.
[140] T. Farouk, B. Farouk, A. Gutsol, A. Fridman, Atmospheric pressure methane-hydrogen dc micro-glow discharge for thin film deposition, J Phys D Appl Phys, 41 (2008) 175202.
[141] T. Farouk, B. Farouk, A. Fridman, Computational Studies of Atmospheric-Pressure Methane-Hydrogen DC Micro Glow Discharges, Ieee T Plasma Sci, 38 (2010) 73-85.
[142] J. Gonzalez-Aguilar, I. Deme, L. Fulcheri, G. Flamant, T.M. Gruenberger, B. Ravary, Comparison of simple particle-radiation coupling models applied on a plasma black process, Plasma Chem Plasma P, 24 (2004) 603-623.
[143] J. Ma, A. Cheesman, M.N.R. Ashfold, K.G. Hay, S. Wright, N. Langford, G. Duxbury, Y.A. Mankelevich, Quantum cascade laser investigations of CH(4) and C(2)H(2) interconversion in hydrocarbon/H(2) gas mixtures during microwave plasma enhanced chemical vapor deposition of diamond, J. Appl. Phys., 106 (2009) 033305.
[144] K. Tachibana, M. Nishida, H. Harima, Y. Urano, Diagnostic and modeling of methane plasma used in the chemical vapor deposition of amorphous carbon films, Journal of Physics D-Applied Physics, 17 (1984) 1727.
[145] G.P. Smith, D.M. Golden, M. Frenklach, M.W. Moriarty, B. Eiteneer, M. Goldenberg, T. Bowman, R.K. Hanson, S. Song, W.C. Gardiner, V.V. Lissianski, Z. Qin, in.
[146] S. Ravasio, M. Masi, C. Cavallotti, Analysis of the Gas Phase Reactivity of Chlorosilanes, J Phys Chem A, 117 (2013) 5221-5231.
[147] C. Cavallotti, F. Rossi, S. Ravasio, M. Masi, A kinetic analysis of the growth and doping kinetics of the SiC chemical vapor deposition process, Industrial & Engineering Chemistry Research, in press (2014).
[148] M.A. Hall, C. Mui, C.B. Musgrave, DFT study of the adsorption of chlorosilanes on the Si(100)-2 x 1 surface, Journal of Physical Chemistry B, 105 (2001) 12068-12075.

[149] K.L. Walker, R.E. Jardine, M.A. Ring, H.E. O'Neal, Mechanisms and kinetics of the thermal decompositions of trichlorosilane, dischlorosilane, and monochlorosilane, Int J Chem Kinet, 30 (1998) 69-88.
[150] J. Nishizawa, M. Saito, Mechanism of chemical vapor deposition of silicon, J Cryst Growth, 52, Part 1 (1981) 213-218.
[151] U. Narusawa, Si deposition from chlorosilanes.1. Deposition modeling, J Electrochem Soc, 141 (1994) 2072-2077.
[152] M. Hierlemann, A. Kersch, C. Werner, H. Schafer, A gas-phase and surface kinetics model for Silicon epitaxial-growth with SiH2Cl2 in an RTCVD reactor, J Electrochem Soc, 142 (1995) 259-266.
[153] H. Habuka, T. Suzuki, S. Yamamoto, A. Nakamura, T. Takeuchi, M. Aihara, Dominant rate process of silicon surface etching by hydrogen chloride gas, Thin Solid Films, 489 (2005) 104-110.
[154] C. Cavallotti, Reactivity of Silicon Surfaces in the Presence of Adsorbed Hydrogen and Chlorine, Chem Vapor Depos, 16 (2010) 329-335.
[155] P. Zhang, W.W. Wang, G.H. Cheng, J.L. Li, Effect of Boundary Layers on Polycrystalline Silicon Chemical Vapor Deposition in a Trichlorosilane and Hydrogen System, Chinese J Chem Eng, 19 (2011) 1-9.
[156] A. Kunz, P. Roth, High-temperature kinetics of some Si- and Cl-containing ceramic precursors, Int J Chem Kinet, 33 (2001) 741-754.
[157] N.S. Shuman, A.P. Spencer, T. Baer, Experimental Thermochemistry of SiCl3R (R = Cl, H, CH3, C2H5, C2H3, CH2Cl, SiCl3), SiCl3+, and SiCl3 center dot, J Phys Chem A, 113 (2009) 9458-9466.
[158] O. Danielsson, A. Henry, E. Janzen, Growth rate predictions of chemical vapor deposited silicon carbide epitaxial layers, J Cryst Growth, 243 (2002) 170-184.
[159] O. Danielsson, P. Sukkaew, L. Ojamae, O. Kordina, E. Janzen, Shortcomings of CVD modeling of SiC today, Theoretical Chemistry Accounts, 132 (2013).
[160] M.D. Allendorf, R.J. Kee, A Model of Silicon-Carbide Chemical Vapor-Deposition, J Electrochem Soc, 138 (1991) 841-852.
[161] S. Leone, O. Kordina, A. Henry, S. Nishizawa, O. Danielsson, E. Janzen, Gas-Phase Modeling of Chlorine-Based Chemical Vapor Deposition of Silicon Carbide, Cryst Growth Des, 12 (2012) 1977-1984.
[162] A. Veneroni, F. Omarini, D. Moscatelli, M. Masi, S. Leone, M. Mauceri, G. Pistone, G. Abbondanza, Modeling of epitaxial silicon carbide deposition, J Cryst Growth, 275 (2005) E295-E300.
[163] M. Masi, A. Veneroni, A. Fiorucci, F. La Via, G. Foti, M. Mauceri, S. Leone, G. Pistone, G. Condorelli, G. Abbondanza, G.L. Valente, D. Crippa, Film morphology and process conditions in epitaxial silicon carbide growth via chlorides route, Silicon Carbide and Related Materials 2006, 556-557 (2007) 93-96.
[164] Y. Fukushima, N. Sato, Y. Funato, H. Sugiura, K. Hotozuka, T. Momose, Y. Shimogaki, Multi-Scale Analysis and Elementary Reaction Simulation of SiC-CVD Using CH3SiCl3/H-2, Ecs Journal of Solid State Science and Technology, 2 (2013) P492-P497.
[165] M.W.j. Chase, Nist-Janaf Themochemical Tables,Fourth Edition, Journal of Physical and Chemical Reference Data, Monograph 9, 1-1951 (1998).

[166] D.L. Baulch, C.J. Cobos, R.A. Cox, P. Frank, G. Hayman, T. Just, J.A. Kerr, T. Murrells, M.J. Pilling, J. Troe, R.W. Walker, J. Warnatz, EVALUATED KINETIC DATA FOR COMBUSTION MODELING SUPPLEMENT-I, Journal of Physical and Chemical Reference Data, 23 (1994) 847-1033.
[167] A. Kunz, P. Roth, A shock tube study of the reaction of Si atoms with HCl, Physical Chemistry Chemical Physics, 2 (2000) 221-226.
[168] M. Camarda, A. La Magna, A. Severino, F. La Via, Extended study of the step-bunching mechanism during the homoepitaxial growth of SiC, Thin Solid Films, 518 (2010) S159-S161.
[169] M. Camarda, A. Canino, A. La Magna, F. La Via, G. Feng, T. Kimoto, M. Aoki, H. Kawanowa, Structural and electronic characterization of (2,3(3)) bar-shaped stacking fault in 4H-SiC epitaxial layers, Appl Phys Lett, 98 (2011).
[170] M. Camarda, A. La Magna, P. Fiorenza, F. Giannazzo, F. La Via, Defect formation and evolution in the step-flow growth of silicon carbide: A Monte Carlo study, J Cryst Growth, 310 (2008) 971-975.
[171] M. Camarda, A. La Magna, P. Fiorenza, G. Izzo, F. La Via, Theoretical Monte Carlo study of the formation and evolution of defects in the homoepitaxial growth of SiC, Mater Sci Forum, 600-603 (2009) 135-138.
[172] M. Camarda, A. La Magna, F. La Via, A kinetic Monte Carlo method on super-lattices for the study of the defect formation in the growth of close packed structures, J Comput Phys, 227 (2007) 1075-1093.
[173] A. Severino, M. Camarda, G. Condorelli, L.M.S. Perdicaro, R. Anzalone, M. Mauceri, A. La Magna, F. La Via, Effect of the miscut direction in (111) 3C-SiC film growth on off-axis (111)Si, Appl Phys Lett, 94 (2009).
[174] S.A. Safvi, J.M. Redwing, A. Thon, J.S. Flynn, M.A. Tischler, T.F. Kuech, MOVPE GaN gas phase chemistry for reactor design and optimization, Mater Res Soc Symp P, 449 (1997) 101-106.
[175] M. Dauelsberg, C. Martin, H. Protzmann, A.R. Boyd, E.J. Thrush, J. Kaeppeler, M. Heuken, R.A. Talalaev, E.V. Yakovlev, A.V. Kondratyev, Modeling and process design of III-nitride MOVPE at near-atmospheric pressure in close coupled showerhead and planetary reactors, J Cryst Growth, 298 (2007) 418-424.
[176] K. Matsumoto, H. Tokunaga, A. Ubukata, K. Ikenaga, Y. Fukuda, T. Tabuchi, Y. Kitamura, S. Koseki, A. Yamaguchi, K. Uematsu, High growth rate metal organic vapor phase epitaxy GaN, J Cryst Growth, 310 (2008) 3950-3952.
[177] T. Shioda, Y. Tomita, T. Sugiyama, Y. Shimogaki, Y. Nakano, GaN selective area metal-organic vapor phase epitaxy: Prediction of growth rate enhancement by vapor phase diffusion model, Jpn. J. Appl. Phys. Part 2 - Lett. Express Lett., 46 (2007) L1045-L1047.
[178] T. Shioda, M. Sugiyama, Y. Shimogaki, Y. Nakano, Selectivity enhancement by hydrogen addition in selective area metal-organic vapor phase epitaxy of GaN and InGaN, Physica Status Solidi a-Applications and Materials Science, 207 (2010) 1375-1378.
[179] M. Sugiyama, Ieee, SELECTIVE AREA GROWTH OF III-V SEMICONDUCTORS: FROM FUNDAMENTAL ASPECTS TO DEVICE STRUCTURES, in: 2010 22nd International Conference on Indium Phosphide and Related Materials, 2010.

[180] U. Bergmann, V. Reimer, B. Atakan, An experimental study of the reactions of trimethylgallium with ammonia and water over a wide temperature range, Physical Chemistry Chemical Physics, 1 (1999) 5593-5599.
[181] J. Schafer, A. Simons, J. Wolfrum, R.A. Fischer, Detection of gas-phase species in MOCVD of GaN using molecular beam quadrupole mass spectrometry, Chem Phys Lett, 319 (2000) 477-481.
[182] A. Demchuk, J. Porter, B. Koplitz, Laser-assisted reactivity of triethylgallium or trimethylgallium with ammonia in constrained pulsed nozzle expansions, J Phys Chem A, 102 (1998) 8841-8846.
[183] F. Glocking, R.G. Strafford, ELECTRON IMPACT STUDIES ON SOME GROUP III METAL ALKYLS, JOURNAL OF THE CHEMICAL SOCIETY A -INORGANIC PHYSICAL THEORETICAL, (1971) 1761.
[184] O. Naji, J. Zhang, T. Kaneko, T.S. Jones, J.H. Neave, B.A. Joyce, A detailed time of flight study of the cracking pattern of trimethylgallium; Implications for MOMBE growth, J Cryst Growth, 164 (1996) 58-65.
[185] J.D. Meng, Y. Jaluria, Asme, NUMERICAL SIMULATION OF GaN GROWTH IN A MOCVD PROCESS, Amer Soc Mechanical Engineers, New York, 2012.
[186] K. Fu, Y. Fu, P. Han, Y. Zhang, R. Zhang, Kinetic Monte Carlo study of metal organic chemical vapor deposition growth dynamics of GaN thin film at microscopic level, J. Appl. Phys., 103 (2008).
[187] H. Hardtdegen, N. Kaluza, R. Steins, R. Schmidt, K. Wirtz, E.V. Yakovlev, R.A. Talalaev, Y.N. Makarov, MOVPE process for horizontal reactors with reduced parasitic deposition, J Cryst Growth, 272 (2004) 407-414.
[188] J.A. Jegier, S. McKernan, W.L. Gladfelter, Solution chemistry of cyclotrigallazane: Supercritical ammonia and Lewis base catalyzed dehydrogenation to produce poly(imidogallane), Inorg Chem, 38 (1999) 2726-2733.
[189] M.E. Bartram, J.R. Creighton, GaN CVD reactions: Hydrogen and ammonia decomposition and the desorption of gallium, Mrs Internet J N S R, 4 (1999) art. no.-G3.68.
[190] N. Grandjean, J. Massies, F. Semond, S.Y. Karpov, R.A. Talalaev, GaN evaporation in molecular beam epitaxy environment (vol 74, pg 1854, 1999), Appl Phys Lett, 75 (1999) 3035-3035.
[191] D.D. Koleske, M.E. Coltrin, A.A. Allerman, K.C. Cross, C.C. Mitchell, J.J. Figiel, In situ measurements of GaN nucleation layer decompostion, Appl Phys Lett, 82 (2003) 1170-1172.